FOURIE, FRANCOIS DANIEL

MODELLING THE TRANSIENT RESPONSE OF MULTIPLE CONDUCTORS FOR A STEP-FUNCTION TIME-DOMAIN ELECTROMAGNETIC SYSTEM

MSc **UP** **1996**

Modelling the transient response of multiple conductors for a step-function time-domain electromagnetic system

by

Francois Daniel Fourie

Submitted to the Faculty of Science in partial fulfillment
of the requirements for the MSc degree
in Exploration Geophysics.

University of Pretoria
May 1996

Modelling the transient response of multiple conductors for a step-function time-domain electromagnetic system

by

Francois Daniel Fourie

Supervisor : Prof WJ Botha
Department : Geology
Degree : Magister Scientiae in Exploration Geophysics

ABSTRACT

The time-domain electromagnetic response from multiple conductors in a resistive environment is studied by using wire loops in free space to model conductive sheets. This approach provides a relatively simple way of qualitatively examining the transient effects that two closely separated conductors have on the measured response.

Results from model studies indicate that the response from a multiple conductor system is not the sum of the individual conductor responses. When two conductors occur near a transmitter loop, the influence that exists between them can have a detrimental effect on the resolvability of the conductors. A conductor between a transmitter loop and a second conductor causes the response of the second conductor to be partially surpressed. This masking phenomena is particularly severe when the conductor that is closer to the transmitter loop has a lower conductance than the other conductor.

When dealing with a multiple conductor system where the conductors have conductances of similar magnitudes, the distance separating the conductors has to exceed their depths if both conductors are to be resolved from the electromagnetic profile plots. Only when the separation/depth ratio approaches 2, can the presence of two conductors be established with any certainty.

When large differences (in the order of a few tenths of a Siemens) exist in model conductances, the cross-overs and amplitude peaks shift in the direction of the conductor of higher conductance. These shifts are observed even when the conductor separations are very small (less than 1.5 m) .

Calculating pseudo decay (time) constants, for each station along the survey profiles, can provide additional information that is helpful to determine whether a multiple conductor situation exists. The pseudo decay constants can indicate the presence of multiple conductors even when the separation/depth ratio is less than unity.

Modelling the transient response of multiple conductors for a step-function time-domain electromagnetic system

deur

Francois Daniel Fourie

Studieleier : Prof WJ Botha
Departement : Geologie
Graad : Magister Scientiae in Eksplorasiegeofisika

SAMEVATTING

Die tydbestek elektromagnetiese responsie van veelvoudige geleiers in 'n weerstandbiedende omgewing word ondersoek deur van draadlusse in vrye ruimte gebruik te maak om geleidende plate te modelieer. Hierdie metode verskaf 'n relatief eenvoudige manier om die tydafhanklike effekte van twee nabyliggende geleiers op die gemete responsie te ondersoek.

Uit modelstudies blyk dit dat die responsie van 'n multigeleiersisteem nie die som van die twee individuele responsies is nie. Wanneer twee geleiers naby 'n senderlus voorkom, kan die invloed wat die twee geleiers op die totale gemete responsie het, veroorsaak dat die oplosvermoë negatief beïnvloed word. 'n Geleier tussen die senderlus en 'n tweede geleier veroorsaak dat die tweede geleier se teenwoordigheid uitgedoof word. Hierdie uitdowingseffek is veral groot wanneer die geleier wat nader aan die senderlus is 'n laer geleiding het as die ander geleier.

Wanneer daar met multigeleiermodelle gewerk word waar die geleiers geleidings van soortgelyke grootte het, moet die afstand wat die geleiers skei groter as hul dieptes wees indien beide geleiers opgelos moet word uit die elektromagnetiese profileringskurwes. Slegs wanneer die skeiding/diepte verhouding strewe na 2, kan daar met sekerheid vasgestel word dat daar twee geleiers teenwoordig is.

Wanneer daar groot verskille (in die orde van 'n paar tiendes van 'n Siemens) in die geleidings van die lusse bestaan, skuif die oorkruisingsposisies en die amplitudepieke van die profileringskurwes in die rigting van die sterker geleier. Hierdie waarneming word gemaak al is die skeiding tussen die geleiers baie klein (minder as 1.5 m).

Deur pseudo-vervalkonstantes te bereken vir elke posisie langs die traverse van die opname, kan addisionele inligting verkry word wat gebruik kan word om te bepaal of 'n multigeleiersisteem aanleiding gee tot die gemete responsie. Die pseudo-vervalkonstantes kan die teenwoordigheid van veelvoudige geleiers aandui selfs al is die skeiding/diepte verhouding kleiner as een.

ACKNOWLEDGEMENTS

I would like to express my gratitude to everybody that has contributed to my education in Physics, Geology and specifically in Exploration Geophysics.

Firstly I would like to thank my promoter, prof WJ Botha, who introduced me to this special intertwined branch of physics and geology, and kept my interests alive throughout my studies. Thanks also to prof PJ Hattingh for his part in my graduate studies. Dr EH Stettler and Mr A du Plooy contributed greatly to my understanding of the electromagnetic methods, and I would like to express my thanks to them. Jacques Markram's computer knowledge proved invaluable during the programming stages of this thesis.

Financial support for my post-graduate studies came from the Foundation for Research Development, and was much appreciated.

Thanks also to all my fellow students for hours of enlightening conversation (not necessarily on topics concerning Geophysics), and to Louise Claassen for providing inspiration when it was most needed.

Lastly, I would like to thank the genius of Led Zeppelin for providing me with the necessary relief at times when frustration was getting the upper hand.

INDEX

List of Figures and Tables

Figures

Tables

CHAPTER 1

INTRODUCTION

1.1 General

Since 1973 time domain electromagnetic (TDEM) methods have been widely used in mineral exploration. Transient systems have played a particularly important role in the search for base-metals. Their popularity is due to their greater depth of penetration as compared to frequency domain systems, as well as the ability to detect targets through conductive overburden (Telford et al, 1990).

In mineral exploration, TDEM systems, such as the GEONICS EM37 system, usually employ a large, stationary transmitter loop with a time-varying current. According to Faraday's law, the transient nature of the source current and associated source magnetic field causes eddy currents to flow in any nearby subsurface conductors. The induced currents decay with time constants that are dependent on the sizes, shapes and conductivities of the conductors (McNeill, 1980). Due to this dependance the time constants are said to be characteristic of the conductors. The decaying eddy currents give rise to decaying secondary electromagnetic fields that can be measured at any desired survey locations by means of an induction coil. The measured responses contain information about the subsurface positions, orientations, sizes, shapes and conductivity-thickness values of the conductors (Telford et al, 1990).

When two conductive plates occur close to one another in the earth, it is often not possible to resolve them individually from EM data alone. The observed cross-overs are displaced away from the actual locations of the sheets, and if the separation between the conductors is less than some minimum distance, the measured response is similar to that from a single conductor of thickness greater than that of either conductor (Telford et al, 1990).

In addition, two closely separated conductors will cause the measured EM response to differ from that which would be expected for two individual isolated conductors. A time varying current flowing in one conductor causes a transient magnetic induction field that induces an emf in the other conductor. This induced emf causes eddy currents to flow in the second conductor. The transient magnetic field associated with these eddy currents has a similar effect on the first conductor. Two conductors influencing each other in this fashion, are said to be coupled through mutual inductance. Due to this coupling the time constants for the decay of the secondary magnetic fields measured during an EM survey will differ from that expected for two uncoupled conductors.

There is a need to investigate the influence that two inductively coupled conductors have on one another and to determine the physical parameters that would allow two closely separated conductors to be resolved. An understanding of the mutual influences will help to avoid erroneous interpretation of conductor position, thickness and conductivity.

1.2 Objectives

This study aims at developing a modelling method that will provide qualitative information on the effects that two closely situated conductors in a resistive host rock have on the measured electromagnetic response. The modelling scheme must allow a great deal of flexibility as far as model parameters are concerned, to facilitate the modelling of a wide variety of geological occurences of sheet conductors. The modelling scheme can then be employed to adress questions such as:

- What is the measured response from two closely separated conductors?
- What should the minimum separation between two conductive plates be in order to resolve them both?
- What is the influence of different time constants on the measured anomaly?
- How should an EM survey be planned to achieve maximum resolution if the presence of multiple conductors are expected?

1.3 Previous Work

Due to their complex 3-dimensional nature, Maxwell's equations for the electric and magnetic field can be solved analytically for only a few simple conductivity distributions. It is therefore of great importance that efficient methods of modelling be developed and employed to gain insight into electromagnetic behaviour and to understand electromagnetic phenomena.

A great deal of numerical and scale modelling work has been done over the past thirty years. Constant progress is being made in obtaining faster and cheaper desktop digital computers, a process that is increasingly making the numerical modelling option more viable and less time consuming. Many modelling methods have yielded only limited successes due to the approximations that had to be made in employing them. The problem of numerical modelling is usually that of approximating the solution to Maxwell's equations when given a certain set of boundary conditions. Three methods have been widely employed to solve the differential equations:

1) finite element modeling (Coggon, 1971),
2) finite difference modeling (Lamontagne and West, 1971),
3) obtaining integral equation approximations (Hohmann, 1971).

In the early stages of numerical modelling, the 3-dimensional problem was reduced to two dimensions by considering conductors of infinite strike. By means of this simplification Maxwell's equations become scalar in two directions. Pioneers of this approach were Coggon (1971), using a finite element approach, Hohmann (1971), employing an integral equation method, and Swift (1971), working with a network solution.

Due to discrepancies between the results obtained from the various 2-dimensional methods, it became clear that a more realistic 3-dimensional approach had to be taken. Lamontagne and West (1971) described a finite difference technique to study the response of a thin plate conductor. Annan (1974) investigated a similar target by utilising an eigencurrent solution. Raiche (1974) and Hohmann (1975) also had some success in applying integral equation methods.

Best and Shammas (1976) used a 2-dimensional network solution in an attempt to model multiple conductors.

Pridmore (1978) modelled 3-dimensional electric and electromagnetic responses using a finite element method. Lee et al (1981) developed a hybrid 3-dimensional electromagnetic modeling scheme to compute the electromagnetic scattering of arbitrary local inhomogeneities in a uniform or two-layered earth. Pridmore et al (1981) investigated finite element modelling in 3 dimensions and found that one advantage of the 3-dimensional approach is that earths with arbitrary conductivity distributions can be modelled.

Goldman (1983) described the integral finite difference method for calculating transient electromagnetic fields in a horizontally stratified medium. Goldman and Stoyer (1983) calculated the transient field of an axially symmetric earth for vertical magnetic dipole excitation by using a finite difference approach. Wannamaker et al (1984) modelled the electromagnetic response of 3-dimensional bodies in layered earths using integral equations. A finite difference approach was used by Oristaglio and Hohmann (1984) to model the diffusion of electromagnetic fields into a 2-dimensional earth. Once again the infinite strike approximation was used. The rectangular source loop usually used in transient surveys, was approximated by considering the field due to two infinitely long line sources. Nabighian and Oristaglio (1984) showed that presenting a finite loop source by 2-dimensional line sources is an inaccurate approximation to make. They found a slower decay for infinite line sources. Best et al (1985) and SanFilipo and Hohmann (1985) used integral equation methods to model the electromagnetic response of 3-dimensional conductors in a layered earth, and a conductive half-space, respectively. SanFilipo et al (1985) described the effect of a conductive half-space on the electromagnetic response of a 3-dimensional body.

Adhidjaja et al (1985) reformulated the 2-dimensional finite difference approach of Oristaglio and Hohmann (1984) in terms of the secondary magnetic field, and found this approach to be roughly 5 times faster. Goldman et al (1986) studied the finite element solution for the transient electromagnetic response of arbitrary 2-dimensional resistivity distributions.

Leppin (1992) presented a 2.5-dimensional numerical method to model the response of 3-dimensional sources over 2-dimensional inhomogeneities.

Liu and Asten (1993) derived fast transient electromagnetic solutions for a thin plate conductive target, by approximating the target by a wire loop.

The electromagnetic response of thin sheets have been studied extensively.
Wesley (1958) found the response of an idealized dyke with infinite conductivity, vanishing thickness, infinite strike and semi-infinite depth extent. He extended his work to approximate the response from a geometrically thin dyke (Wesley (1958)). Lamontagne and West (1971) studied plate responses by means of a finite difference technique. Annan (1974) developed a method of finding the plate response by calculating a set of eigencurrents induced in the target conductor. Valleé (1981) approximated conductive plates by loops and found an exact solution to the multiple loop problem in terms of the mutual inductances between the loops. Weidelt (1983) calculated the harmonic and transient electromagnetic responses of a thin dipping dyke. He used the Wiener-Hopf technique to find the solution. Hanneson and West (1984) constructed a numerical method for calculating the electromagnetic induction response of a rectangular thin plate conductor in one stratum of a layered conductive half-space. Rai (1985) calculated the transient electromagnetic response of a thin conducting plate in a conducting host rock. Gallagher et al (1985) developed the computer program PLATE, which calculates the response from a sheet conductor with arbitrary conductance, dip, depth and size. The program employs the eigencurrent method developed by Annan. Smith and West (1987) studied electromagnetic induction in an inhomogeneous conductive sheet. Walker and West (1991) found a robust integral equation solution for electromagnetic scattering by a thin plate in conductive media. Hanneson (1992) developed an algorithm to calculate the transient electromagnetic response of a dipping plate in a conductive half-space.

1.4 Methodology

In Section 2.1 a description of the EM37 system and its operation is given. The time constant and its importance to a transient EM survey is briefly discussed in Section 2.2. The magnetic field of a current-carrying source loop in a whole space is calculated in Section 2.3. The results are used in the subsequent sections.

Chapter 3 forms the basis of this study. It deals with the modelling of conductive plates by making loop approximations. In Section 3.2 the magnetic field of a steady current carrying loop with arbitrary dip, strike and plunge is calculated. Section 3.3 states the 4-loop problem and gives the differential equations that describe current flow in the model loops. These differential equations are subsequently solved by making use of a method developed by Valleé (1981). Section 3.4 deals with the problem of calculating Self- and Mutual inductances.

A number of models are studied in Chapter 4. These model studies were done with a computer program that was developed by making use of loop approximations as discussed in the previous sections. Section 4.4.3 investigates the influence that two closely separated conductors with different conductivities have on the measured decay. In this section a pseudo decay constant is defined that proves to be helpful when trying to determine whether a multiple conductor situation exists.

In Chapter 5 the results from model studies are summarized and conclusions are drawn.

CHAPTER 2

BASIC THEORY

2.1 Field procedure

The EM37 system is a ground time-domain electromagnetic system utilising a step-function current waveform, manufactured by Geonics Ltd of Mississauga, Ontario, Canada. In the profiling mode (TURAM-type operation), it consists of a large transmitter loop, typically 300X600 m, and a small, mobile receiver loop. The source loop is laid out in the vicinity of the area under investigation, with the long edge parallel to the geological strike, if it is known. Surveying takes place at stations on traverses that are perpendicular to the long sides of the source loop. These traverses can extend to either side and go through the source loop. Figure 2.1 shows the survey configuration.

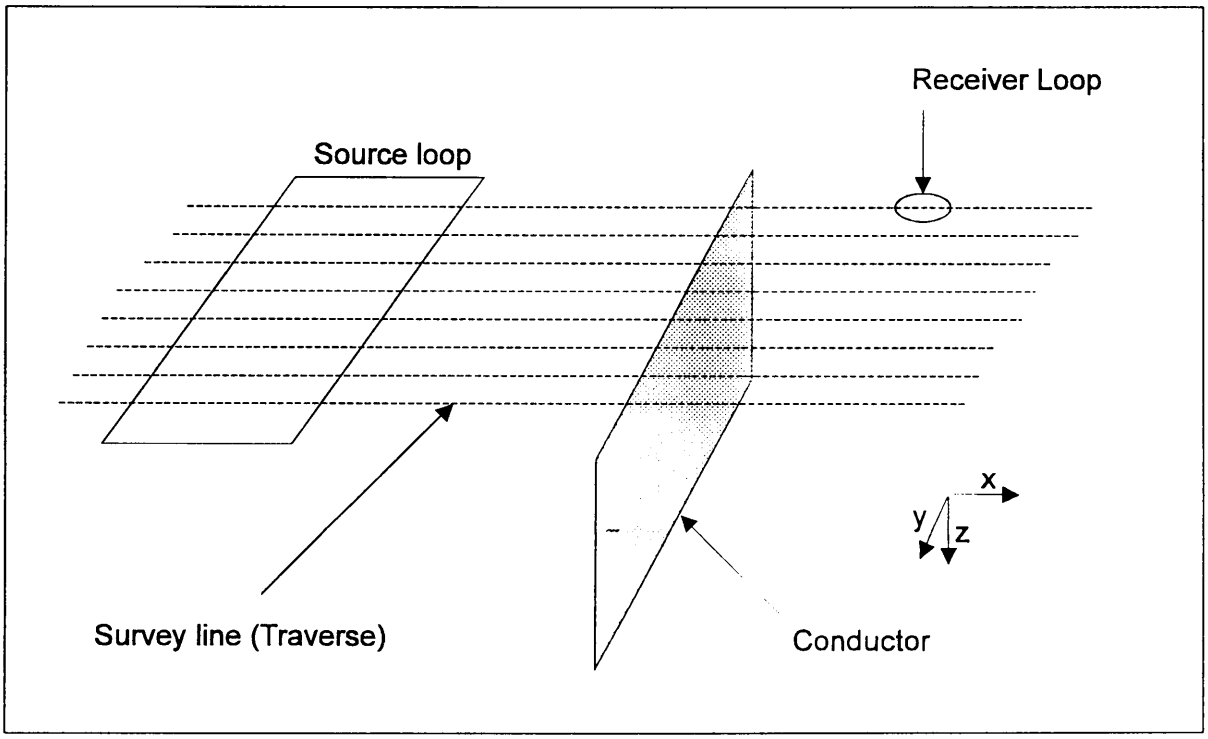

Figure 2.1: *Schematic presentation of a typical transient profiling survey setup.*

The current waveform in the source loop is shown in Figure 2.2. It consists of alternating bipolar current pulses with slow exponential turn-on and rapid linear turn-off. Due to the abruptness of the turn-off, the GEONICS EM37 system measures the impulse response of the earth. According to Faraday's law (see Section 2.3.2., equation 2.10), the abrupt changes in source current and source magnetic field (primary field) induce current flow (eddy currents) in the target conductors. The decay of these eddy currents, and the secondary magnetic fields associated with them, is a sum of exponentials (Gallagher et al,1985). The late time decay is a pure exponential decay with a decay constant that is determined by the size, shape and conductivity of the conductor. Because of this relation between conductor parameters and decay constants, the decay constants are said to characterize the conductors. The time-rates of change of the secondary magnetic fields are now measured by the receiver coil at 20 preset time intervals (channels). Three spatial components of the changing field can be measured by varying the receiver loop orientation. Conventionaliy these are the z-component, which is the vertical component, the x-component, which is parallel to the survey line, and the y-component, which is perpendicular to the survey line.

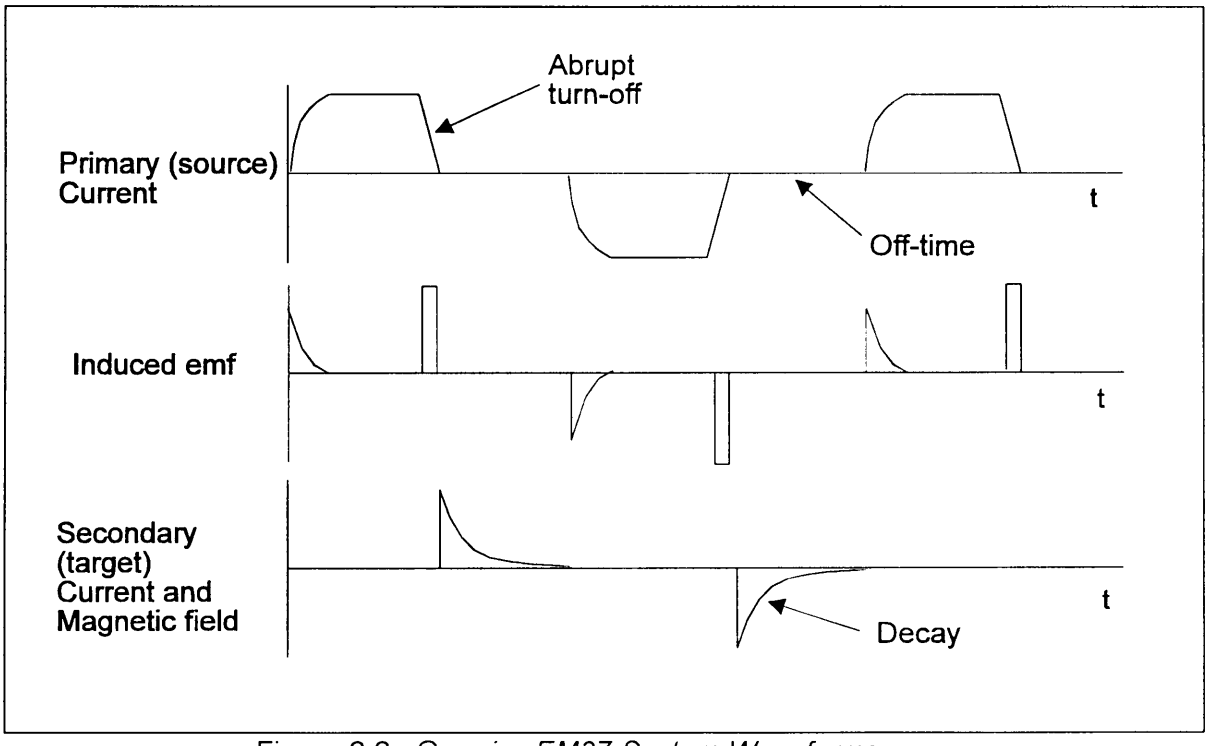

Figure 2.2: *Geonics EM37 System Waveforms.*

Measurements are only made during 'off' times. The time channels are separated on a logarithmic scale. The base frequency for the alternating source current can be set at 2.5, 7.5 or 25 Hz. With a choice of 25 Hz the off-time window has a maximum size of 8 ms. Table 2.1 gives the centres of the different time channels with this choice of base frequency.

CHANNEL	Time (ms)	CHANNEL	Time (ms)
1	0.089	11	0.881
2	0.100	12	1.096
3	0.140	13	1.411
4	0.177	14	1.795
5	0.220	15	2.224
6	0.280	16	2.850
7	0.355	17	3.600
8	0.443	18	4.490
9	0.564	19	5.700
10	0.713	20	7.190

Table 2.1: *The time gates of the Geonics EM37 operating at 25 Hz.*

2.2 The time constant

The late time dependence of the induced eddy currents and associated secondary magnetic fields on the time (decay) constant, can be expressed as follows (McNeill, 1980):

$$\mathbf{I}(t) \propto e^{-t/\tau}$$
$$\mathbf{B}(t) \propto e^{-t/\tau} \qquad (2.1)$$

with τ the time constant. Since the time rate of change of the secondary magnetic field is the quantity that is measured by the Geonics EM37 system, the response will be of the form:

$$\frac{d\mathbf{B}}{dt} \propto \frac{1}{\tau} e^{-t/\tau} \qquad (2.2)$$

This inverse relation of the response to the time constant is a constraint on the system. The time constant is directly proportional to the conductivity of the conductor. Therefore the initial response (early channels) of a good conductor is smaller than that of a poor conductor, but will decay less rapidly in time. Good conductors are often the targets of a time-domain EM survey, and have responses that show up only on the later channels, while the presence of poorer conductors will dominate the early channels.

2.3 The Magnetic field associated with a current carrying loop in a whole-space

2.3.1 The Law of Biot-Savart

The law of Biot-Savart describes the magnetic field of a long wire carrying a steady or slowly varying current. In differential form it is given as:

$$\mathbf{dB} = \mu_0 \frac{\mathbf{I}\mathbf{dl} \times \hat{\mathbf{r}}}{4\pi r^2} \qquad (2.3)$$

Through integration an expression for the magnetic field of an infinitely long wire source lying in the y-direction can be found (see Appendix A):

$$\mathbf{B}(x,z) = \frac{\mu_0 \mathbf{I}}{2\pi\rho^2}\left[z\mathbf{u}_x - x\mathbf{u}_z\right] \qquad (2.4)$$

with $\rho^2 = x^2 + z^2$, and $\mathbf{u}_x$ and $\mathbf{u}_z$ unit vectors pointing in the x and z directions respectively.

2.3.2 Electromagnetic induction

The magnetic flux through a surface S enclosed by a circuit is defined as:

$$\Phi = \int_S \mathbf{B} \bullet \mathbf{dA} \tag{2.5}$$

and is measured in webers (Wb). When the magnetic flux changes with time, an emf is induced in the circuit. From experiments this emf (ε) is found to be:

$$\varepsilon = -\frac{d\Phi}{dt} \tag{2.6}$$

The emf is furthermore defined in terms of the electric field $\mathbf{E}$ as:

$$\varepsilon = \oint_C \mathbf{E} \bullet \mathbf{dl} \tag{2.7}$$

where $\mathbf{dl}$ is a line element of the closed circuit C. Thus, from equations 2.5, 2.6 and 2.7 we get:

$$\oint_C \mathbf{E} \bullet \mathbf{dl} = -\frac{d}{dt}\iint_S \mathbf{B} \bullet \mathbf{dA} \tag{2.8}$$

If the circuit is rigid and stationary, the time derivative can be taken inside the integral. Stoke's theorem allows us to write the line integral of $\mathbf{E}$ into the surface integral of $\nabla \times \mathbf{E}$:

$$\iint_S (\nabla \times \mathbf{E}) \bullet \mathbf{dA} = -\iint_S \frac{d\mathbf{B}}{dt} \bullet \mathbf{dA} \tag{2.9}$$

This must hold true for all surfaces S, so that it follows:

$$\nabla \times \mathbf{E} = -\frac{d\mathbf{B}}{dt} \qquad (2.10)$$

which is the differential form of Faraday's law, and one of the four Maxwell equations.

Faraday's law states that a change in the magnetic field induces an electric field (and emf) that opposes the change that produces it.

2.3.3 The Transient Magnetic Response of a Line Source

Ward and Hohmann (1988) derived an expression for the transient magnetic response of a line source in a whole-space with conductivity σ, carrying a step current (going from an initial value of zero to a final value of I ampéres):

$$\mathbf{B} = \frac{\mu_0 I}{2\pi\rho^2}\left[z\mathbf{u}_x - x\mathbf{u}_z\right]e^{-\theta^2\rho^2} \qquad (2.11)$$

with

$$\theta^2 = \frac{\mu_0\sigma}{4t} \qquad (2.12)$$

Equation 2.11 is seen to be similar to that of a infinite line source with a steady current (eq 2.4), but contains an extra exponential term which describes the bounded exponential growth with time after turn-on.

2.3.4 The Transient Magnetic Response of a Rectangular Loop

By using Biot-Savart's law, it is possible to calculate the magnetic field of a line source of finite length (see Appendix A). When a rectangular source loop is viewed as consisting of 4 line sources, the field of this loop can now easily be calculated. For a loop lying in the xy-plane with the long sides (length a) lying in the y-direction,

and short sides (length b) in the x-direction, we find the three components of the magnetic field to be:

$$B_x(\mathbf{r}) = \frac{\mu_0 Iz}{4\pi}\left[\frac{1}{\rho_{xz1}^{\ 2}}\left(\frac{y_{d2}}{R_2} - \frac{y_{d1}}{R_1}\right) - \frac{1}{\rho_{xz2}^{\ 2}}\left(\frac{y_{d2}}{R_4} - \frac{y_{d1}}{R_3}\right)\right] \tag{2.13a}$$

$$B_y(\mathbf{r}) = \frac{-\mu_0 Iz}{4\pi}\left[\frac{1}{\rho_{yz1}^{\ 2}}\left(\frac{x_{d2}}{R_3} - \frac{x_{d1}}{R_1}\right) - \frac{1}{\rho_{yz2}^{\ 2}}\left(\frac{x_{d2}}{R_4} - \frac{x_{d1}}{R_2}\right)\right] \tag{2.13b}$$

$$\begin{aligned} B_z(\mathbf{r}) = \frac{-\mu_0 I}{4\pi}\Bigg[&\frac{x_{d1}}{\rho_{xz1}^{\ 2}}\left(\frac{y_{d2}}{R_2} - \frac{y_{d1}}{R_1}\right) - \frac{x_{d2}}{\rho_{xz2}^{\ 2}}\left(\frac{y_{d2}}{R_4} - \frac{y_{d1}}{R_3}\right) \\ &+ \frac{y_{d1}}{\rho_{yz1}^{\ 2}}\left(\frac{x_{d2}}{R_3} - \frac{x_{d1}}{R_1}\right) - \frac{y_{d2}}{\rho_{yz2}^{\ 2}}\left(\frac{x_{d2}}{R_4} - \frac{x_{d1}}{R_2}\right)\Bigg] \end{aligned} \tag{2.13c}$$

The symbols in these expressions are explained in Figure 2.3. In a similar way the transient magnetic field due to a loop carrying a step current can be found by using equation 2.11 and integrating over the sides of the loops. Equation 2.11 describes the magnetic field caused by a current that instantaneously increases from zero to a maximum value of I ampéres. The abrupt turn-off of the current in the source loop of the Geonics EM37 is an approximation to an instantaneous step in the source current, going from an initial value of I to a final value of zero ampéres. Keeping this in mind, we find the following expressions for the components of the transient magnetic field:

$$B_x(\mathbf{r},t) = \frac{\mu_0 Iz}{4\pi}\left[\frac{1}{\rho_{xz1}^{\ 2}}\left(\frac{y_{d2}}{R_2} - \frac{y_{d1}}{R_1}\right)\left(1 - e^{-\theta^2\rho_{xz1}^{\ 2}}\right) - \frac{1}{\rho_{xz2}^{\ 2}}\left(\frac{y_{d2}}{R_4} - \frac{y_{d1}}{R_3}\right)\left(1 - e^{-\theta^2\rho_{xz2}^{\ 2}}\right)\right]$$

(2.14a)

$$B_y(\mathbf{r},t) = \frac{-\mu_0 Iz}{4\pi}\left[\frac{1}{\rho_{yz1}^{\ 2}}\left(\frac{x_{d2}}{R_3} - \frac{x_{d1}}{R_1}\right)\left(1 - e^{-\theta^2\rho_{yz1}^{\ 2}}\right) - \frac{1}{\rho_{xz2}^{\ 2}}\left(\frac{x_{d2}}{R_4} - \frac{x_{d1}}{R_2}\right)\left(1 - e^{-\theta^2\rho_{yz2}^{\ 2}}\right)\right]$$

(2.14b)

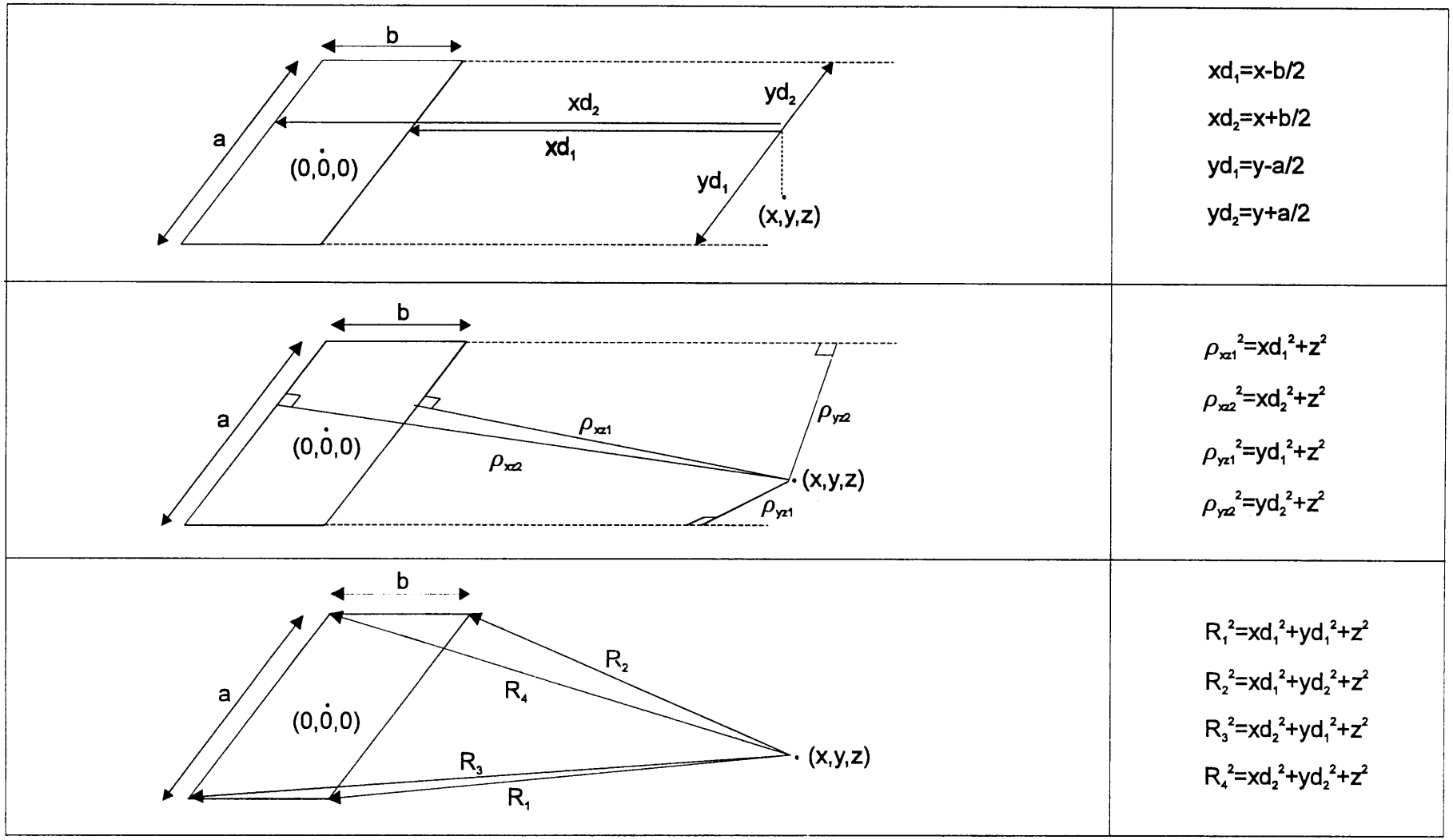

Figure 2.3.: *Schematic representation of a loop to explain the symbols in equations 2.13*

$$B_z(\mathbf{r},t) = \frac{-\mu_0 I}{4\pi}\left[\frac{x_{d1}}{\rho_{xz1}^{\ 2}}\left(\frac{y_{d2}}{R_2}-\frac{y_{d1}}{R_1}\right)\left(1-e^{-\theta^2\rho_{xz1}^{\ 2}}\right)-\frac{x_{d2}}{\rho_{xz2}^{\ 2}}\left(\frac{y_{d2}}{R_4}-\frac{y_{d1}}{R_3}\right)\left(1-e^{-\theta^2\rho_{xz2}^{\ 2}}\right)\right.$$
$$\left.+\frac{y_{d1}}{\rho_{yz1}^{\ 2}}\left(\frac{x_{d2}}{R_3}-\frac{x_{d1}}{R_1}\right)\left(1-e^{-\theta^2\rho_{yz1}^{\ 2}}\right)-\frac{y_{d2}}{\rho_{xz2}^{\ 2}}\left(\frac{x_{d2}}{R_4}-\frac{x_{d1}}{R_2}\right)\left(1-e^{-\theta^2\rho_{yz2}^{\ 2}}\right)\right] \quad (2.14c)$$

with $\theta^2 = \frac{\mu_0\sigma}{4t}$. These equations allow us to easily calculate the transient magnetic field at any location within a three-dimensional whole-space. As an example Figure 2.4 shows the magnitude of the transient magnetic field as measured at a distance of 400 m from the centre of an 800 by 400m loop lying in the xy-plane, and at a depth of 400 m as measured from the xy-plane.

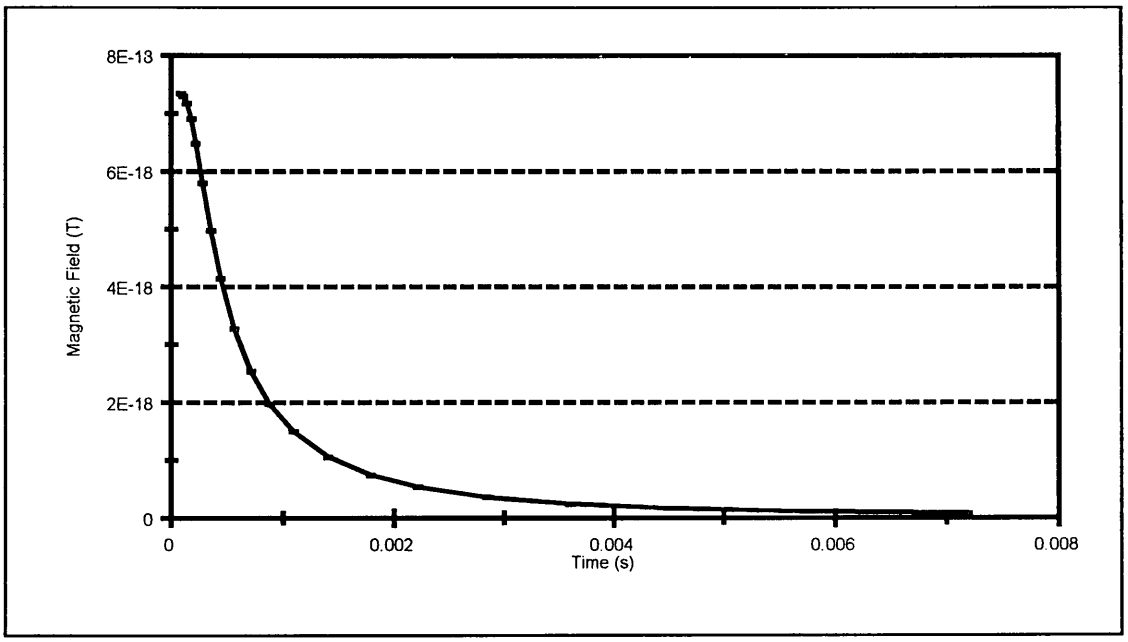

Figure 2.4: *Example of transient magnetic field calculations by making use of equations 2.14. The field due to an 800 by 400 m rectangular loop, carrying a step current with turn-on value of 20A, was calculated at a position 400m away from the loop centre and at a depth of 400m as measured from the xy-plane, for an earth with a conductivity of 0.01 S/m.*

CHAPTER 3

MODELLING CONDUCTIVE PLATES BY LOOPS

3.1 Introduction

Using loops to approximate the transient response of conductive plates is an over-simplification of the problem, especially when working with multiple conductors. Liu and Asten (1993) used this approach to find approximate solutions to the transient EM response of a thin-plate conductor. They made the assumption that the plate can be represented by a singular rectangular wire loop with dimensions 70% of the plate size. McNeill (1982) showed that this assumption is valid at late times when the observation point is at some distance away from the target.

When the multiple conductor problem is considered, it is often desirable to study the interaction of two closely separated shallow conductors, and the loop approximation therefore introduces problems. Valleé (1981) also states that the coupling between two plates is much stronger and more complex than the coupling between two loops.

In modelling thin plates by wire loops, the finite thickness of the plate is ignored. The conductivity-thickness product (conductance), which is a diagnostic parameter in EM interpretation (Telford et al,1990), therefore has no physical meaning when dealing with wire loops. The conductance thus needs to be calculated in a different manner.

Despite all the mentioned problems, the loop approach does provide a relatively simple way of qualitatively modelling the response from plate conductors in a resistive host rock. It also allows easy computation of the coupling between arbitrarily orientated conductors.

Modelling plates by loops enables us to gain insight into the effects that multiple conductors have on the measured transient EM response. It is therefore of great heuristic value.

3.2 The magnetic field of a loop with arbitrary dip, strike, and plunge

Equations 2.13 give the three components of the magnetic field from a steady current-carrying loop lying in the xy-plane. With the xy-plane the reference plane and the z-direction pointing downwards, the rotational parameters dip, strike, and plunge, can be introduced. Taking positive dip as a rotation θ of the loop from the x-axis in the direction of the z-axis (see Figure 3.1), the magnetic field at a position $\mathbf{r}_{dip}$ relative to the centre of the dipping loop can be calculated as follows:

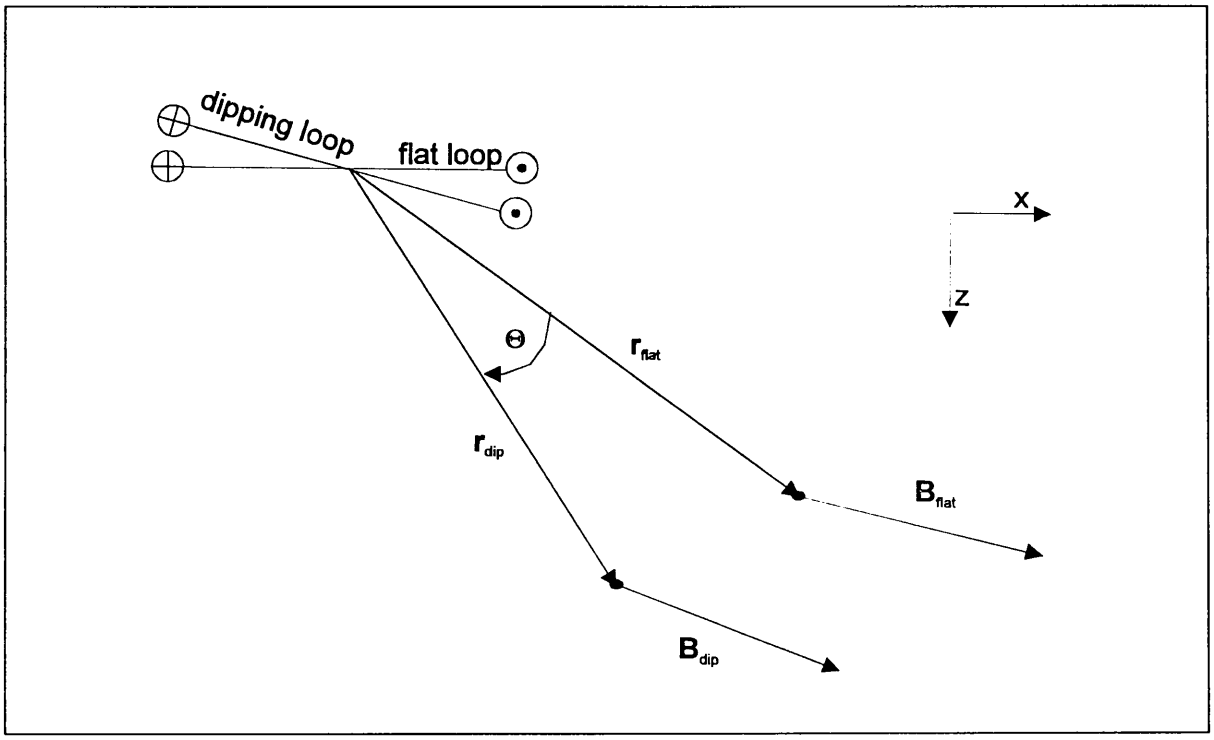

Figure 3.1: *Calculating the magnetic field of a dipping loop.*

1. find the position $\mathbf{r}_{flat}$ which has the same position relative to a similar loop lying in the xy-plane,
2. apply equations 2.13 to calculate the field at the position $\mathbf{r}_{flat}$,
3. rotate the calculated field according to the dip of the loop.

The processes described above can be represented mathematically as follows:

1. Since $\mathbf{r}_{dip}$ is just a rotation of the vector $\mathbf{r}_{flat}$, we have:

$$\mathbf{r}_{dip} = [\mathbf{ROT}] \bullet \mathbf{r}_{flat} \tag{3.1}$$

with $[\mathbf{ROT}]$ being a rotational matrix containing the dip (θ) of the loop.

Therefore $\mathbf{r}_{flat}$ can be found from:

$$\mathbf{r}_{flat} = [\mathbf{ROT}]^{-1} \bullet \mathbf{r}_{dip} \tag{3.2}$$

2. The magnetic field $\mathbf{B}_{flat}(\mathbf{r}_{flat})$ is calculated by using equations 2.13.
3. The calculated field is rotated:

$$\begin{aligned} \mathbf{B}_{dip}(\mathbf{r}_{dip}) &= [\mathbf{ROT}] \bullet \mathbf{B}_{flat}(\mathbf{r}_{flat}) \\ &= [\mathbf{ROT}] \bullet \mathbf{B}_{flat}\left([\mathbf{ROT}]^{-1} \bullet \mathbf{r}_{dip}\right) \end{aligned} \tag{3.3}$$

For this case in which the loop is only rotated according to dip, the rotational matrix is simply given by:

$$[\mathbf{ROT}] = \begin{bmatrix} \cos\theta & 0 & -\sin\theta \\ 0 & 1 & 0 \\ \sin\theta & 0 & \cos\theta \end{bmatrix} \tag{3.4}$$

Defining strike as a rotation ϕ of the loop from the y-axis in the direction of the z-axis, and plunge as a rotation γ from the x-axis in the direction of the y-axis, we can calculate the magnetic field from a dipping, striking and plunging loop from:

$$\begin{aligned} \mathbf{B}_{dip,strike,plunge}(\mathbf{r}_{dip,strike,plunge}) &= [\mathbf{ROT}] \bullet \mathbf{B}_{flat}(\mathbf{r}_{flat}) \\ &= [\mathbf{ROT}] \bullet \mathbf{B}_{flat}\left([\mathbf{ROT}]^{-1} \bullet \mathbf{r}_{dip,strike,plunge}\right) \end{aligned} \tag{3.5}$$

with

$$[\mathbf{ROT}] = \underbrace{\begin{bmatrix} \cos\theta & 0 & -\sin\theta \\ 0 & 1 & 0 \\ \sin\theta & 0 & \cos\theta \end{bmatrix}}_{\text{dip}} \underbrace{\begin{bmatrix} 1 & 0 & 0 \\ 0 & \cos\phi & -\sin\phi \\ 0 & \sin\phi & \cos\phi \end{bmatrix}}_{\text{strike}} \underbrace{\begin{bmatrix} \cos\gamma & -\sin\gamma & 0 \\ \sin\gamma & \cos\gamma & 0 \\ 0 & 0 & 1 \end{bmatrix}}_{\text{plunge}}$$

$$= \begin{bmatrix} \cos\theta\cos\gamma & -\cos\theta\cos\phi\sin\gamma - \sin\theta\sin\phi & \cos\theta\sin\phi\sin\gamma - \sin\theta\cos\phi \\ \sin\gamma & \cos\phi\cos\gamma & -\sin\phi\cos\gamma \\ \sin\theta\cos\gamma & -\sin\theta\cos\phi\sin\gamma + \cos\theta\sin\phi & \sin\theta\sin\phi\sin\gamma + \cos\theta\cos\phi \end{bmatrix} \quad (3.6)$$

3.3 The 4-loop problem and its solution

In modelling two conductive plates in a resistive host rock by loops in free space, we encounter the problem of 4 inductively coupled loops: the source and receiver loops, and the two model loops. Each loop has its own resistance (R) and inductance (L). Figure 3.2 shows the situation schematically.

The differential equations that govern the flow of currents in the two model loops (loops 1 and 2) follow from circuit theory, and are given by:

$$-R_1 i_1 - L_1 i_1' - M_{12} i_2' - M_{01} i_0' = 0 \quad (3.7a)$$

$$-R_2 i_2 - L_2 i_2' - M_{21} i_1' - M_{02} i_0' = 0 \quad (3.7b)$$

with i_1 and i_2 the currents flowing in the loops, and i_1' and i_2' their time derivatives. In these equations M_{ij} indicates the mutual inductance between loop i and loop j. Section 3.4 deals with the calculation of mutual inductances.

Valleé (1981) solved these equations for the UTEM transient system with its triangular source (primary) current. He found the solution by employing Laplace Transforms. The expression he found for the time derivatives of the currents flowing in the model loops are:

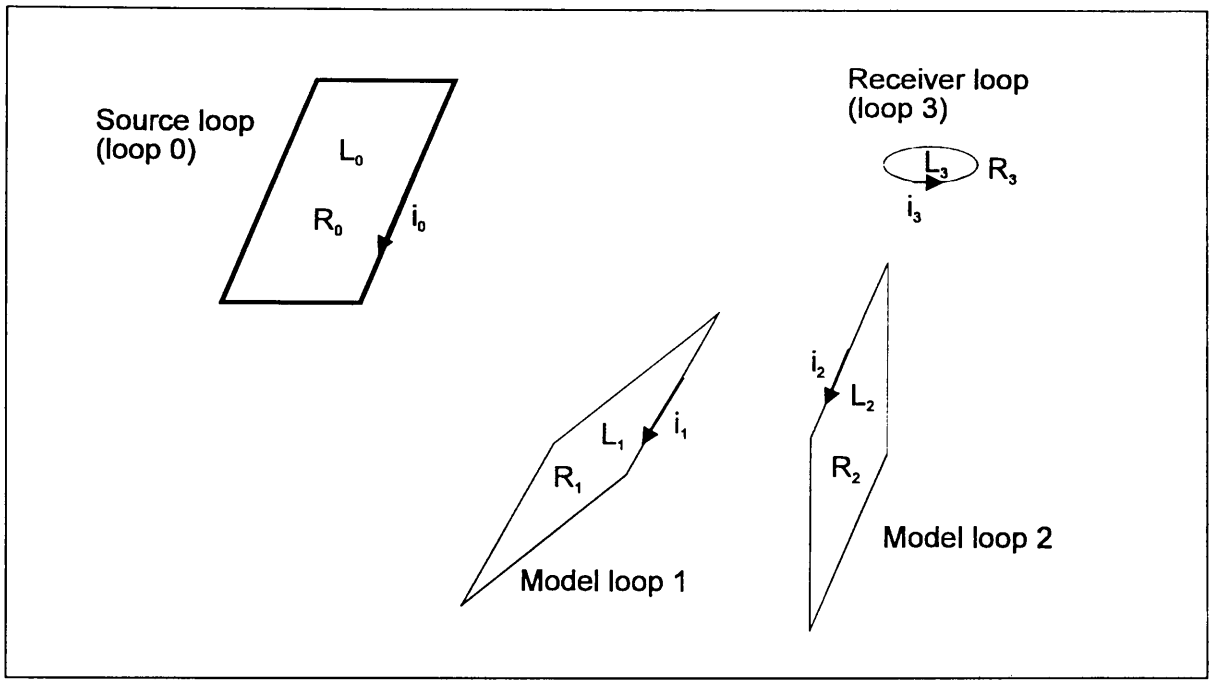

Figure 3.2 *:Schematic presentation of the 4-loop problem.*

$$i_1'(t) = -\frac{M_{01}}{L_1\left(1-k_{12}^2\right)(t_1-t_2)}\left[t_2\left(\frac{t_1}{\tau_2}-\frac{k_{01}-k_{02}k_{12}}{k_{01}}\right)e^{-\frac{t}{t_1}} - t_1\left(\frac{t_2}{\tau_2}-\frac{k_{01}-k_{02}k_{12}}{k_{01}}\right)e^{-\frac{t}{t_2}}\right] \tag{3.8a}$$

and

$$i_2'(t) = -\frac{M_{02}}{L_2\left(1-k_{12}^2\right)(t_1-t_2)}\left[t_2\left(\frac{t_1}{\tau_1}-\frac{k_{02}-k_{01}k_{12}}{k_{02}}\right)e^{-\frac{t}{t_1}} - t_1\left(\frac{t_2}{\tau_1}-\frac{k_{02}-k_{01}k_{12}}{k_{02}}\right)e^{-\frac{t}{t_2}}\right] \tag{3.8b}$$

with

$$t_1, t_2 = \frac{(\tau_1+\tau_2) \pm \sqrt{(\tau_1+\tau_2)^2 - 4\tau_1\tau_2\left(1-k_{12}^2\right)}}{2}, \tag{3.9}$$

$$k_{ij} = \frac{M_{ij}}{\sqrt{L_i L_j}} \tag{3.10}$$

and

$$\tau_i = \frac{L_i}{R_i} \tag{3.11}$$

t_1 and t_2 are the coupled decay constants of the loops, while k_{ij} and τ_i respectively give the coupling coefficients between loops i and j, and the uncoupled time constant of loop i. The emf induced in the receiver loop follows from circuit theory, and is given by:

$$\begin{aligned} \varepsilon_{\text{receiver}} &= -\left(\frac{d\Phi_{13}}{dt} + \frac{d\Phi_{23}}{dt}\right) \\ &= -\left(M_{13}i_1' + M_{23}i_2'\right) \end{aligned} \tag{3.12}$$

with Φ_{ij} the magnetic flux through loop i due to the magnetic field caused by the current flowing in loop j.

Systems that measure the impulse response of the earth have source currents that ideally make instantaneous steps. A step current is the time derivative of a triangular current. Valleé (1981) stated that, for this reason, the impulse response of the earth can be found by taking the time derivative of the response from a triangular source current. For a system sampling the impulse response of the ground, the emf induced in the receiver loop is found to be:

$$\begin{aligned} \varepsilon_{\text{receiver}} = -\frac{M_{03}}{k_{03}\left(1-k_{12}^2\right)\left(t_1-t_2\right)}\Bigg[& k_{01}k_{13}\left\{\frac{t_2}{t_1}\left[\frac{t_1}{\tau_2} - \left(\frac{k_{01}-k_{02}k_{12}}{k_{01}}\right)\right]e^{-\frac{t}{t_1}}\right. \\ & \left. - \frac{t_1}{t_2}\left[\frac{t_2}{\tau_2} - \left(\frac{k_{01}-k_{02}k_{12}}{k_{01}}\right)\right]e^{-\frac{t}{t_2}}\right\} \\ & + k_{02}k_{23}\left\{\frac{t_2}{t_1}\left[\frac{t_1}{\tau_1} - \left(\frac{k_{02}-k_{01}k_{12}}{k_{02}}\right)\right]e^{-\frac{t}{t_1}}\right. \\ & \left. - \frac{t_1}{t_2}\left[\frac{t_2}{\tau_1} - \left(\frac{k_{02}-k_{01}k_{12}}{k_{02}}\right)\right]e^{-\frac{t}{t_2}}\right\} \Bigg] \end{aligned} \tag{3.13}$$

Problems arise when $t_1=t_2$. This happens only when $k_{12}=0$ and $\tau_1 = \tau_2$. It is interesting to note the case where the coupling coefficient (k_{12}) between the model loops 1 and 2 is zero. This corresponds to the unrealistic case where the model loops are not inductively coupled. From equation 3.9 we see that $t_1 = \tau_1$ and $t_2 = \tau_2$. That is, the time constants are equal to their uncoupled values. The expression for the emf induced in the receiver coil reduces to:

$$\varepsilon_{\text{receiver}} = -\frac{M_{03}}{k_{03}}\left[k_{01}k_{13}\frac{1}{\tau_1}e^{-\frac{t}{\tau_1}} + k_{02}k_{23}\frac{1}{\tau_2}e^{-\frac{t}{\tau_2}}\right] \qquad (3.14)$$

This expression is the sum of the two individual responses of the loops and is of the same form as equation 2.2.

3.4 Numerical Calculation of Mutual- and Self-Inductances

The self-inductance (L) of a circuit is a constant that describes the relation between current flowing in the circuit and the magnetic flux through the circuit due to the current. Likewise, the mutual inductance (M_{ab}) between two circuits gives the dependance of the magnetic flux through loop a on the current flowing in loop b. When the circuits are simple loops, the inductances can be expressed as:

$$L_a = \frac{\Phi_{aa}}{i_a}$$
$$M_{ab} = \frac{\Phi_{ab}}{i_b} \qquad (3.15)$$

Figure 3.3 shows two simple loops with arbitrary orientations in 3-D. Loop b is carrying a constant current of i_b ampéres.

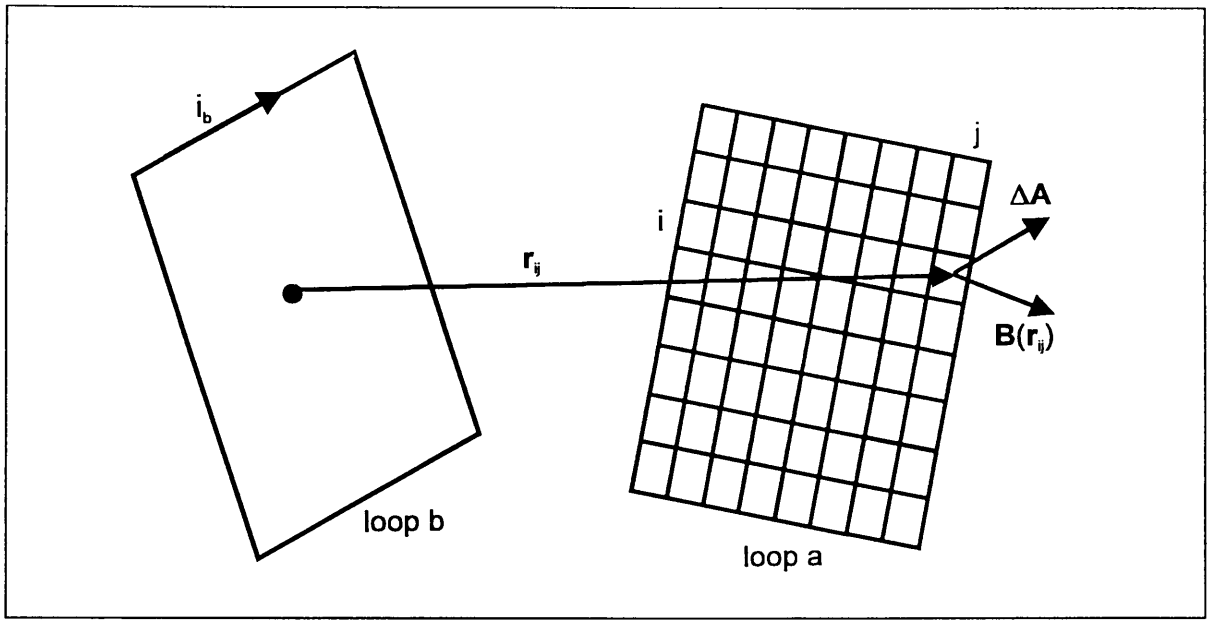

Figure 3.3: *Calculating Mutual- and Self-inductances.*

Using the expression for the magnetic field of a loop with dip, strike, and plunge (equations 3.5 and 3.6), the mutual inductance between loop a and loop b can be calculated through numerical integration as follows:

1) Divide the area enclosed by loop a into $M \times N$ equal areas ΔA. All of these areas will have the same area vector $\Delta \mathbf{A}$.

2) The magnetic flux through one of these areas can be approximated from:

$$\Delta\Phi_{ij} = \mathbf{B}\left(\mathbf{r}_{ij}\right) \bullet \Delta\mathbf{A} \qquad (3.16)$$

with $\mathbf{r}_{ij}$ the position vector from the centre of loop b to the centre of the area ΔA_{ij}.

3) The total magnetic flux is just the sum of the fluxes through all such areas:

$$\Phi_{ab} = \sum_{i}\sum_{j} \Delta\Phi_{ij} \qquad (3.17)$$

4) Use equation 3.15 to find the mutual inductance.

The self-inductance of a loop is found in a similar way, by numerically calculating the flux through the loop due to a current flowing in itself.

CHAPTER 4

MODEL INVESTIGATIONS

4.1 Aim of investigations

In this chapter a number of models are examined by making use of a computer program that was developed to model the response from multiple conductive sheets by considering the response from inductively coupled wire loops, as was discussed in Chapter 3. The investigations concentrate on the resolvability of multiple conductors and study the parameters that influence this resolvability. The ways in which conductor separation and dip affect the resolvability are examined. The mutual influence that exists between conductors is also considered, since it can have a great impact on the resolvabilty.

The results of the model investigations are discussed in Section 4.4. The figures with the model results are numbered Figure M1 through Figure M14 and appear at the end of Chapter 4.

4.2 Model Considerations

The late-time decay constant measured during a TDEM survey over a finite conductor, is a function of the conductor parameters, and is directly proportional to the conductivity-thickness of the target. For a 2-D conducting plate of finite depth extent, it is given by (Nabighian and Macnae (1991) after Khomenyuk (1963)):

$$\tau = \frac{2(t\sigma)\mu_0 l}{\pi^2} = \frac{2S\mu_0 l}{\pi^2} \qquad (4.1)$$

with l the depth extent, t the thickness and S the conductivity-thickness product, or conductance.

A thin sheet conductor can be modelled using a wire loop of resistance R ohm, with a self-inductance of L henry. The decay constant for such a loop is given by equation 3.11:

$$\tau = \frac{L}{R}$$

that is

$$\tau = LS \qquad (4.2)$$

with S the conductance and L the inductance of the loop. Since the inductance of a loop is dependant on its size, the decay constant will also be a function of loop size.

4.3 Model description

Some parameters of the models studied in this chapter are shown in Figure 4.1. The source loop has dimensions 800 by 400m with the long axis of the loop lying in the y-direction, and the short axis in the x-direction. The origin of the coordinate system is taken at the centre of the source loop. Profiling traverses go through the centre of the loop.

The model loops have sizes of 400 by 400 m. A square loop of this size has a self-inductances of around 0.001 henry. The decay constants for targets of interest vary between 0.5 and 20 ms (Nabighian and Macnae, 1991). From equation 4.2 it follows that the loop conductances must vary between 0.5 and 20 S (siemens) to represent geological targets and be less than 0.5 S when modelling conductors of average to low conductivity. The strike and plunge of the model loops are taken as 90^0 and 0^0 respectively, for all the models .

The amplitude of the source current has a maximum value of 20A in all the models.

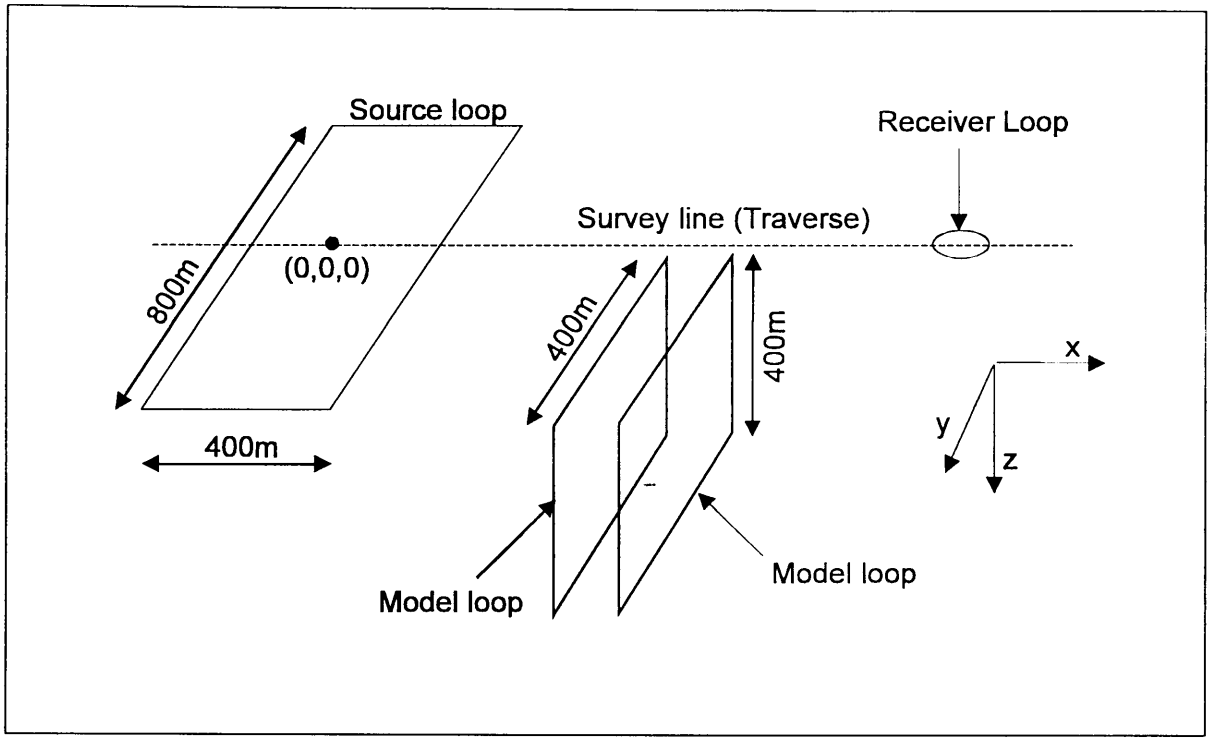

Figure 4.1: *Description of model parameters.*

4.4 Model results

Model investigation was done on a 486 Dx personal computer running at 66MHz with 16 MB of RAM. The software was developed in Turbo C++. A listing of the modelling program is given in Appendix B. When numerical integration was done, the loop areas were divided into 50 by 50 smaller areas. With this choice of subdivision the program took approximately 4 seconds to run a model.

4.4.1 Masking

Valleé (1981) studied the response of multiple conductors through scale modelling. He found that a weak conductor situated between the transmitter loop and a good conductor, blanks the early time response of the good conductor.

To investigate this phenomenon numerically, the coupled and uncoupled responses of multiple conductors (equations 3.13 and 3.14, respectively,) were compared. Figure M1 shows the results of a model with two loops of moderate conductances.

Only the vertical measurements of the emf's (proportional to $\frac{dB_z}{dt}$) are shown. The masking effect of loop 1 on the response of loop 2 is quite apparent.

When a weak conductor is placed between the source loop and a good conductor (Figure M2), the presence of the good conductor only becomes clear at later channels. This is in accordance with Valleé's scale model results.

A good conductor between the source and a bad conductor has a detrimental effect on the responses from both conductors (Figure M3), but the masking effect is not nearly as severe as when the weak conductor is closer to the source loop.

Masking has a similar effect on the measured response when the conductors have dips that are less than 90°. Figure M4 shows the results of a model study in which the model loops have dips of 70°. Once again the presence of the weaker conductor, situated between the source loop and the better conductor, blanks out the early time response of this conductor.

4.4.2 Conductor separation

When two conductors occur too close to one another, it is often not possible to resolve them from EM data alone. Conductor depth plays an important role in determining the minimum separation that will allow both conductors to be recognised.

As was shown in Section 4.4.1, masking can seriously affect resolvability, and its effects have to be taken into account. In this section two different cases of sheet conductor occurences are discussed. Firstly the case where the conductors have conductances of similar magnitudes is studied. The effects of masking is much less severe in this case. Secondly we deal with the presence of a poor and a good conductor and examine the combined effects of masking and conductor separation on the resolvability.

Figure M5a shows two conductors at a depth of 40m and at a separation of 40m. The conductors have conductances of 0.5S and 0.4S. The measured response looks similar to the response one would expect from a single conductor. Note how

the cross-over in the vertical response is displaced from the true conductor positions. As the separation between the conductors increases (Figures M5b and M5c), the presence of two conductors can be detected through the skewness of the profile curves. Only when the separation between the conductors approaches twice the depth, do two peaks form in the response. This dependance of resolvability on the separation/depth ratio was observed for all choices of conductor depths where the conductances of the two conductors were of similar magnitude. The dependance also exists when the conductors have dips of less than 90^{o}, as in Figures M6a and M6b.

Figures M7a and M7b show the responses measured near two conductors with large differences in conductances. Although the responses look similar to the responses from single sheet conductors, there are indications that we are dealing with two-conductor systems. The peaks of the profile curves move in the direction of the stronger conductor in later time channels. In the horizontal responses (proportional to $\frac{dB_x}{dt}$), the cross-overs that are closer to the strong conductor shift towards this conductor in time. The cross-over positions of the vertical responses (proportional to $\frac{dB_z}{dt}$) undergo similar shifts. As a result, the measured vertical responses undergo changes in sign at positions between the conductors. These observations are in accordance with the physical scale model results of Valleé (1981). An interesting observation is that the shifts in cross-over position can be seen even when the separation/depth ratio is less than unity, as in Figure M7a. This fact can prove helpful in establishing whether an anomaly is due to a multiple conductor system. These shifts are also observed when dealing with conductors of varying dips, as can be seen in Figures M8a through M8c.

The shifts in cross-over positions are present even when two conductors occur very close to one another. Figures M9a through M9c study the shifts in the cross-over positions of the vertical response of conductors with small separations. In all these figures the model loops have conductances of 0.8S and 0.3S, respectively. The subsurface positions of the 0.8S conductors are indicated by the dashed lines, while the locations of the weaker conductors are shown in solid lines. The depths of the conductors are 40m in all the examples.

From Figures M9a through M9c it seems theoretically possible to determine the presence of a multiple conductor system for conductors with very small separations. In practice it is often not possible to define the anomalies caused by multiple sheet conductors with small separation with the accuracy required to observe this drift. The anomalies from field data have to be isolated from the total measured response by the removal of the host rock response. The processes used to remove the host rock response have certain limitations as far as accuracy is concerned, and can therefore cause an anomaly to be described inaccurately.

Figure M10 compares the drift in cross-over positions of the vertical responses of 4 geological models. The weak and strong conductors in all the models have conductances of 0.3S and 0.8S, respectively. The distances between the cross-over positions of the first and fifteenth time channels are plotted as functions of conductor separation. It is interesting to note that conductor depth has little influence on the observed cross-over drift. Only when the conductor separation exceeds 20m, do the magnitudes of the drifts start to differ for the various models. When conductor separation is large, a shallow two-conductor system causes greater drift than a deep two-conductor system. Very little cross-over drift can be distinguished when the conductor separation approaches 1m. This is observed for all the models.

4.4.3 Effect of different decay constants

The late time response from a single conductor is an exponential decay (see equation 2.2). An example of such a response is shown in Figure 4.2. When logarithms of the measured channel amplitudes are plotted versus their measurement times, the late time responses lie on a straight line. The decay constant is given by the inverse of the slope of this line:

$$\ln\left[\frac{d\mathbf{B}}{dt}(t)\right] \propto -\frac{t}{\tau} \qquad (4.3)$$

Figure 4.3 shows an example of the semi-log plots used in the determination of the decay constant.

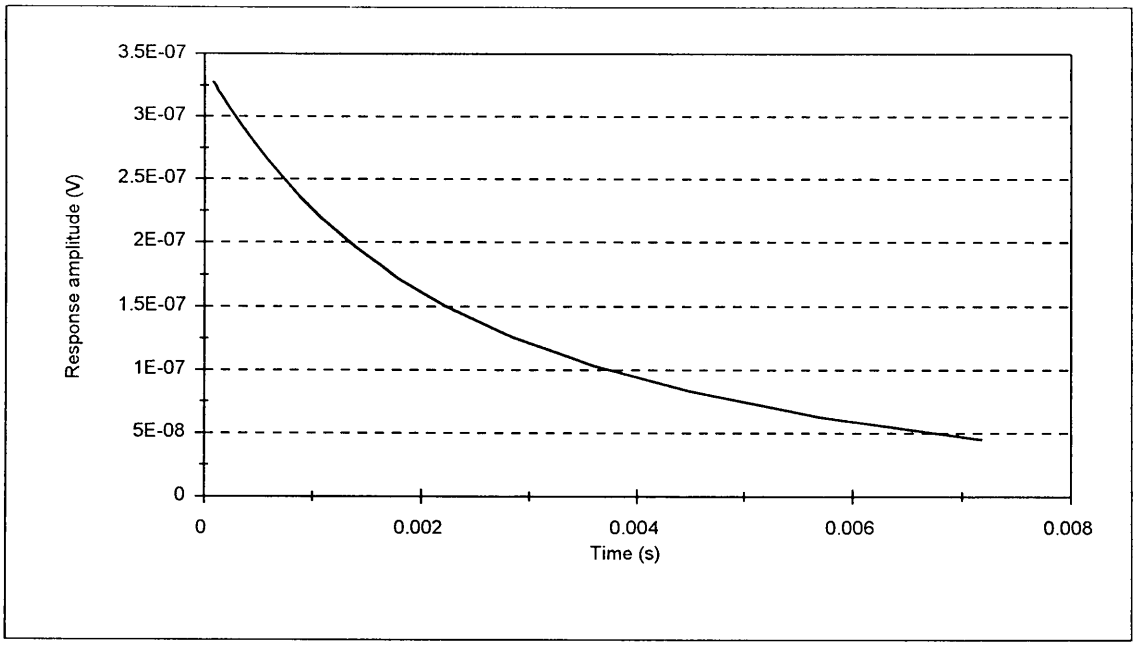

Figure 4.2: *Example of a measurement of the secondary magnetic field from a single sheet conductor.*

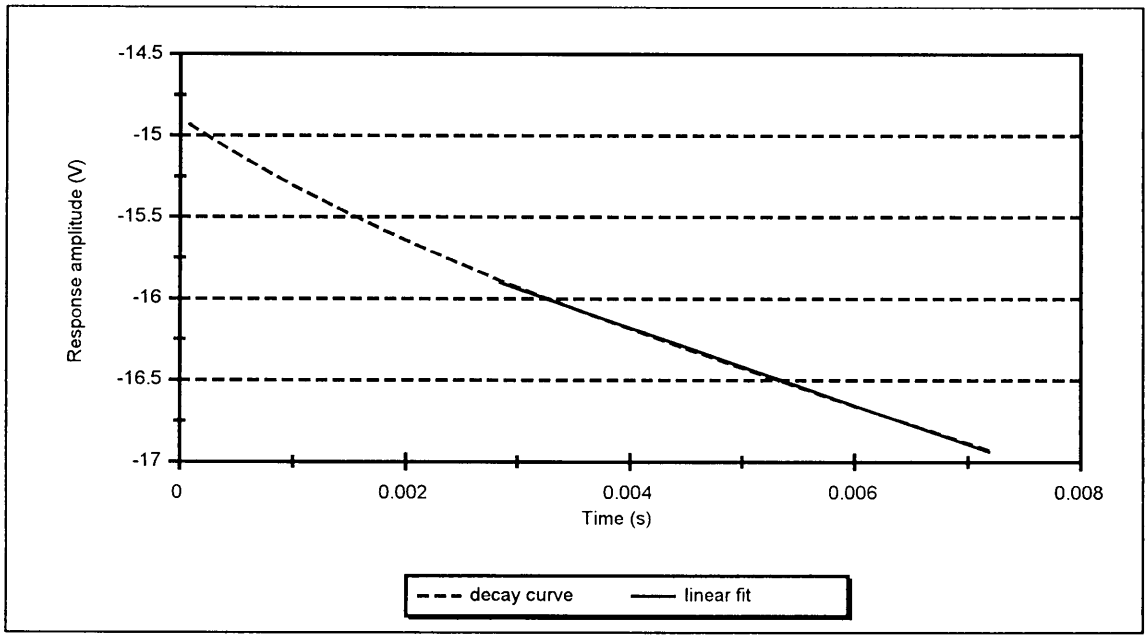

Figure 4.3: *Decay curve plot from measurements made at a position close to a single sheet conductor illustrating the late time linear dependance between the log values of the response and the time after turn-off.*

The equation describing the response from two coupled conducting wire loops (equation 3.13) is not purely exponential, but is a sum of two exponential decays

with decay constants t_1 and t_2. The decay of the secondary magnetic field is now also position dependant, due to the fact that the coupling coefficients between the various loops and the receiver loop vary with position. Since the response from a multiple conductor system is a sum of exponentials, its behaviour can not be described exactly by a single exponential decay. At positions between two conductors, the influence that exists between them causes the measured response to be very different from a true exponential decay. In Section 4.4.2 it was shown that the measured response can undergo changes in sign at these positions due to the shifting of the cross-overs. Figure 4.4 illustrates how the response measured at a position between two conductors can have a behaviour that is different from a true exponential decay. In the example of Figure 4.4 the response even undergoes a change in sign.

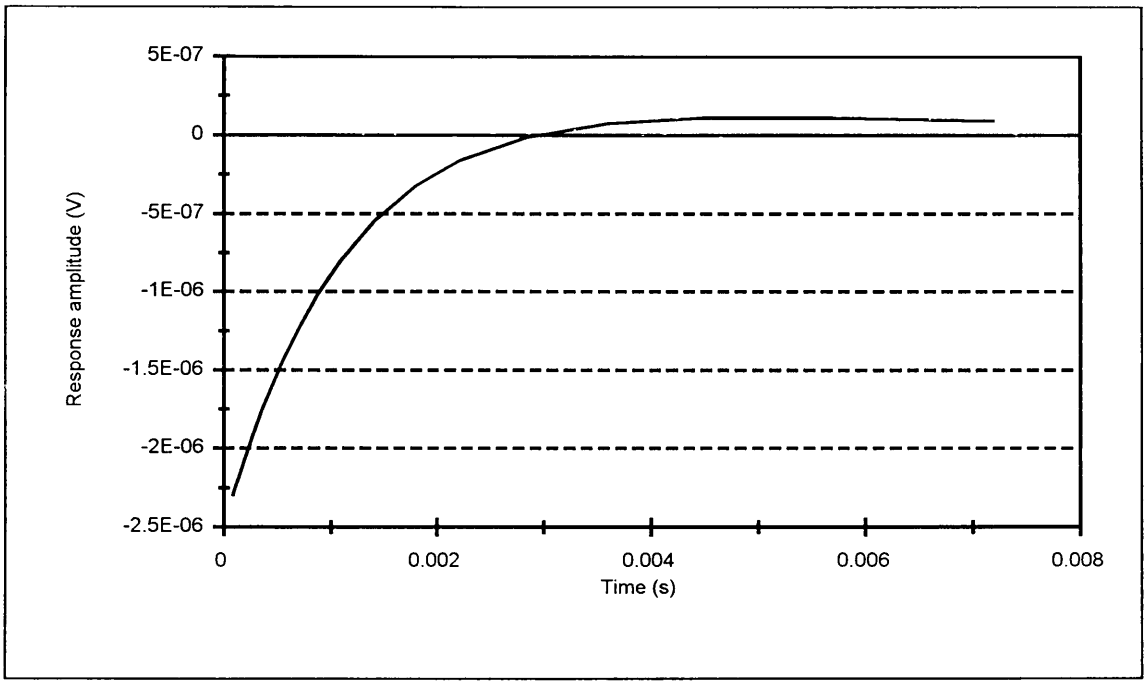

Figure 4.4: *Example of the electromagnetic response measured at a position between two conductors. Note how the decay is not of the true exponential form.*

Since the decay constant of a conductor is defined in terms of the exponential decay of its secondary magnetic field, it is not practical to define this constant for positions between two conductors where exponential decay is not exhibited. This fact can be exploited to ascertain whether a TDEM response is caused by a multiple conductor system. A pseudo decay constant can be calculated at each position along the survey traverse by taking the natural logarithm of the absolute value of the

last five channels of the measured vertical responses, and applying least square linear fits to these data sets. At positions where the behaviour of the measured response has an exponential form, the pseudo decay constant agrees with the true decay constant (as calculated in Figure 4.3). Figure 4.5 illustrates this method of calculating the pseudo decay constant at a survey station situated between two conductors.

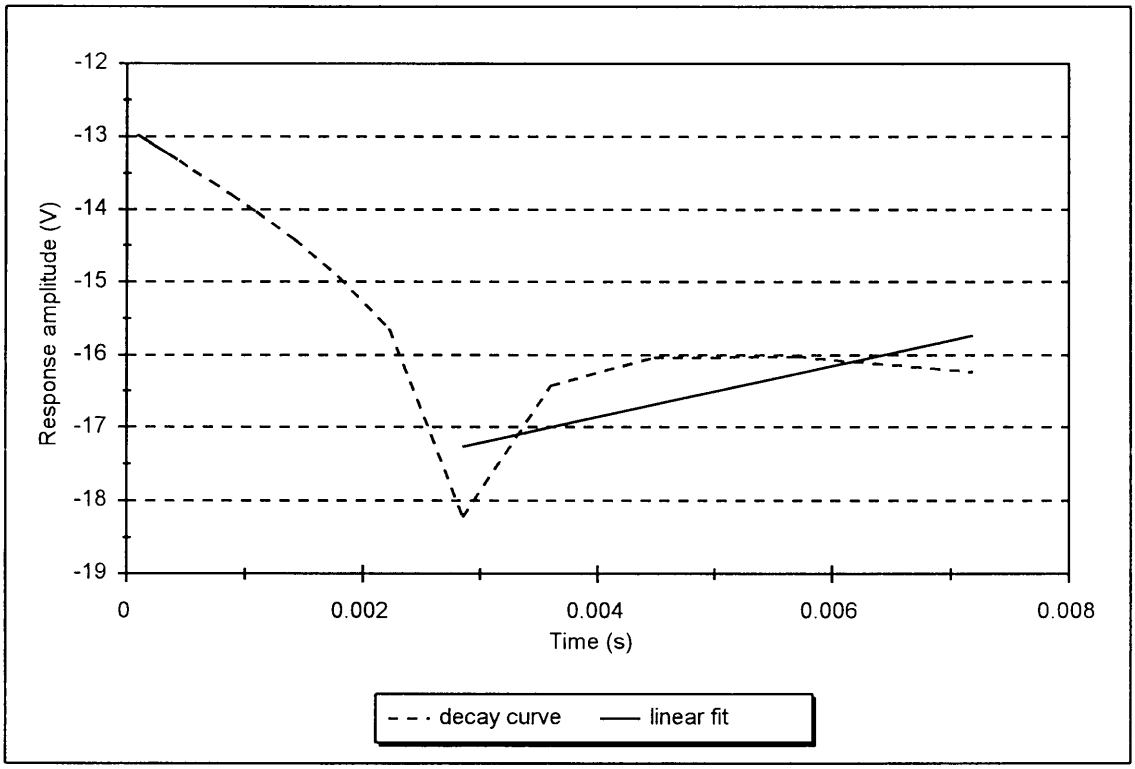

Figure 4.5: *Calculating the pseudo decay constant from the response measured at a position between two conductors. In this example the pseudo decay constant for the measured response of Figure 4.4 is calculated.*

From Figure 4.5 it is seen that the linear fit is unaccurate when calculated at a position between two conductors (compare with Figure 4.3). Figure M11 shows an example of a profile plot of the pseudo decay constant over a two-conductor system. The errors made in applying linear fits are also shown at each survey position.

When the separation between the conductors is large as compared to their depths, the calculated pseudo decay constant is approximately equal to the larger decay constant of the two individual model loops (shown in a dashed line) at positions on

either side of the two-conductor system. This can be understood by noting that a large separation implies a small coupling coefficient between two conductors, therefore the measured response (equation 3.13) approaches the response from two uncoupled conductors (equation 3.14). Since a larger decay constant implies slower decay, the larger decay constant of the multiple circuit system of large separation, is approximately equal to the larger decay constant of the two individual loops (Valleé, 1981). The pseudo decay constant varies much more drastically in positions situated between the conductors where the linear fits were unaccurate.

Figures M12 through M14 show profile plots of the pseudo decay constants for various two conductor problems in which the separation/depth ratio is smaller than unity. The strong coupling between the conductors causes the pseudo decay constant to be much higher than that of either conductor at positions on the sides of the two-conductor system. When such a situation is encountered during a TDEM survey, the calculated decay constant could lead to the erroneous interpretation of the presence of a conductor of high conductivity.

Figures M12 through M14 illustrate how the calculation of the pseudo decay constant can be diagnostic of a two-conductor system. From the figures it can be seen that the calculated pseudo decay constants, and the errors associated with the least square fits, indicate the presence of two conductors through the sharp variation in their values at positions situated between the conductors. It is therefore possible to establish that we are dealing with a multiple conductor situation, even though it may not be possible to determine this from the profile plots of the measured responses alone.

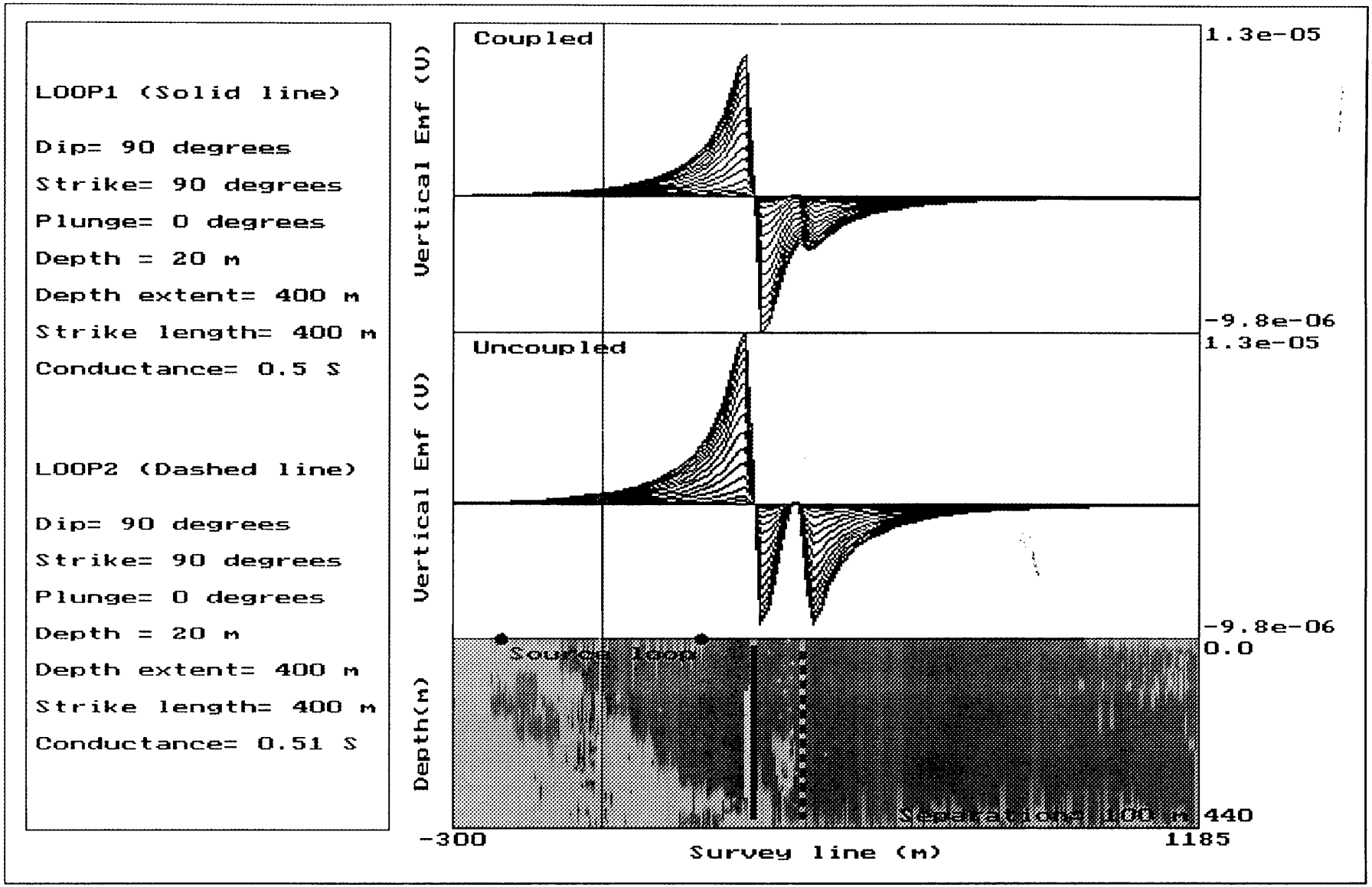

Figure M1: *Model example illustrating the effects of masking.*

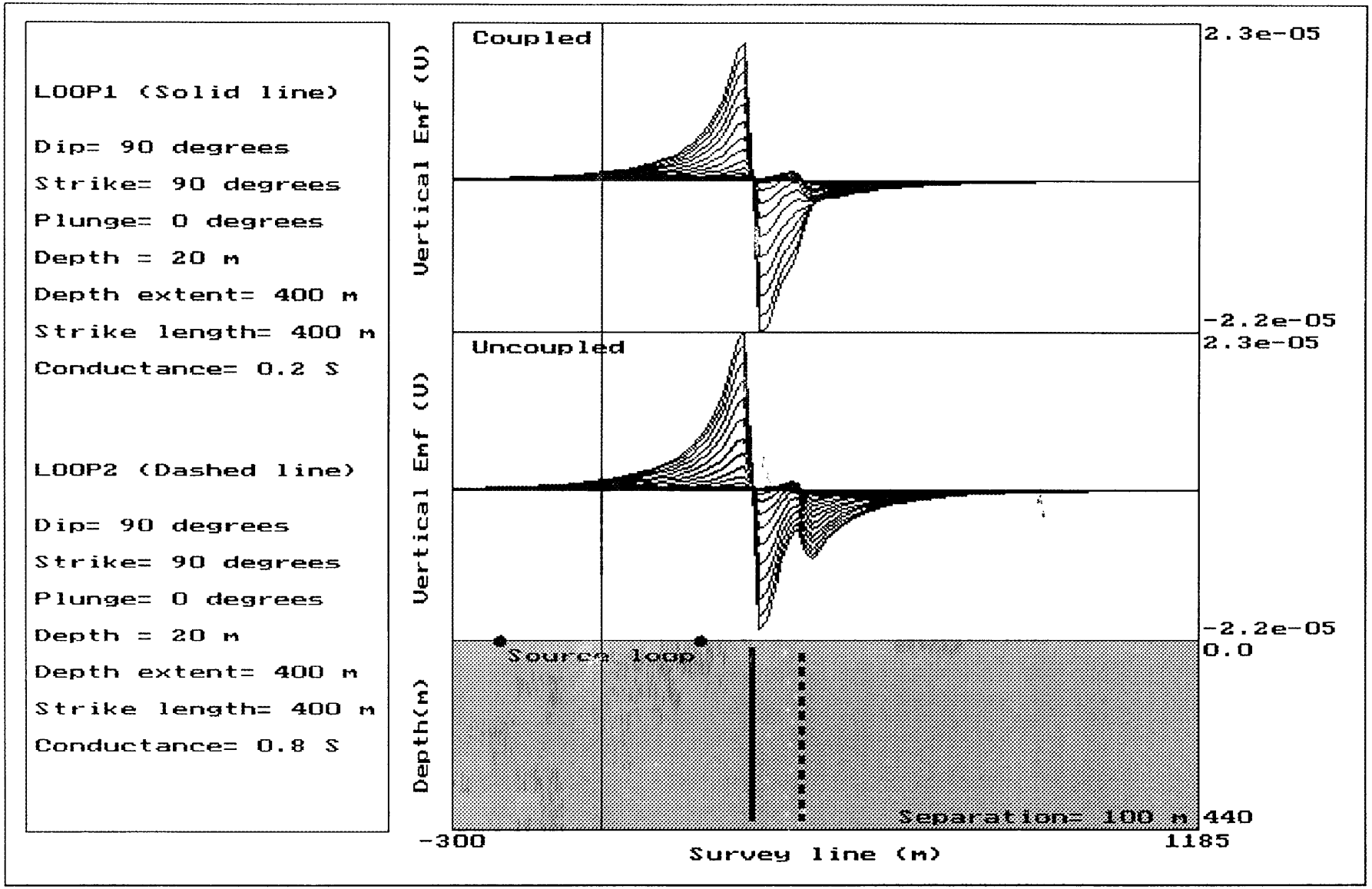

Figure M2: *Model example illustrating the effects of masking.*

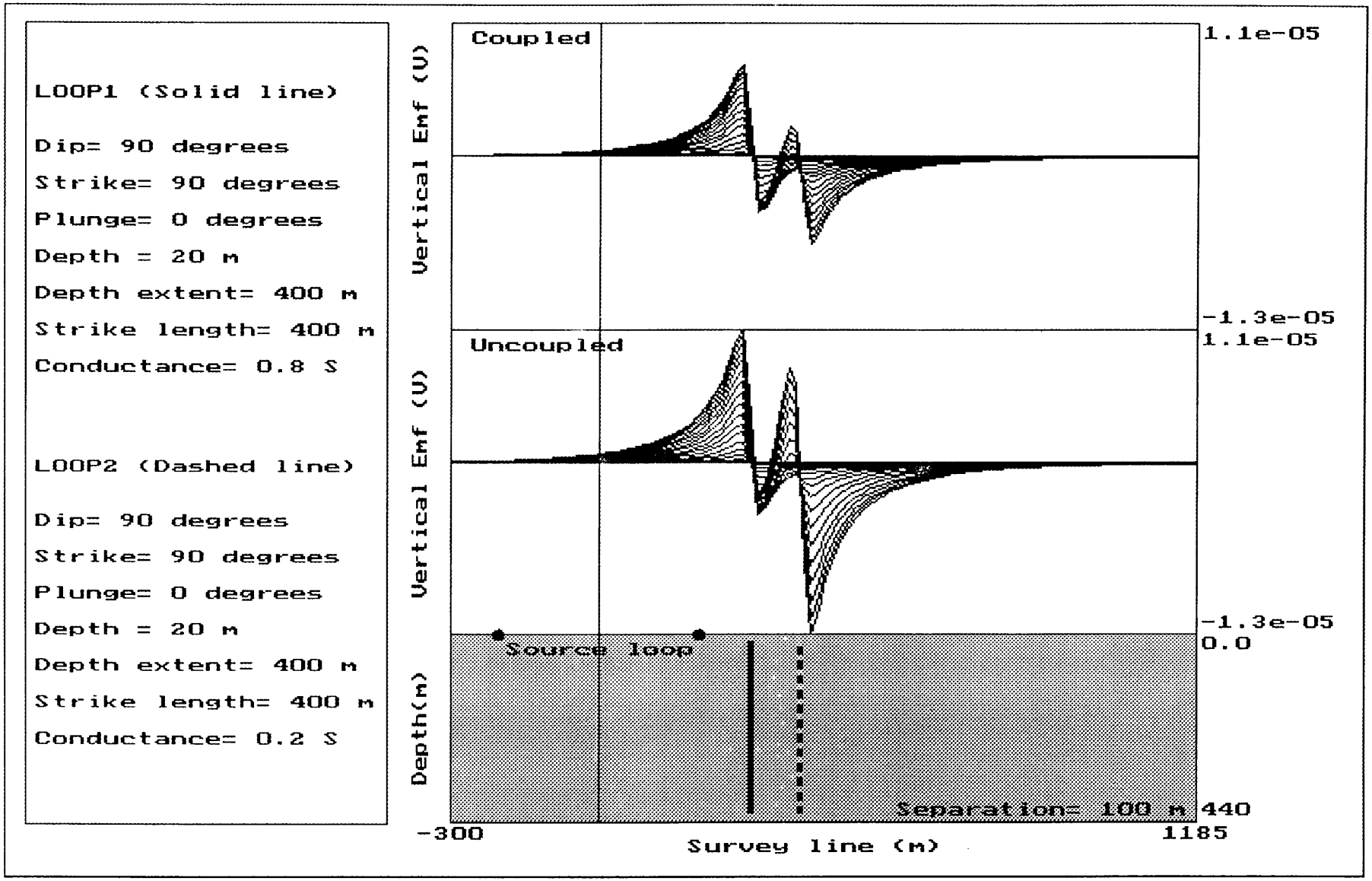

Figure M3: *Model example illustrating the effects of masking.*

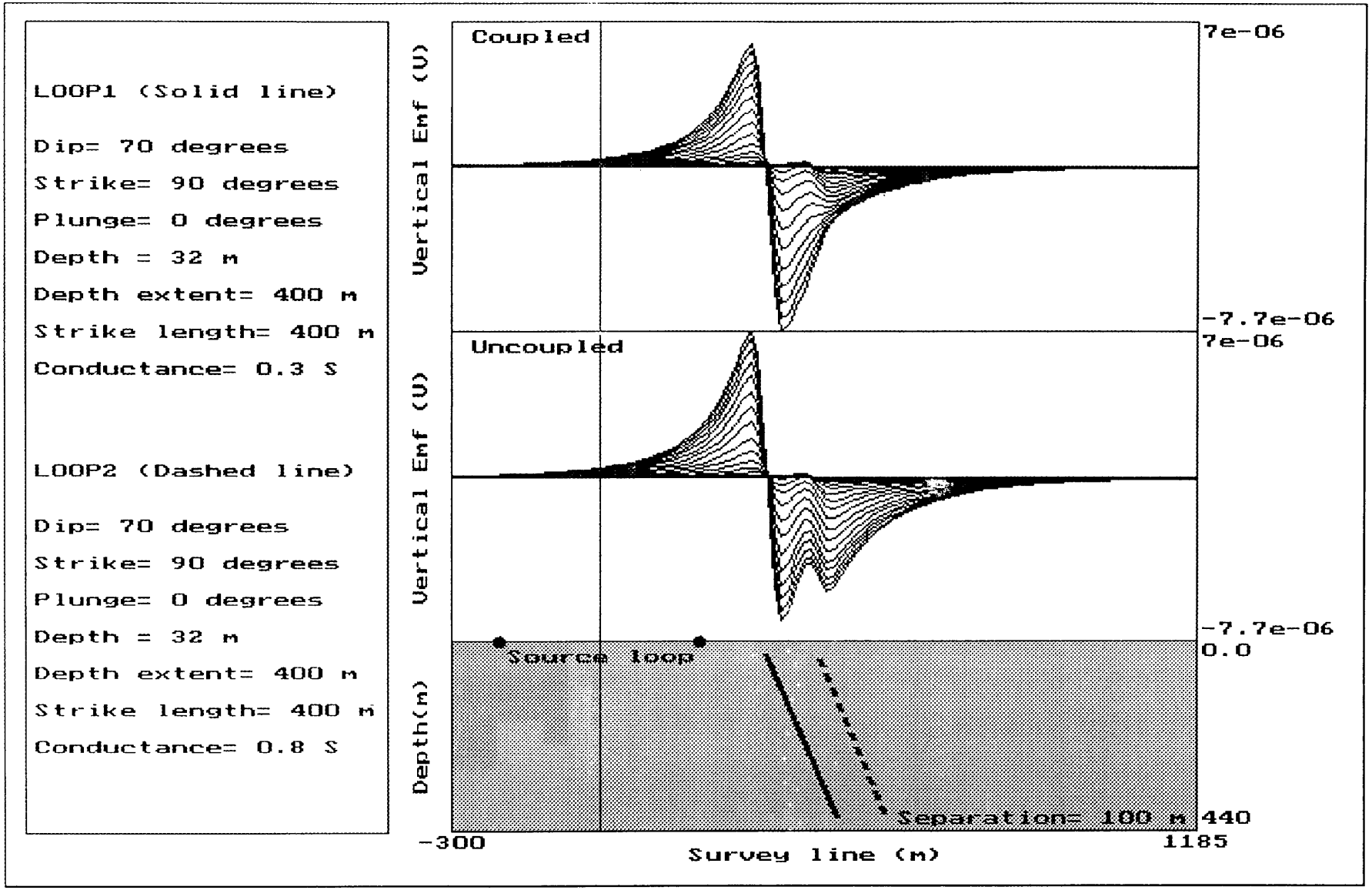

Figure M4: *Model example illustrating the effects of masking.*

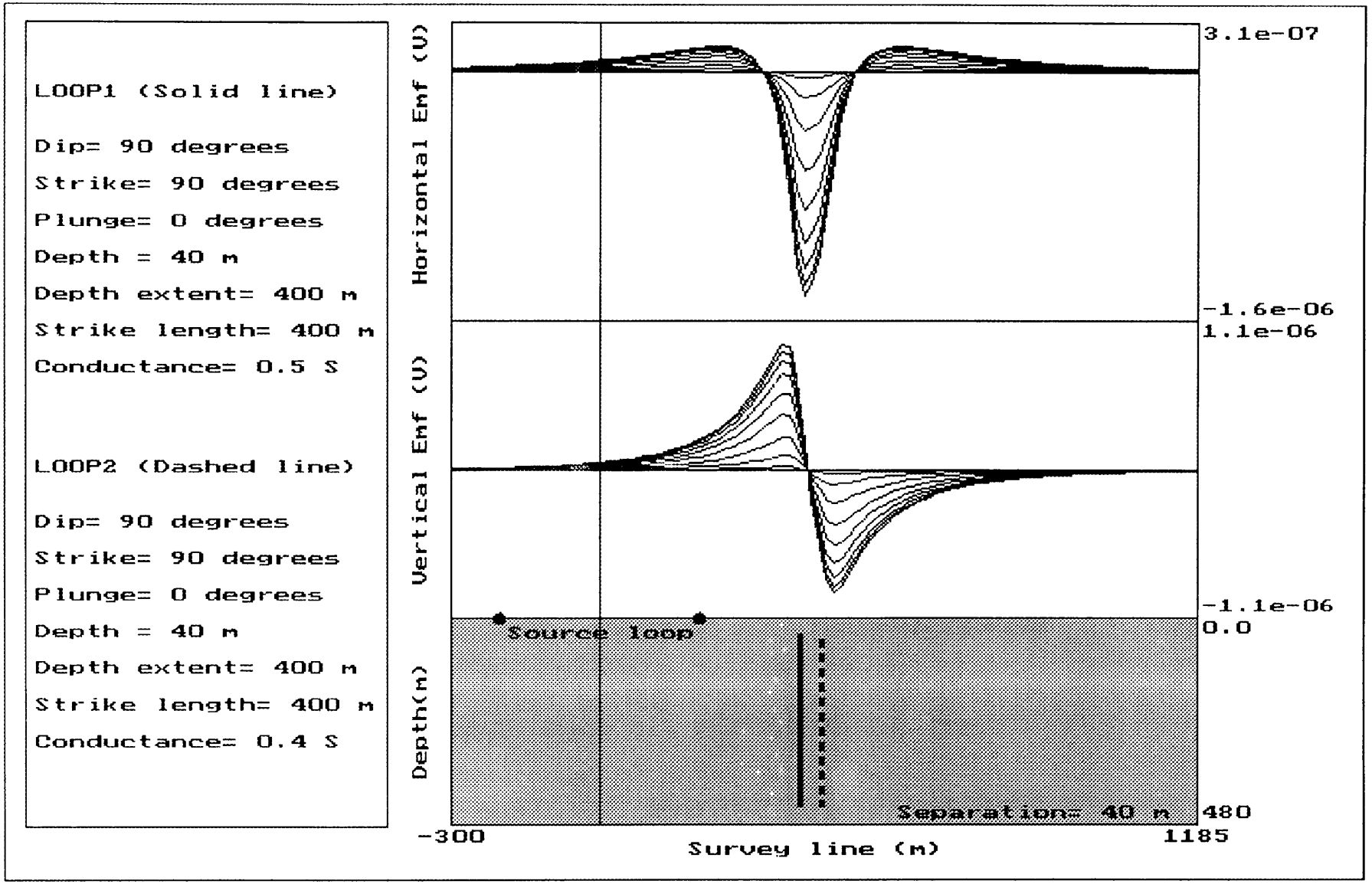

Figure M5a: *Model example examining the effects of conductor separation.*

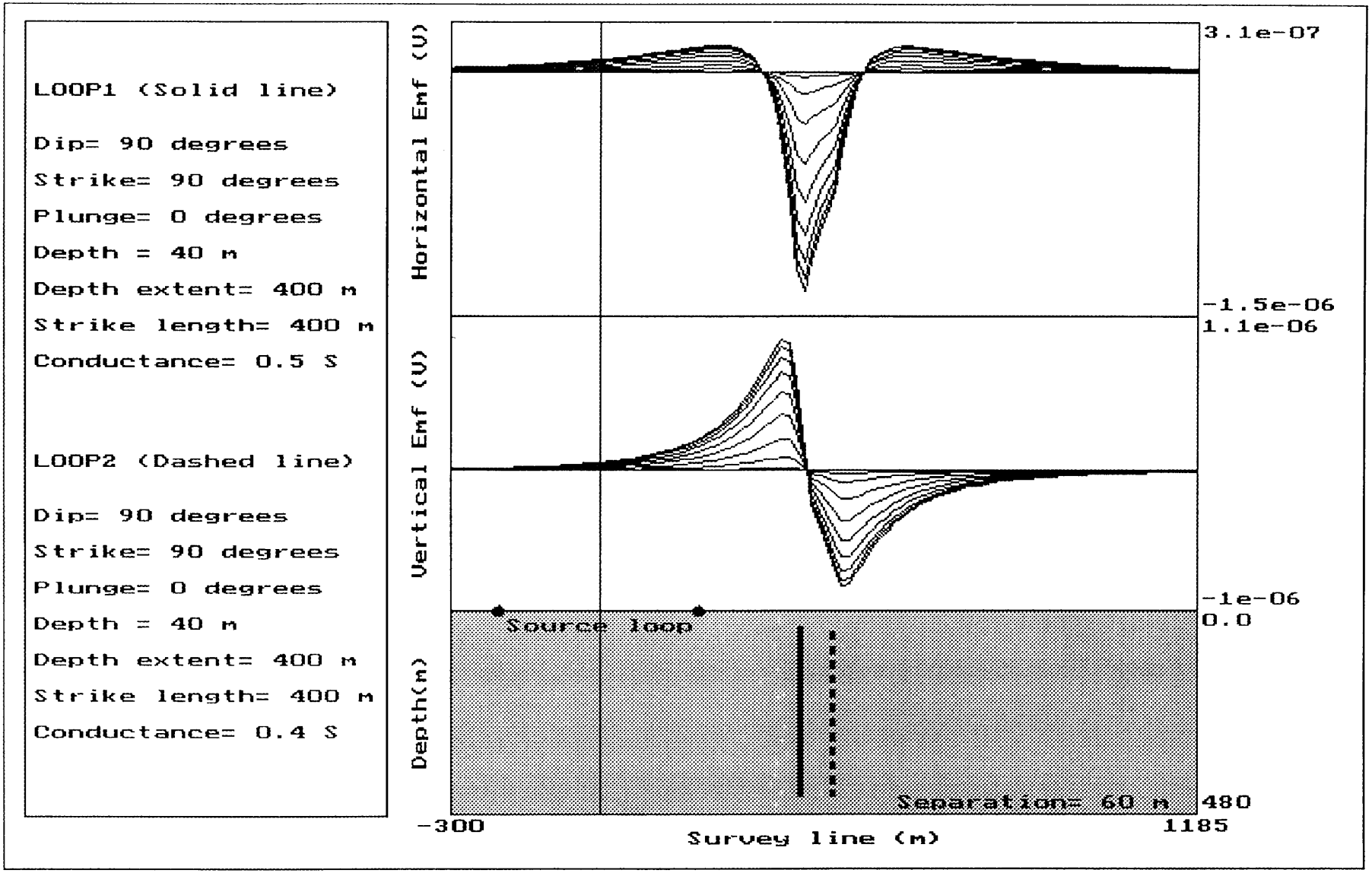

Figure M5b: *Model example examining the effects of conductor separation.*

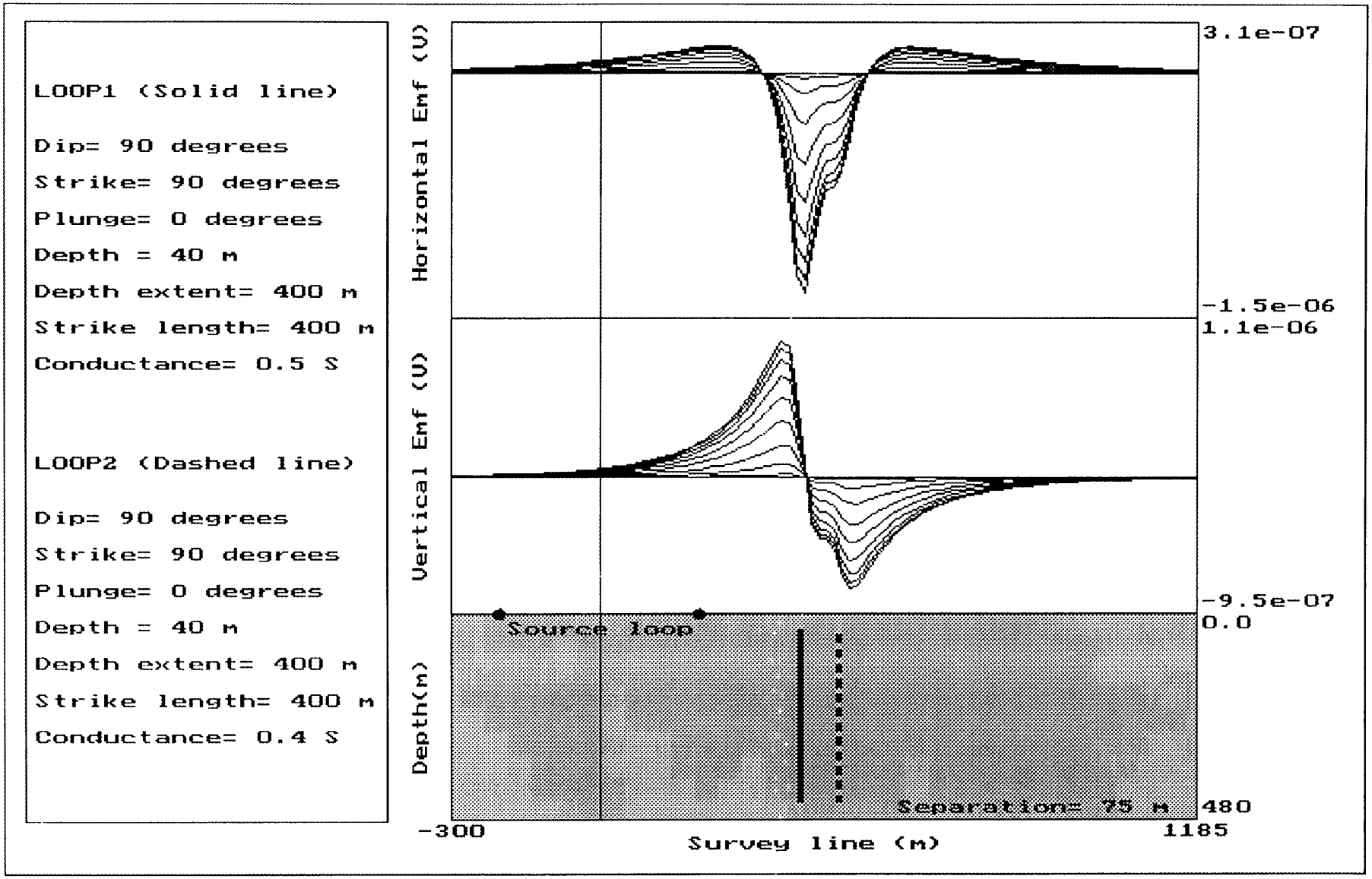

Figure M5c: *Model example examining the effects of conductor separation.*

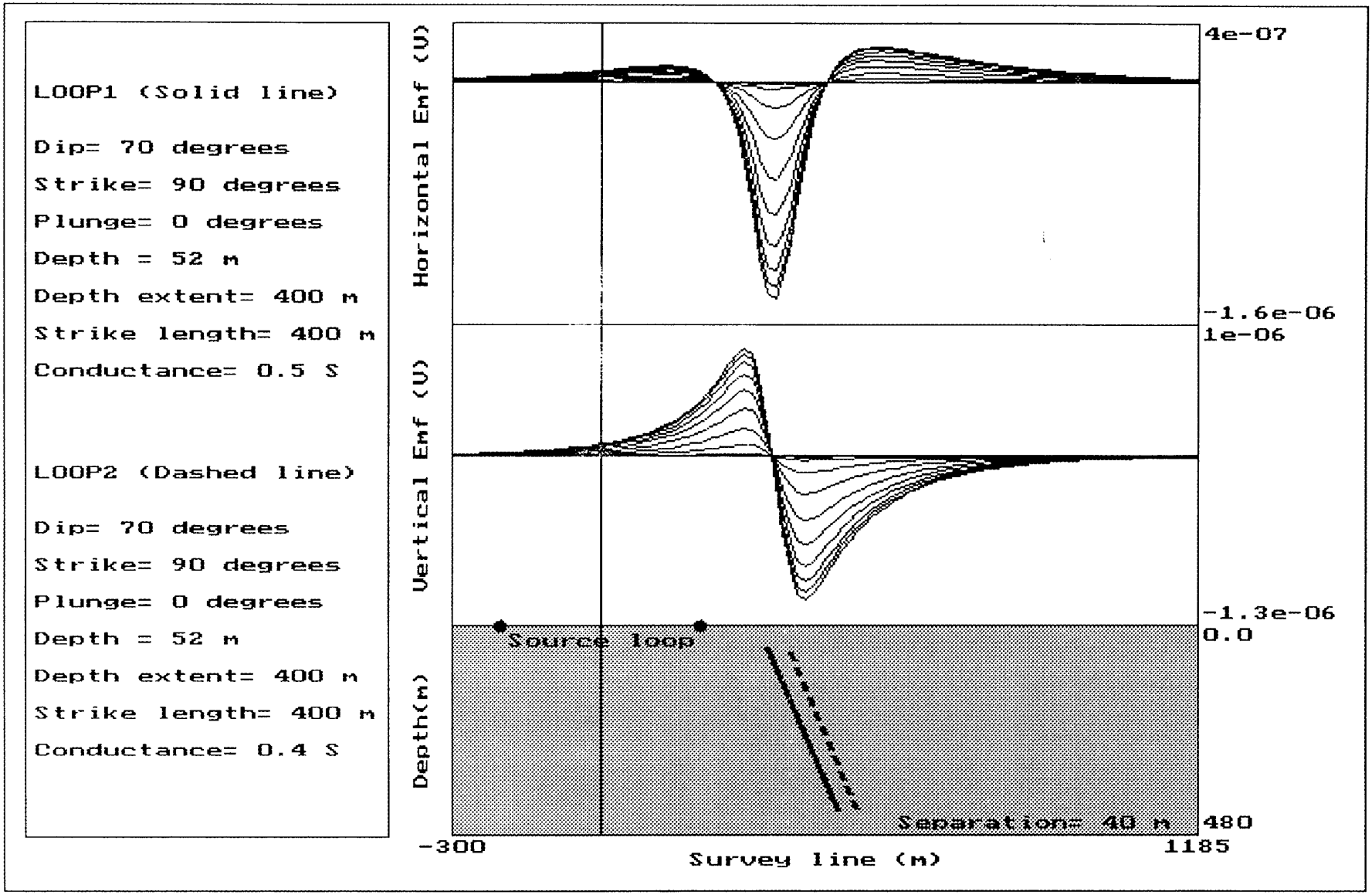

Figure M6a: *Model example examining the effects of conductor separation.*

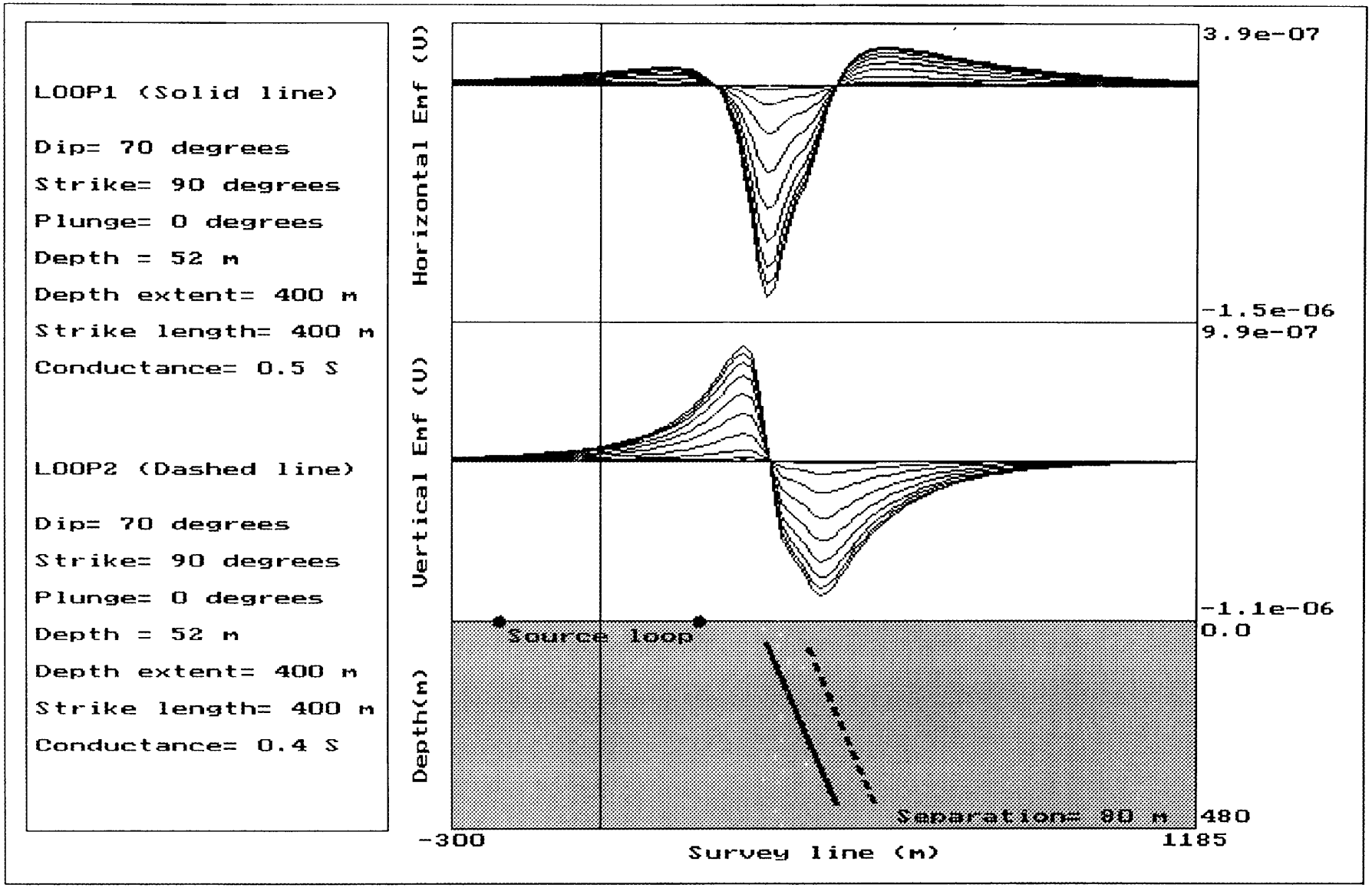

Figure M6b: *Model example examining the effects of conductor separation.*

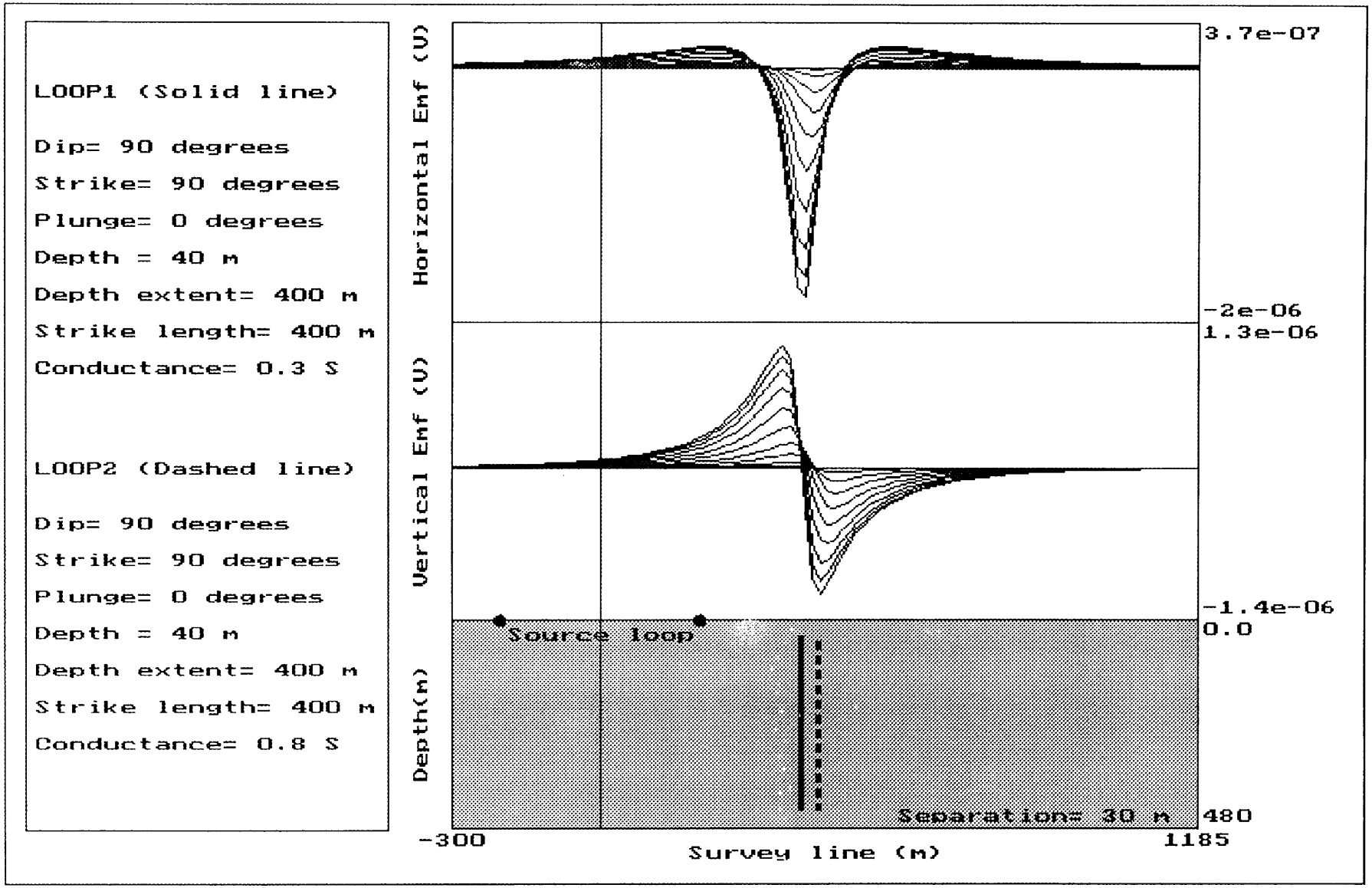

Figure M7a: *Model example examining the effects of conductor separation.*

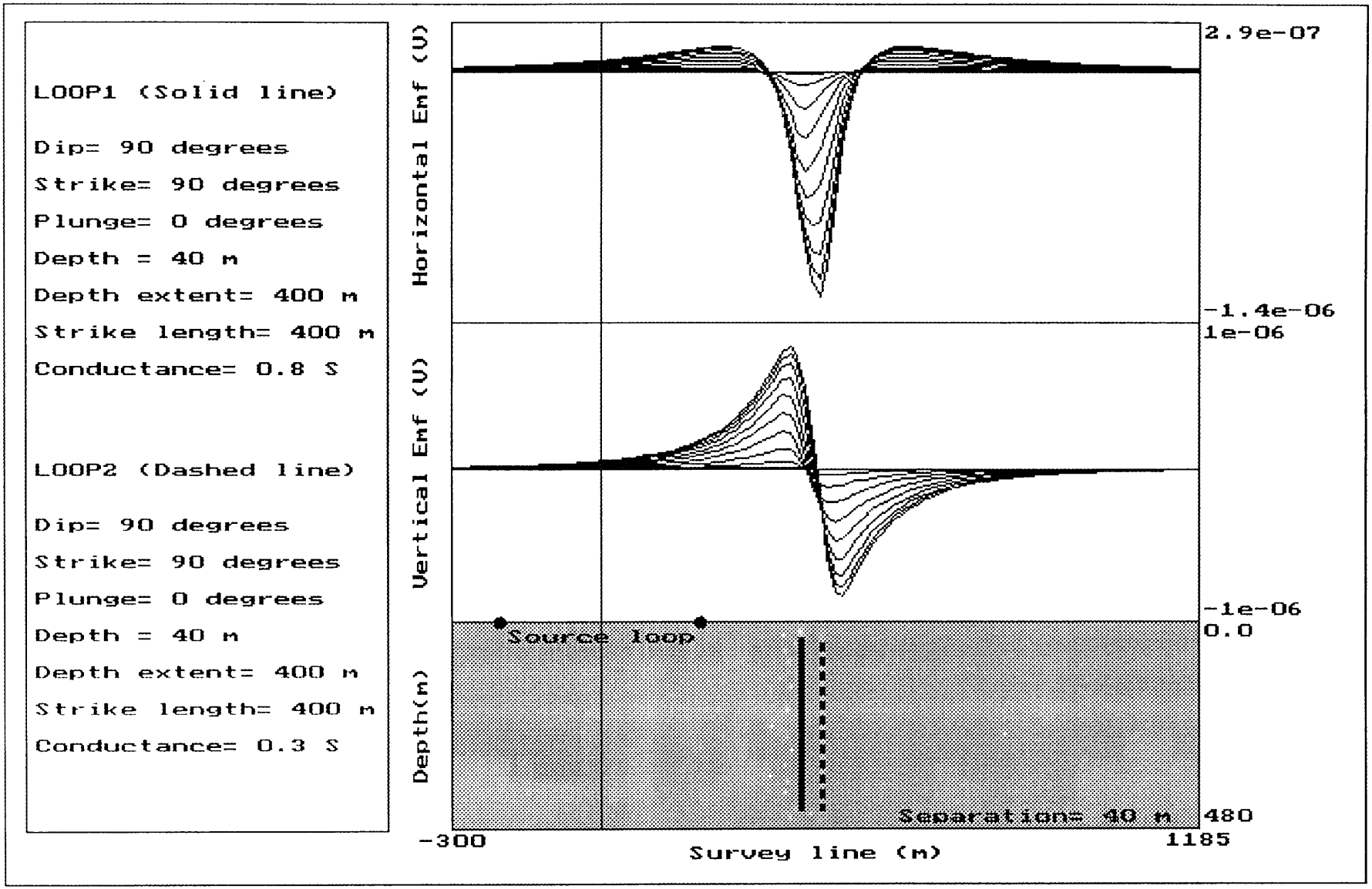

Figure M7b: *Model example examining the effects of conductor separation.*

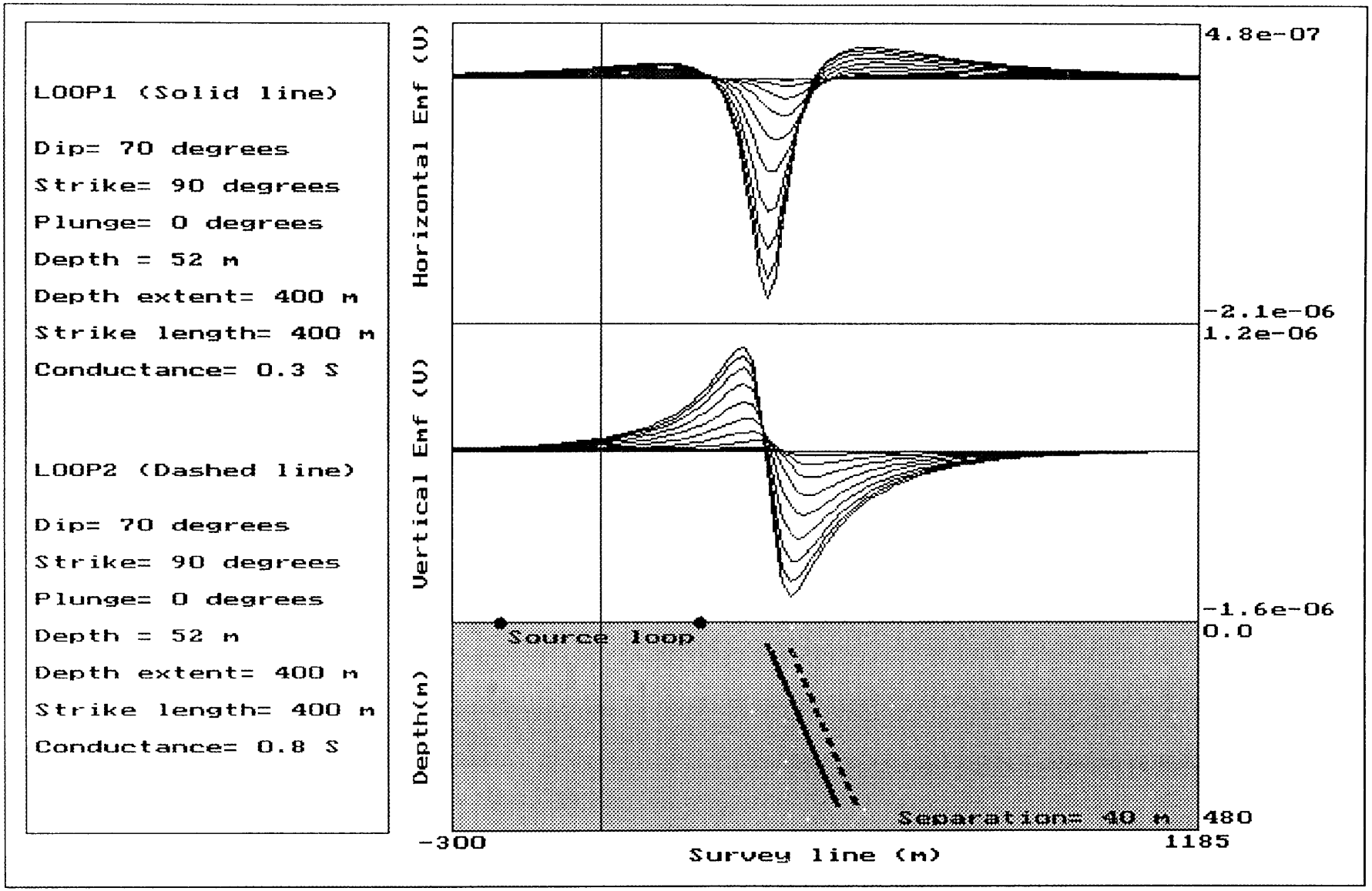

Figure M8a: *Model example examining the effects of conductor separation.*

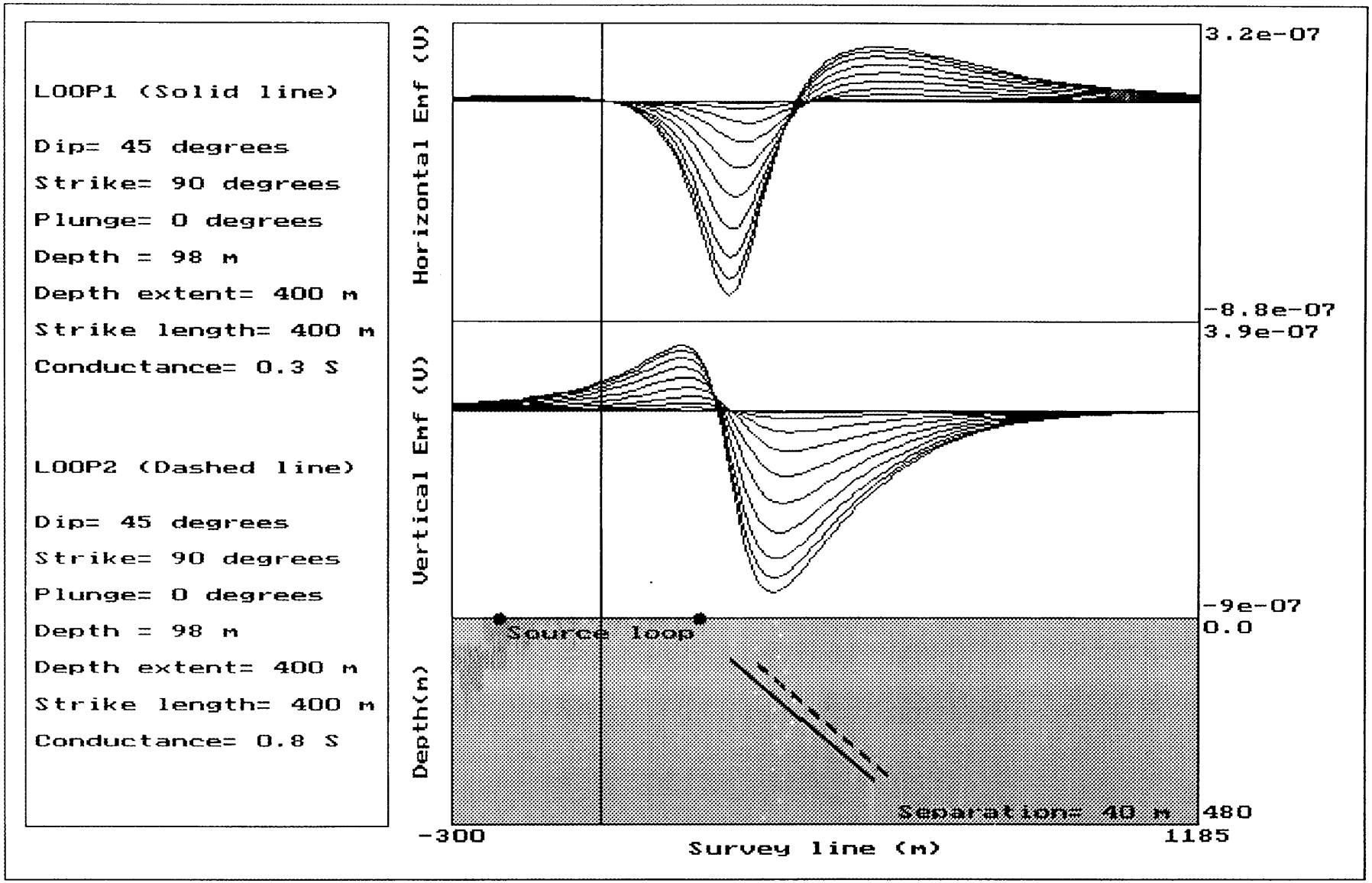

Figure M8b: *Model example examining the effects of conductor separation.*

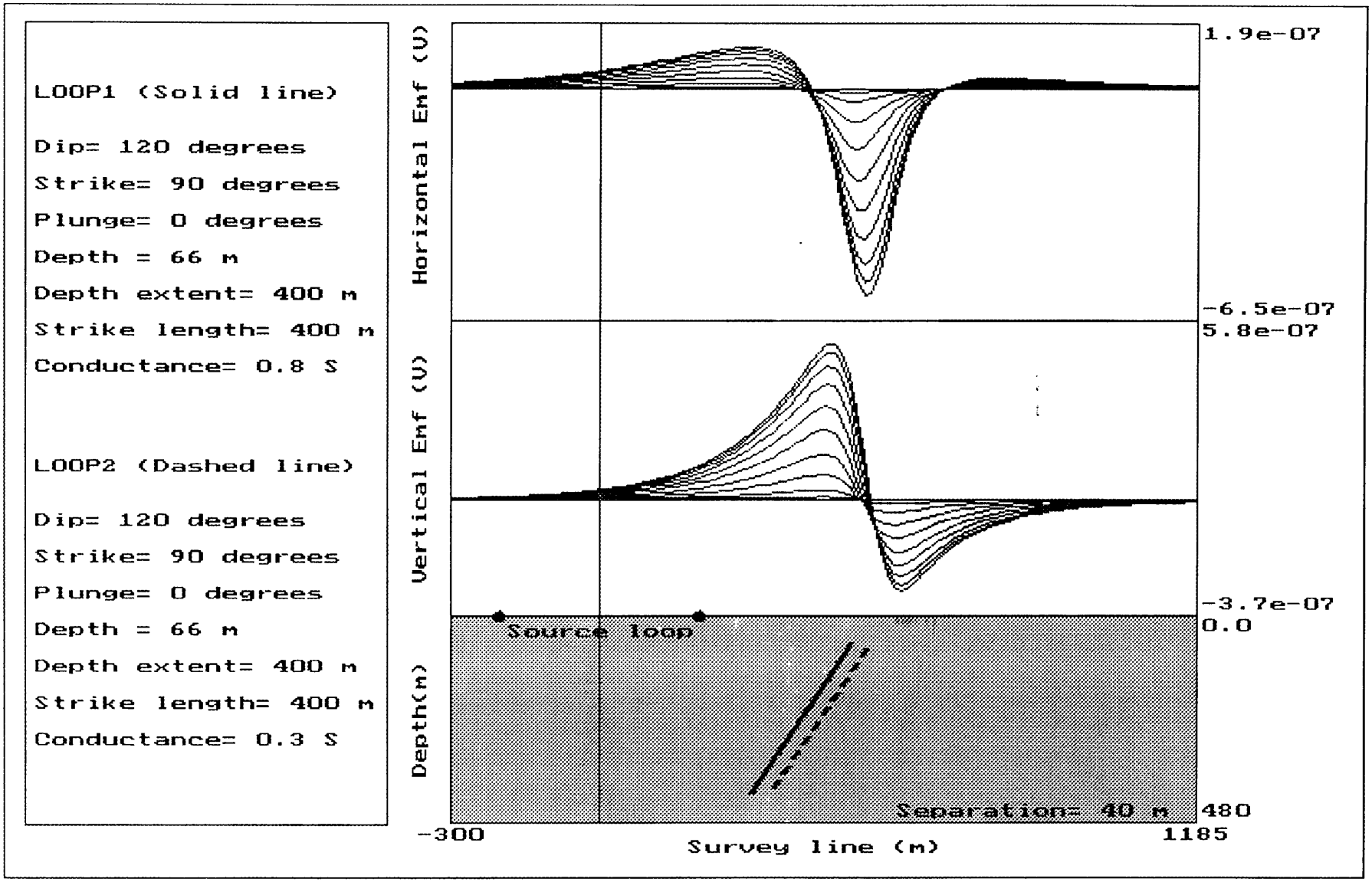

Figure M8c: *Model example examining the effects of conductor separation.*

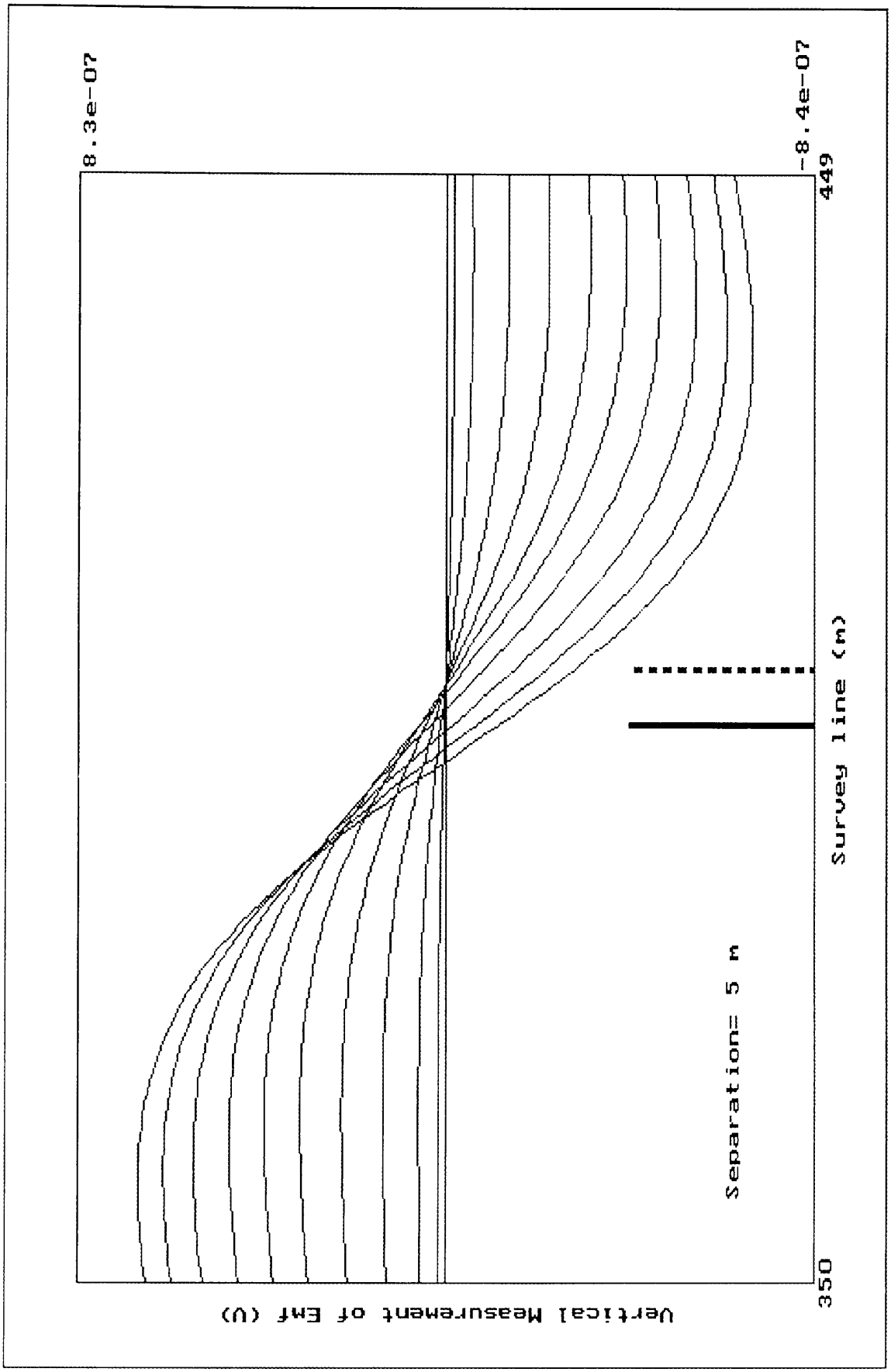

Figure M9a: *Model example studying the shift in cross-over position for multiple conductor models.*

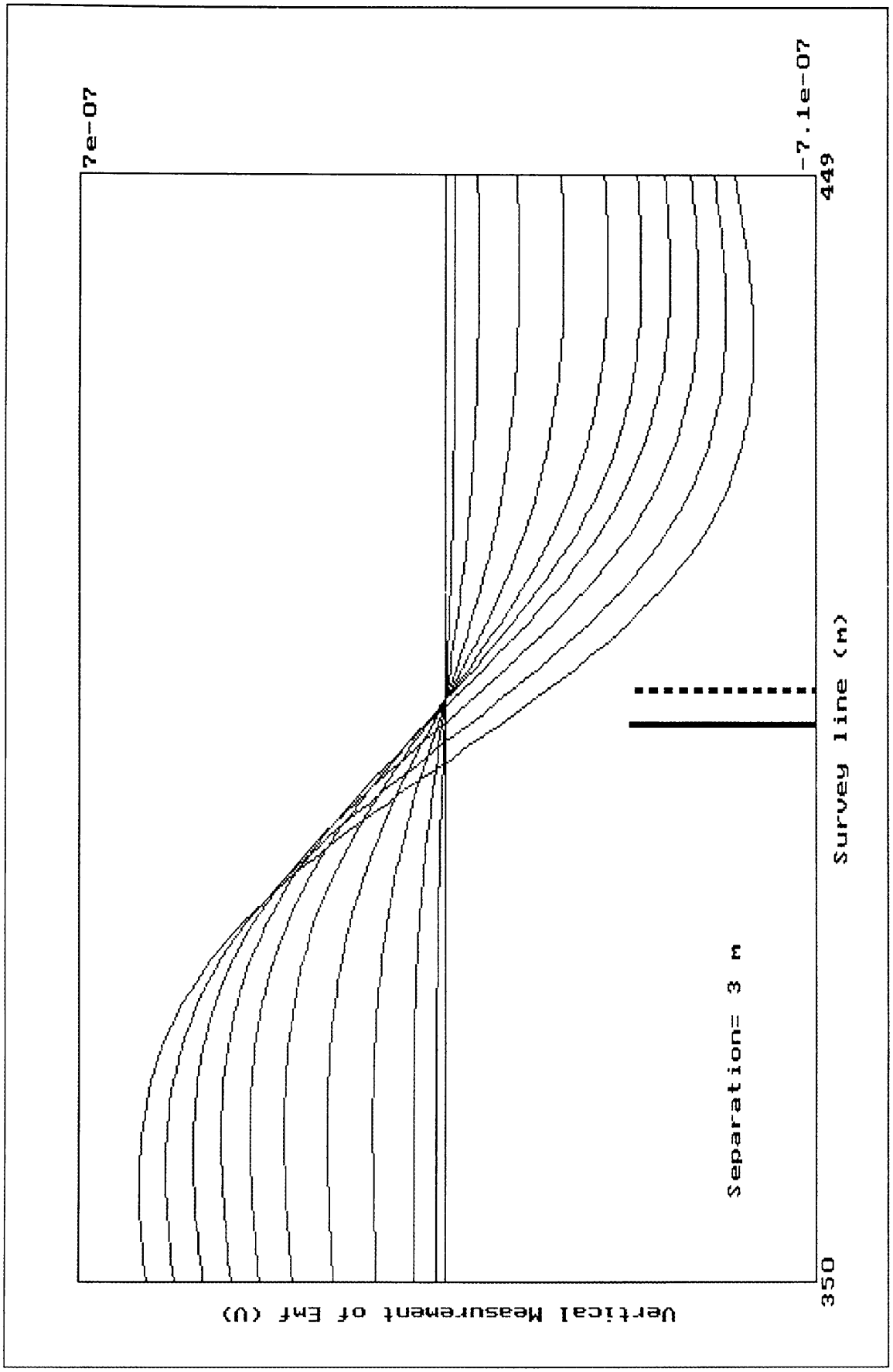

Figure M9b: *Model example studying the shift in cross-over position for multiple conductor models.*

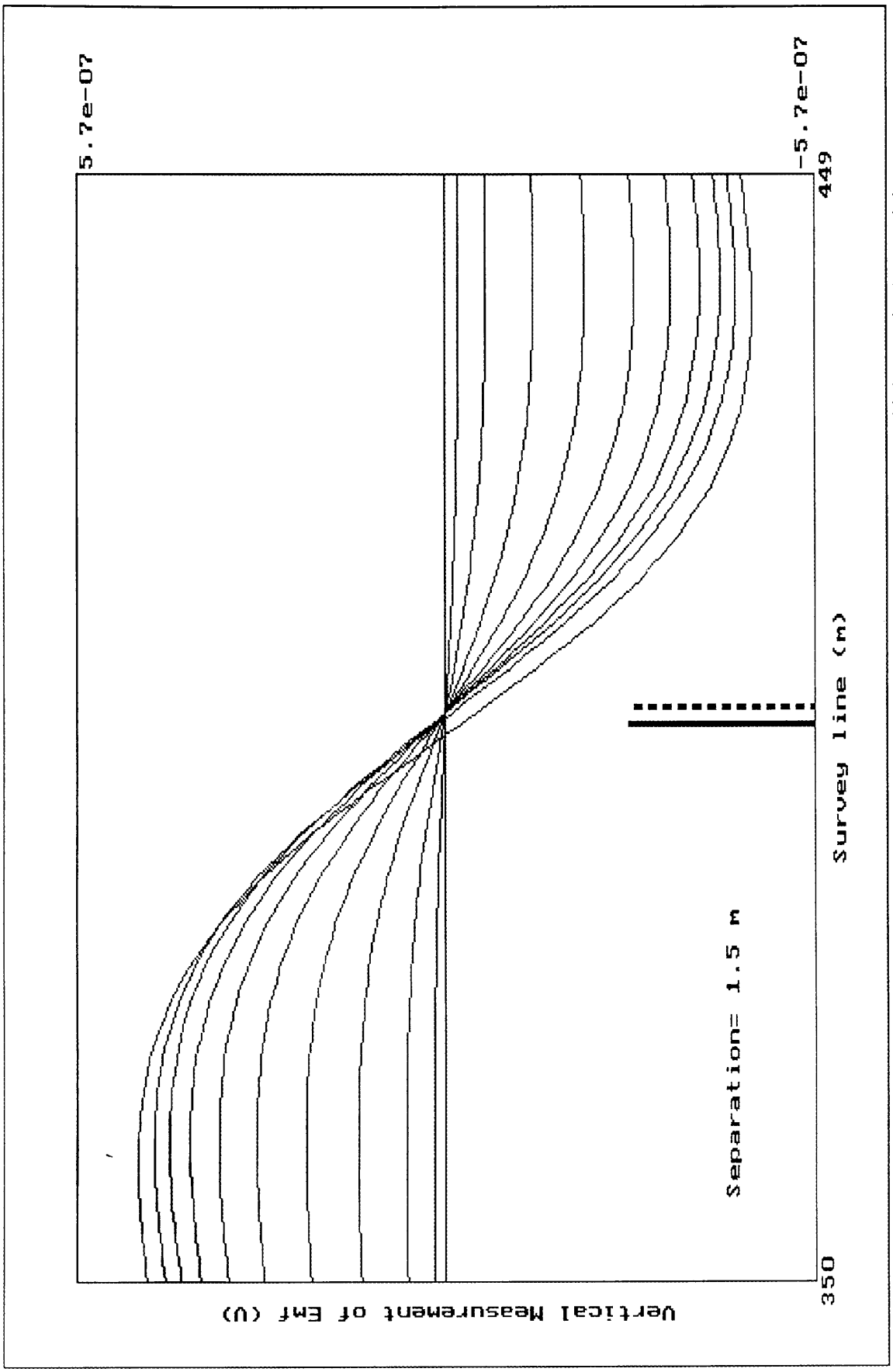

Figure M9c: *Model example studying the shift in cross-over position for multiple conductor models.*

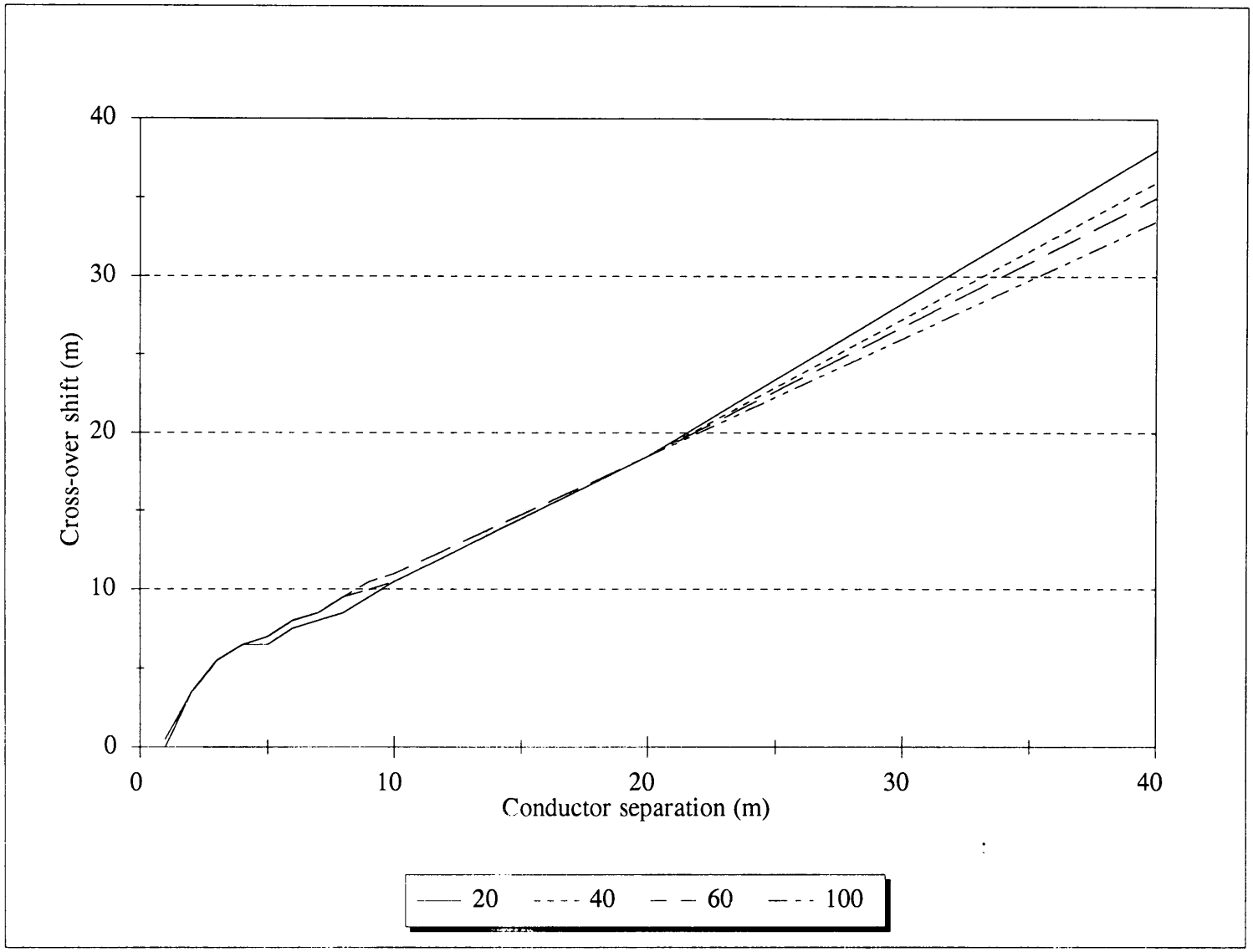

Figure M10: *Comparing the relationship between conductor separation and cross-over drift for multiple conductors with depths of 20, 40, 60 and 100m.*

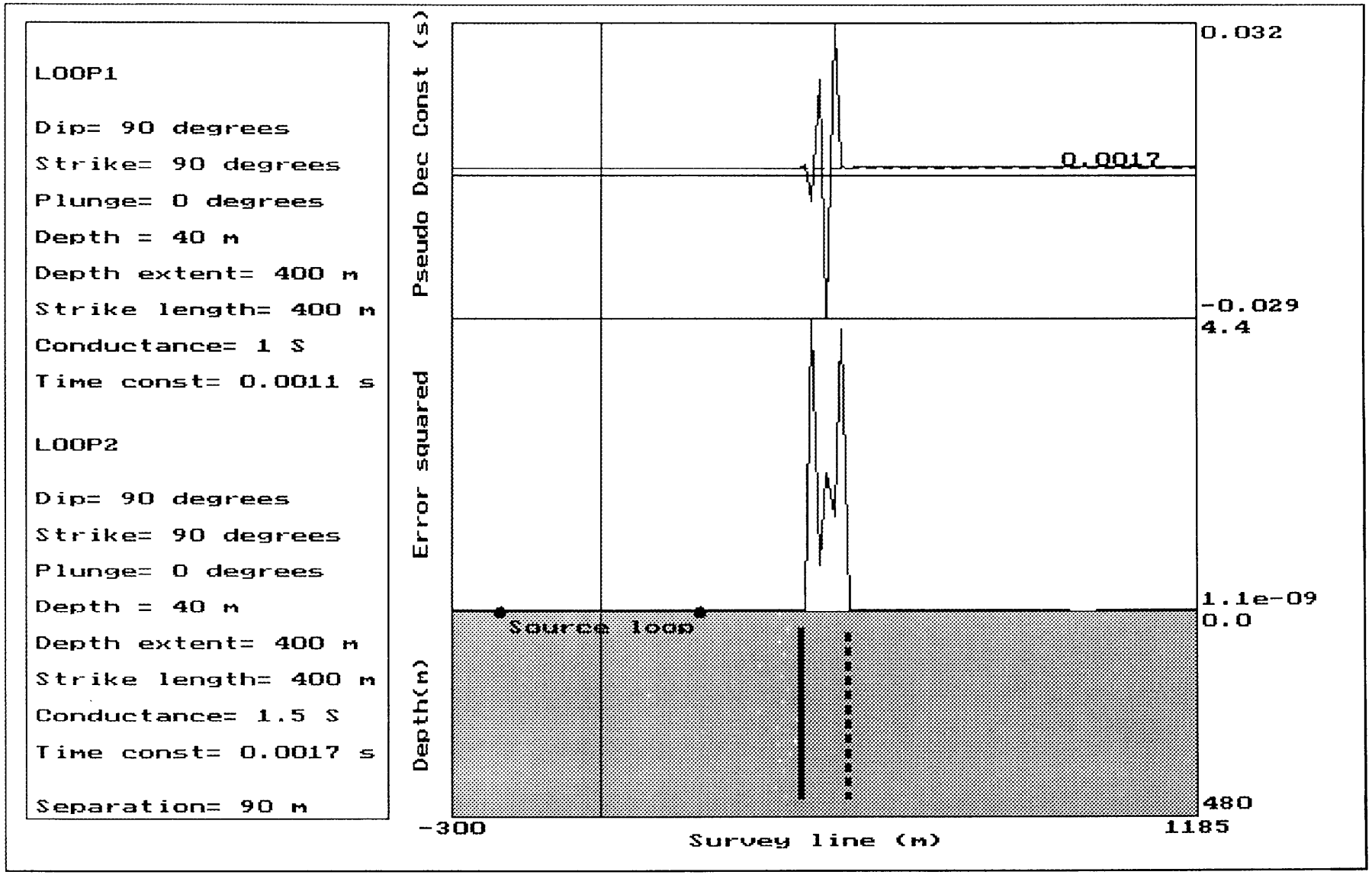

Figure M11: *Model example showing how the pseudo decay constant can indicate the presence of multiple conductors.*

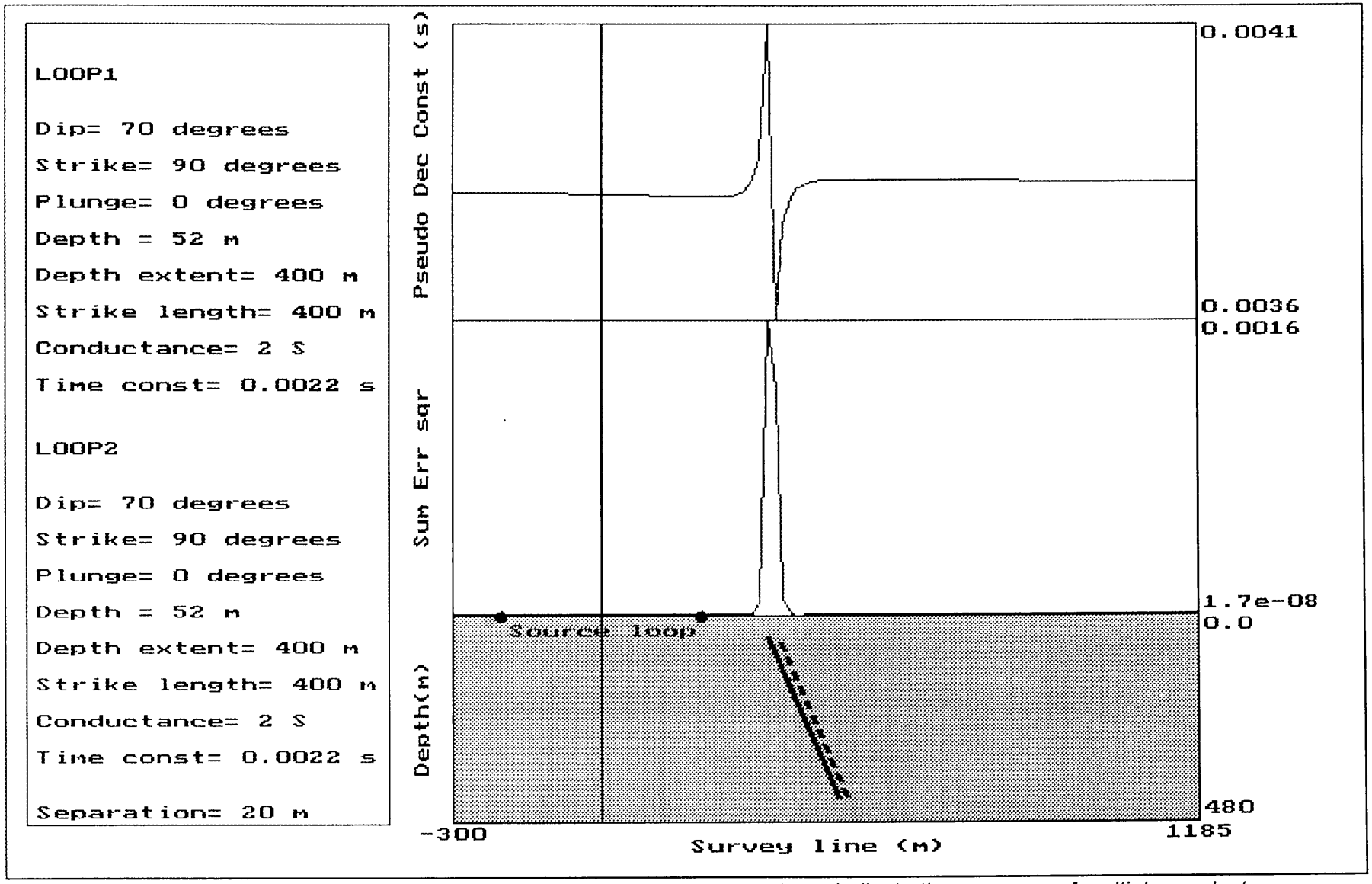

Figure M12: *Model example showing how the pseudo decay constant can indicate the presence of multiple conductors.*

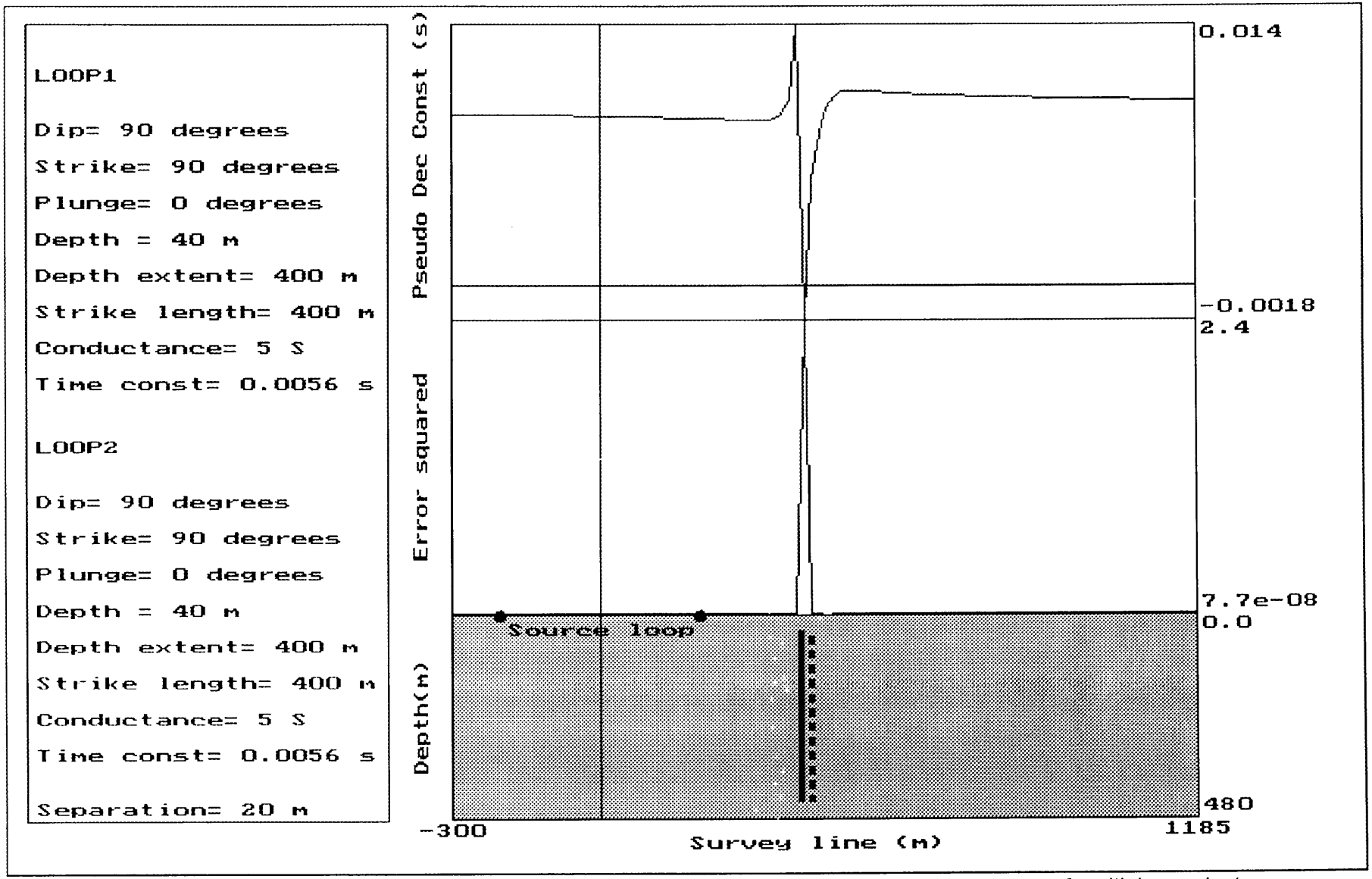

Figure M13: *Model example showing how the pseudo decay constant can indicate the presence of multiple conductors.*

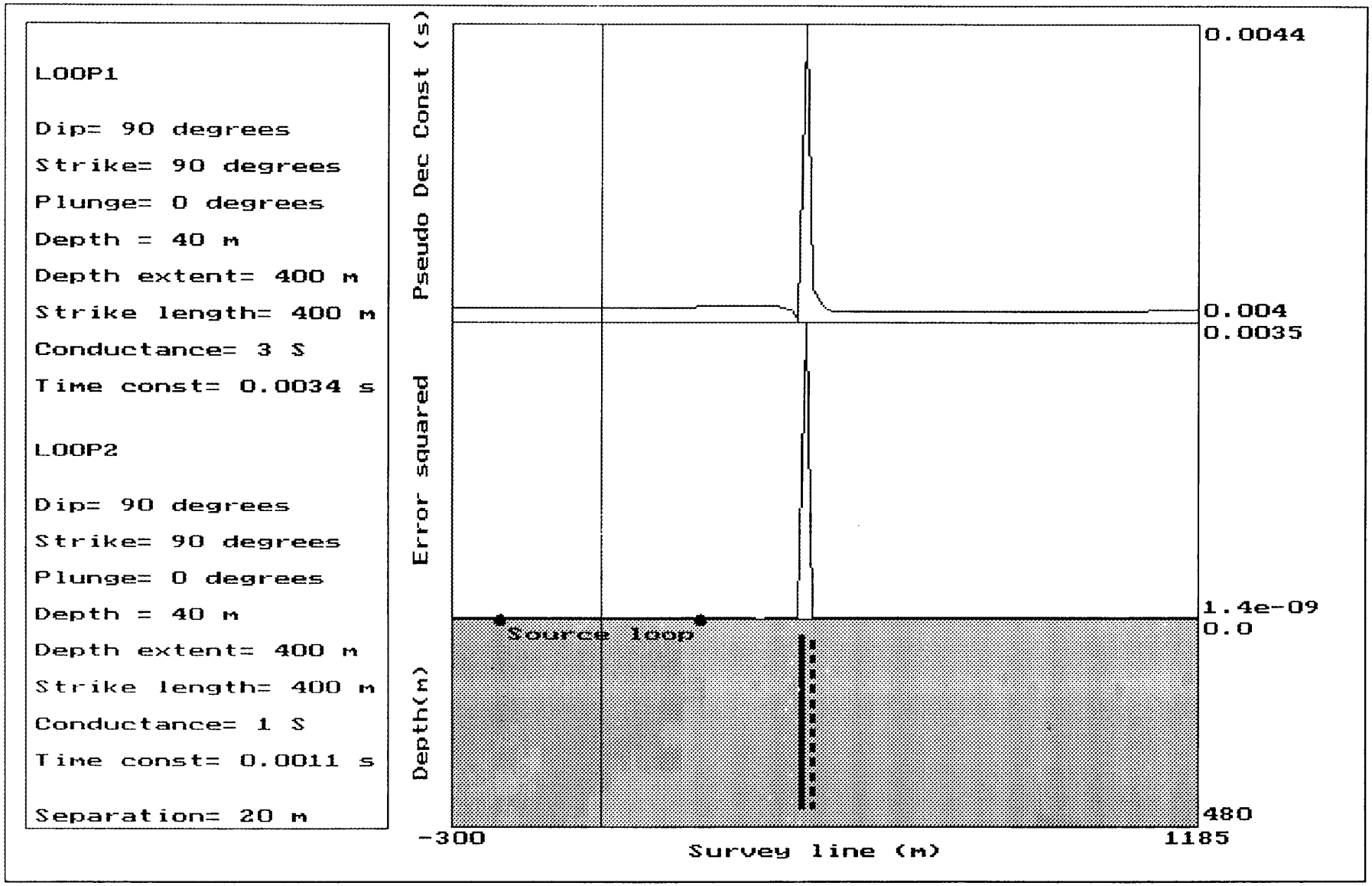

Figure M14: *Model example showing how the pseudo decay constant can indicate the presence of multiple conductors.*

CHAPTER 5

CONCLUSIONS

The objective of this thesis was to develop a method of modelling the TDEM response of multiple sheet conductors in resistive host rocks for TDEM systems that employ step-function source currents, and to use this to study the influence mutual coupling will have on the observed data. The method used was to approximate the response from two inductively coupled conductive plates by the response from two interacting wire circuits.

Modelling conductive plates by loops provided a relatively simple way of qualitatively predicting the time-domain response from multiple conductors. Although it is an oversimplification of the problem at hand, it is of heuristic value since it allows much insight into the phenomena of electromagnetic coupling. Due to the simplicity of the mathematics involved in the modelling process, a fast computer program was written that allows the study of a great number of geological sheet conductor problems.

The results of this study are:

- The TDEM response of multiple conductors is not the sum of their individual uncoupled responses, but is given by a sum of exponentials.
- When a weak conductor is situated between the source loop and a good conductor, the response of the good conductor is masked by the presence of the poor conductor, and only becomes apparent on the late time channels.
- A good conductor situated between the source loop and a weak conductor has a similar, though less severe, effect on the measured response.
- The separation/depth ratio of two conductors of similar conductances affects their resolvability. When the ratio is less than 1 it is not possible to resolve them both from the measured secondary magnetic profile plots. Only when the ratio approaches 2, do two peaks appear on the profile curves. This behaviour is also observed for conductors with dips less than 90^{o}.

- When the difference between the conductances of two conductors is large, the peaks of the measured responses and the cross-over positions drift in the direction of the stronger conductor. This behaviour can be diagnostic of a multiple conductor system, and is observed even when conductor separation is very small.
- The decay constant for a multiple conductor situation of large conductor separation, is approximately equal to the greater of the two individual decay constants, but is position dependant.
- At positions between two conductors it is not possible to define a true exponential decay constant. By exploiting this fact and defining a pseudo decay constant, it is possible to get additional information that can help to establish whether more than one conductor are present. The pseudo time constant is calculated by fitting straight lines to the natural logarithms of the absolute values of the last five channels in the vertical TDEM response.

Many other geological problems involving sheet conductors can be studied with ease by employing this modelling method. The speed at which the computer program runs ensures that a great number of changes can be made to model parameters without it becoming costly as far as time is concerned.

APPENDIX A - Calculating the Magnetic field of a line source.

A1 Line source of finite length.

Figure A1 shows a line source of length 2L lying in the y-direction, with the origin of the coordinate system coinciding with the centre of the line source.

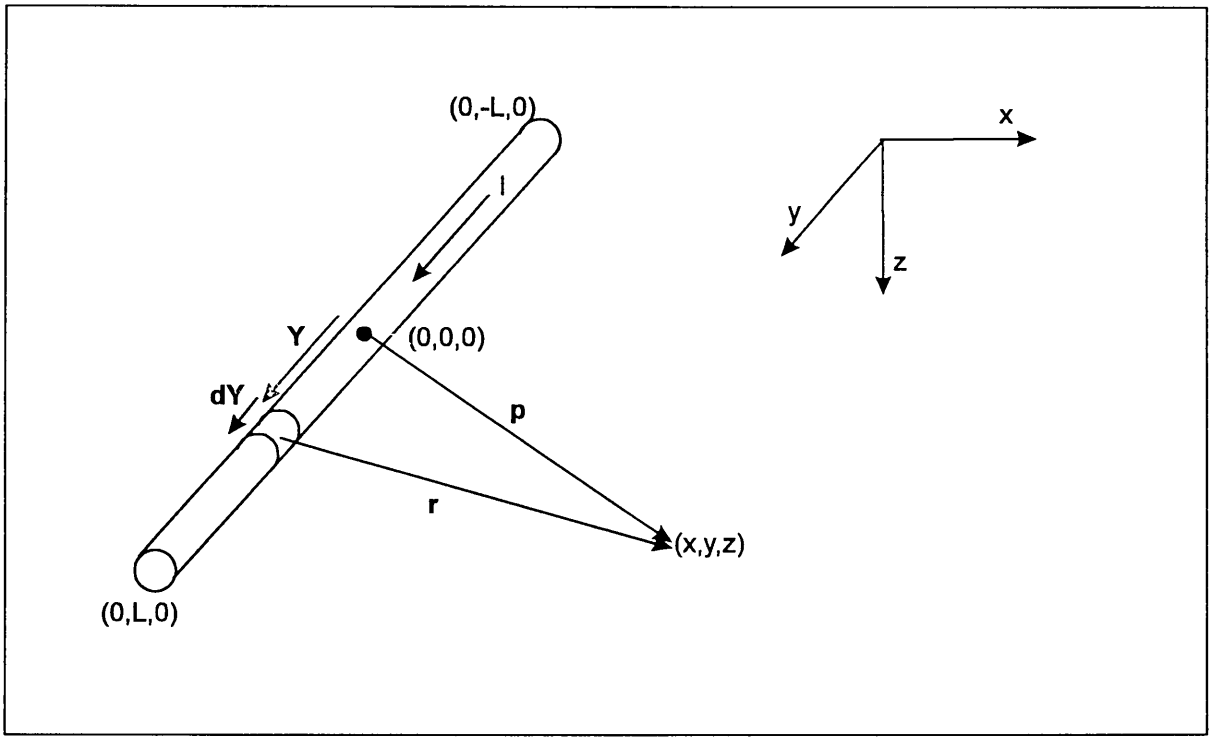

Figure A1: *Schematic presentation of a line source with finite length lying in the y direction.*

The magnetic field due to this source can be calculated at any position in a whole-space by using the law of Biot-Savart (equation 2.3):

$$\mathbf{dB} = \mu_0 \frac{\mathbf{Idl} \times \hat{\mathbf{r}}}{4\pi r^2}$$

We wish to calculate the magnetic field at any survey station with position vector $\mathbf{p}$ relative to the origin of the coordinate system. This station has a position vector $\mathbf{r}$ relative to the line element $\mathbf{dY}$. The position vector $\mathbf{r}$ is given by:

$$\mathbf{r} = \mathbf{p} - \mathbf{Y}, \tag{A1}$$

or

$$\mathbf{r} = (x, y - Y, z) \tag{A2}$$

The vector $\mathbf{dY}$ and the unit vector $\hat{\mathbf{r}}$ are given by:

$$\mathbf{dY} = (0, dY, 0) \tag{A3}$$

and

$$\hat{\mathbf{r}} = \frac{1}{\sqrt{x^2 + (y - Y)^2 + z^2}} (x, y - Y, z) \tag{A4}$$

Equation 2.3 can thus be expressed as:

$$\mathbf{dB} = \frac{\mu_0 I}{4\pi r^3} (0, dY, 0) \times (x, y - Y, z) \tag{A5}$$

Calculation of the vector product yields the following expressions for the components of the magnetic field:

$$dB_x = \frac{\mu_0 I z}{4\pi r^3} dY \tag{A6}$$

and

$$dB_z = -\frac{\mu_0 I x}{4\pi r^3} dY \tag{A7}$$

The x component of the magnetic field can now be calculated from:

$$B_x = \frac{\mu_0 I z}{4\pi} \int_{-L}^{L} \frac{dY}{\left(x^2 + (y - Y)^2 + z^2\right)^{3/2}} \tag{A8}$$

By defining $\rho^2 = x^2 + z^2$, and making the substitusion $y - Y = y^*$, equation A8 reduces to:

$$B_x = \frac{\mu_0 Iz}{4\pi} \int_{y-L}^{y+L} \frac{dy^*}{\left(\rho^2 + y^{*2}\right)^{3/2}} \qquad \text{(A9)}$$

This integral is of a standard form and, when solved, gives the following expression:

$$B_x(r) = \frac{\mu_0 Iz}{4\pi\rho^2}\left[\frac{y+L}{\left((y+L)^2+\rho^2\right)^{1/2}} - \frac{y-L}{\left((y-L)^2+\rho^2\right)^{1/2}}\right] \qquad \text{(A10)}$$

For the case of a finite line source of length a (as is used in Section 2.3.4 as one of the long sides of a loop), equation A10 gives:

$$B_x(r) = \frac{\mu_0 Iz}{4\pi\rho^2}\left[\frac{y_{d2}}{\left(y_{d2}^2+\rho^2\right)^{1/2}} - \frac{y_{d1}}{\left(y_{d1}^2+\rho^2\right)^{1/2}}\right] \qquad \text{(A11)}$$

with $y_{d1} = y - \frac{a}{2}$, and $y_{d2} = y + \frac{a}{2}$.

The z component can be found in a similar way:

$$B_z(r) = -\frac{\mu_0 Ix}{4\pi\rho^2}\left[\frac{y_{d2}}{\left(y_{d2}^2+\rho^2\right)^{1/2}} - \frac{y_{d1}}{\left(y_{d1}^2+\rho^2\right)^{1/2}}\right] \qquad \text{(A12)}$$

A2 Line source of infinite length.

The magnetic field of a line source of infinite length can be calculated by taking the limit as L tends to infinity $(L \to \infty)$ in equation A10. Due to infinite length of the source in the y direction, the magnetic field is not a function of the y position of measurement. By taking y=0 for simplicity's sake, equation A10 reduces to:

$$B_x = \frac{\mu_0 I z}{4\pi\rho^2}\left[\frac{2L}{\left(L^2+\rho^2\right)^{1/2}}\right] \qquad (A13)$$

In the limit as L tends to infinity, this equation becomes:

$$B_x = \frac{\mu_0 I z}{2\pi\rho^2} \qquad (A14)$$

The z component is found in the same way to be given by:

$$B_z = -\frac{\mu_0 I x}{2\pi\rho^2} \qquad (A15)$$

The magnetic field of an infinitely long line source lying in the y-direction, is thus given by:

$$\mathbf{B}(x,z) = \frac{\mu_0 I}{2\pi\rho^2}\left[z\mathbf{u}_x - x\mathbf{u}_z\right] \qquad (A16)$$

APPENDIX B - Computer Code

This program models the response of two mutually coupled plates by calculating the response of two inductively coupled loops. The program allows the model loops to have arbitrary positions, dips, strikes, and plunges in a whole space. The calculations employ results of work done by MA Valleé of the University of Toronto.

```
#include <stdio.h>
#include <math.h>
#include <conio.h>
#include <graphics.h>
#include <stdlib.h>


#define MU 4*M_PI*pow10(-7)
#define Radfact M_PI/180
#define Nchannels 20            //number of time channels//
#define Nsurveypts 100          //number of stations along survey traverse//
#define Nxint 50                //number of equally sized x and y intervals used...//
#define Nyint 50                //...in numerical integration//


//VVVVVVVVVVVVVVVVVV--Define variables--VVVVVVVVVVVVVVVVVVVVVV//

int i,j,k,l;                    // dummy variables //

float a0,b0,current0;           // long and short axes of source loop, source current//
float a1,b1;                    // long and short axes of loop1 //
float a2,b2;                    // long and short axes of loop2 //
float dip1,strike1,plunge1;     // dips, strikes, and plunges of model loops in radians//
float dip2,strike2,plunge2;
```

```
float Dip1,Strike1,Plunge1;   // dips, strikes, and plunges of model loops in degrees//
float Dip2,Strike2,Plunge2;
float cond1,cond2;            // conductances of two model loops in Siemens //
float l1x,l1y,l1z,l2x,l2y,l2z;    // loop midpoint coordinates //

float S0;                     // area of source loop //
float S1,s1x,s1y,s1z;         // area of loop1, components of area vector 1 //
float S2,s2x,s2y,s2z;         // area of loop2, components of area vector 2 //

float times[]={.089,.110,.140,.177,.220,.280,
               .355,.443,.564,.713,.881,1.096,
               1.411,1.795,2.224,2.850,3.600,
               4.490,5.700,7.190};          // array with channel times (ms) //

float t;                                    // time variable //

float xint,yint;                  // sizes of intervals used in numerical integration //
float xnode1[Nxint],ynode1[Nyint];          // node positions //
float xnode2[Nxint],ynode2[Nyint];          // node positions //


double rotx,roty,rotz;                // output from rotational function ROT //
double invrotx,invroty,invrotz;       // output from inverse rotational function InvROT
//
double transx,transy,transz;          // output for translating function Trans //
double xr,yr,zr;                      // coordinates used in calculations //
double xt,yt,zt;                      // coordinates used in calculations //
float xs[Nsurveypts],ys,zs;           // survey coordinates (profile line in x-direction) //


double Phi00,Phi11,Phi22,
       Phi10,Phi20,          // Phi-ij: flux through loop i due to unit current in loop j //
       Phi12,Phi21;
double L0,L1,L2,L3,
       M01,M02,M12,M21,
```

```
        M03x[Nsurveypts],M13x[Nsurveypts],
        M23x[Nsurveypts],
        M03z[Nsurveypts],M13z[Nsurveypts],
         M23z[Nsurveypts];

                    // Self Inductances of and Mutual Inductances between loops //


float xd1,xd2,yd1,yd2;          // x and y components of distances to sides of loops //
float rhoxz1sq,rhoxz2sq,rhoyz1sq,rhoyz2sq;
                                        // Squared distances to sides of loops //
float R1,R2,R3,R4;                  // Distances to corner points of loops //
float term1,term2,term3,term4;          // Terms used in calculations //
double bx,by,bz;                        // Magnetic field components //



double Tau1,Tau2;                   // individual decay constants //
double t1,t2;                       // coupled decay constants //

double k01,k02,k03x[Nsurveypts],k03z[Nsurveypts],
     k12,k13x[Nsurveypts],k13z[Nsurveypts],
     k23x[Nsurveypts],k23z[Nsurveypts];      // coupling coefficients //
double c1,c2,c3,c4,c5;

double i1[Nchannels],i2[Nchannels];         // currents in coupled loops //
double i1prime[Nchannels],
        i2prime[Nchannels];
                                    // time derivatives of currents in coupled loops //
double emfx[Nchannels][Nsurveypts],
        emfz[Nchannels][Nsurveypts];        // emf's induced in receiver loop//
```

```
// graphics: //
float xsmin,xsmax;              // maximum and minimum value of survey coordinates //
float emfxmin,emfxmax;          // maximum and minimum value of emf's induced //
float emfzmin,emfzmax;          // maximum and minimum value of emf's induced //
float cpmax,cpmin,
    cp1max,cp1min,
    cp2max,cp2min;          // maximum and minimum value of loop corner positions //
float cp1z[4],cp2z[4],
    cp1x[4],cp2x[4];                    // loop corner positions //




//FFFFFFFFFFFFFFFFFFFF--Define functions--FFFFFFFFFFFFFFFFFFFFFFFF//

void Areavec();
void Nodes();
void Bfields(int a,int b,float curr,float xb,float yb,float zb);
void Inductances();
void Timeconst();
void Couplingcoef();
void Emfs();
void ROT(float xcomp,float ycomp,float zcomp,float theta,float phi. float gamma);
void InvROT(float xcomp,float ycomp,float zcomp,float theta,float phi, float gamma);
void Trans(float xt,float yt,float zt,float centx,float centy,float centz);
void Maxmin();
float max(float value1, float value2);
float min(float value3, float value4);
void Graph();
void Cornerpts();
```

```
//MMMMMMMMMMMMMMMMMMMM---main---MMMMMMMMMMMMMMMMMMMM//

main()
{

   clrscr();

//--Coordinates of survey line--//
   for(i=0;i<Nsurveypts;i++)
     xs[i]=-300.0+(15*i);          //Determine station spacing and traverse position//
   ys=0;
   zs=0;


//***********************************//
//***MODEL PARAMETERS***//
//***********************************//
// location of the centre of loop1 //
   l1x=400;
   l1y=0;
   l1z=240;

// location of the centre of loop2 //
   l2x=480;
   l2y=0;
   l2z=240;

//--Parameters of source loop--//
   a0=400;
   b0=400;
   current0=20;



//--Parameters of loop1--//
```

```
    a1=400;
    b1=400;
    cond1=0.5;
    Dip1=90.0;
    Strike1=90.0;
    Plunge1=0.0;
    dip1=Dip1*Radfact;
    strike1=(90-Strike1)*Radfact;
    plunge1=Plunge1*Radfact;

//--Parameters of loop2--//
    a2=800;
    b2=400;
    cond2=0.5;
    Dip2=90.0;
    Strike2=90.0;
    Plunge2=0.0;
    dip2=Dip2*Radfact;
    strike2=(90-Strike2)*Radfact;
    plunge2=Plunge2*Radfact;



//--CALCULATE THE COMPONENTS OF THE LOOP AREA VECTORS--//
    Areavec();

//--CALCULATE THE NODE COORDINATES USED IN NUMERICAL
INTEGRATION--//
    Nodes();

//--CALCULATE INDUCTANCES--//
    Inductances();

//--CALCULATE TIMECONSTANTS--//
    Timeconst();
```

```
//--COUPLING COEFICIENTS--//
    Couplingcoef();

//--CALCULATE THE EMF INDUCED IN THE RECEIVER LOOP--//
    Emfs();


//--FUNTIONS THAT CONTROL THE GRAPHICS--//
    Cornerpts();
    Maxmin();
    Graph();



    return(0);

}
//EMEMEMEMEMEMEMEMEMEM---end of main---EMEMEMEMEMEMEMEM//




//*************************************************************************//
// Funtion calculates the mutual and self inductances of the model loops     //
//*************************************************************************//
void Inductances()
{
//L0//
        for(k=0;k<Nxint;k++){
            for(l=0;l<Nyint;l++){
                Bfields(a0,b0,1,xnode1[k],ynode1[l],0);
                Phi00=Phi00+(bz*S0);
```

```
            }
        }
        L0=Phi00;


//L1//
        for(k=0;k<Nxint;k++){
            for(l=0;l<Nyint;l++){
                Bfields(a1,b1,1,xnode1[k],ynode1[l],0);
                Phi11=Phi11+(bz*S1);
            }
        }
        L1=Phi11;


//L2//
        for(k=0;k<Nxint;k++){
            for(l=0;l<Nyint;l++){
                Bfields(a2,b2,1,xnode2[k],ynode2[l],0);
                Phi22=Phi22+(bz*S2);
            }
        }
        L2=Phi22;


//L3//
        L3=0.5*MU/sqrt(M_PI);


//M10=M01//
        for(k=0;k<Nxint;k++){
            for(l=0;l<Nyint;l++){
                ROT(xnode1[k],ynode1[l],0,dip1,strike1,plunge1);
                xr=l1x+rotx;
                yr=l1y+roty;
```

```
                zr=l1z+rotz;
                Bfields(a0,b0,1,xr,yr,zr);
                Phi10=Phi10+(bx*s1x+by*s1y+bz*s1z);
            }
        }
        M01=Phi10;


//M20=M02//
        for(k=0;k<Nxint;k++){
            for(l=0;l<Nyint;l++){
                ROT(xnode2[k],ynode2[l],0,dip2,strike2,plunge2);
                xr=l2x+rotx;
                yr=l2y+roty;
                zr=l2z+rotz;
                Bfields(a0,b0,1,xr,yr,zr);
                Phi20=Phi20+(bx*s2x+by*s2y+bz*s2z);
            }
        }
        M02=Phi20;


//M21=M12//
        for(k=0;k<Nxint;k++){
            for(l=0;l<Nyint;l++){
                ROT(xnode1[k],ynode1[l],0,dip1,strike1,plunge1);
                Trans(l1x+rotx,l1y+roty,l1z+rotz,l2x,l2y,l2z);
                InvROT(transx,transy,transz,dip2,strike2,plunge2);
                Bfields(a2,b2,1.0,invrotx,invroty,invrotz);
                ROT(bx,by,bz,dip2,strike2,plunge2);
                Phi12=Phi12+(rotx*s1x+roty*s1y+rotz*s1z);
            }
        }
        M12=Phi12;
```

```
        for(i=0;i<Nsurveypts;i++){
//M30=M03//
            Bfields(a0,b0,1.0,xs[i],ys,zs);
            M03x[i]=bx;
            M03z[i]=bz;

//M13=M31//
            Trans(xs[i],ys,zs,l1x,l1y,l1z);
            InvROT(transx,transy,transz,dip1,strike1,plunge1);
            Bfields(a1,b1,1.0,invrotx,invroty,invrotz);
            ROT(bx,by,bz,dip1,strike1,plunge1);
            M13x[i]=rotx;
            M13z[i]=rotz;

//M32=M23//
            Trans(xs[i],ys,zs,l2x,l2y,l2z);
            InvROT(transx,transy,transz,dip2,strike2,plunge2);
            Bfields(a2,b2,1.0,invrotx,invroty,invrotz);
            ROT(bx,by,bz,dip2,strike2,plunge2);
            M23x[i]=rotx;
            M23z[i]=rotz;

        }

}



//*********************************//
// Uncoupled time constants //
//*********************************//
void Timeconst()
{
    Tau1=cond1*L1;
    Tau2=cond2*L2;
```

```
}



//*****************************************//
// Calculating the Coupling coefficients //
//*****************************************//
void Couplingcoef()
{
    k01=M01/sqrt(L0*L1);
    k02=M02/sqrt(L0*L2);
    k12=M12/sqrt(L1*L2);
    for(i=0;i<Nsurveypts;i++){
        k03x[i]=M03x[i]/sqrt(L0*L3);
        k13x[i]=M13x[i]/sqrt(L1*L3);
        k23x[i]=M23x[i]/sqrt(L2*L3);
        k03z[i]=M03z[i]/sqrt(L0*L3);
        k13z[i]=M13z[i]/sqrt(L1*L3);
        k23z[i]=M23z[i]/sqrt(L2*L3);
    }
}



//*********************************************************************//
// Calculating the Emf's induced in the receiver loop.          //
// Responses for horizontal and vertical measurements are //
// calculated.                                                  //
//*********************************************************************//
void Emfs()
{

    t1=(Tau1+Tau2)/2+0.5*sqrt( (Tau1-Tau2)*(Tau1-Tau2)+4*Tau1*Tau2*k12*k12 );
    t2=(Tau1+Tau2)/2-0.5*sqrt( (Tau1-Tau2)*(Tau1-Tau2)+4*Tau1*Tau2*k12*k12 );
```

```
    c1=1 / ( (1-k12*k12)*(t1-t2) );
    c2=( (t1/Tau2) - (k01-k02*k12)/k01 );
    c3=( (t2/Tau2) - (k01-k02*k12)/k01 );
    c4=( (t1/Tau1) - (k02-k01*k12)/k02 );
    c5=( (t2/Tau1) - (k02-k01*k12)/k02 );


    for(j=0;j<Nchannels;j++){
        t=times[j]*pow10(-3);
        i1[j]=(M01/L1)*c1*(  t2*c2*exp(-t/t1)
                           -t1*c3*exp(-t/t2)  );
        i2[j]=(M02/L2)*c1*(  t2*c4*exp(-t/t1)
                           -t1*c5*exp(-t/t2)  );
        i1prime[j]=-(M01/L1)*c1*(  t2/t1*c2*exp(-t/t1)
                                 -t1/t2*c3*exp(-t/t2)  );
        i2prime[j]=-(M02/L2)*c1*(  t2/t1*c4*exp(-t/t1)
                                 -t1/t2*c5*exp(-t/t2)  );
    }


    for(i=0;i<Nsurveypts;i++){
        for(j=0;j<Nchannels;j++){
           t=times[j]*pow10(-3);
           emfx[j][i]=-current0*(M13x[i]*i1prime[j]+M23x[i]*i2prime[j]);
           emfz[j][i]=-current0*(M13z[i]*i1prime[j]+M23z[i]*i2prime[j]);
        }
    }
}




//*****************************************************************************//
```

```
// Function calculates Magnetic induction for a horizontal loop. (The field  //
// is calculated with the origin at the centre of the loop.)                  //
// (Positive z-axis points downwards)                                         //
//*****************************************************************************//
void Bfields(int a,int b,float curr,float xb,float yb,float zb)
{

    xd1=xb-b/2;
    xd2=xb+b/2;
    yd1=yb-a/2;
    yd2=yb+a/2;

    rhoxz1sq=xd1*xd1+zb*zb;
    rhoxz2sq=xd2*xd2+zb*zb;
    rhoyz1sq=yd1*yd1+zb*zb;
    rhoyz2sq=yd2*yd2+zb*zb;

    R1=sqrt(xd1*xd1+yd1*yd1+zb*zb);
    R2=sqrt(xd1*xd1+yd2*yd2+zb*zb);
    R3=sqrt(xd2*xd2+yd1*yd1+zb*zb);
    R4=sqrt(xd2*xd2+yd2*yd2+zb*zb);


    term1=(xd1/rhoxz1sq)*(yd2/R2-yd1/R1);
    term2=(xd2/rhoxz2sq)*(yd2/R4-yd1/R3);
    term3=(yd1/rhoyz1sq)*(xd2/R3-xd1/R1);
    term4=(yd2/rhoyz2sq)*(xd2/R4-xd1/R2);
    bz=MU*(-curr/(4*M_PI))*(term1-term2+term3-term4);

    term1=(zb/rhoxz1sq)*(yd2/R2-yd1/R1);
    term2=(zb/rhoxz2sq)*(yd2/R4-yd1/R3);
    bx=MU*(+curr/(4*M_PI))*(term1-term2);

    term1=(zb/rhoyz1sq)*(xd2/R3-xd1/R1);
    term2=(zb/rhoyz2sq)*(xd2/R4-xd1/R2);
```

```
        by=MU*(-curr/(4*M_PI))*(term1-term2);

}




//*************************************************************************//
// Function rotates any vector, with origin at the centre of a loop, in    //
// accordance with the dip,plunge and strike of the loop                    //
//*************************************************************************//
void ROT(float xcomp,float ycomp,float zcomp,float theta,float phi, float gamma)
{

    float r11,r12,r13,r21,r22,r23,r31,r32,r33;

    r11=cos(theta)*cos(gamma);
    r12=-cos(theta)*sin(gamma)*cos(phi)-sin(theta)*sin(phi);
    r13=cos(theta)*sin(gamma)*sin(phi)-sin(theta)*cos(phi);
    r21=sin(gamma);
    r22=cos(gamma)*cos(phi);
    r23=-cos(gamma)*sin(phi);
    r31=sin(theta)*cos(gamma);
    r32=-sin(theta)*sin(gamma)*cos(phi)+cos(theta)*sin(phi);
    r33=sin(theta)*sin(gamma)*sin(phi)+cos(theta)*cos(phi);

    rotx=r11*xcomp+r12*ycomp+r13*zcomp;
    roty=r21*xcomp+r22*ycomp+r23*zcomp;
    rotz=r31*xcomp+r32*ycomp+r33*zcomp;


}
```

```
//*****************************************//
// The inverse rotation of function ROT //
//*****************************************//
void InvROT(float xcomp,float ycomp,float zcomp,float theta,float phi, float gamma)
{

    float r11,r12,r13,r21,r22,r23,r31,r32,r33;

    r11=cos(-theta)*cos(-gamma);
    r12=-cos(-theta)*sin(-gamma)*cos(-phi)-sin(-theta)*sin(-phi);
    r13=cos(-theta)*sin(-gamma)*sin(-phi)-sin(-theta)*cos(-phi);
    r21=sin(-gamma);
    r22=cos(-gamma)*cos(-phi);
    r23=-cos(-gamma)*sin(-phi);
    r31=sin(-theta)*cos(-gamma);
    r32=-sin(-theta)*sin(-gamma)*cos(-phi)+cos(-theta)*sin(-phi);
    r33=sin(-theta)*sin(-gamma)*sin(-phi)+cos(-theta)*cos(-phi);

    invrotx=r11*xcomp+r12*ycomp+r13*zcomp;
    invroty=r21*xcomp+r22*ycomp+r23*zcomp;
    invrotz=r31*xcomp+r32*ycomp+r33*zcomp;


}




//*************************************************************************************//
// Funtion calculates the sizes of the areas used in numeric integration and //
// determines the components of the area vectors.                            //
//*************************************************************************************//
void Areavec()
{
```

```
    S0=(a0*b0)/(Nxint*Nyint);
    S1=(a1*b1)/(Nxint*Nyint);
    S2=(a2*b2)/(Nxint*Nyint);

    ROT(0,0,S1,dip1,plunge1,strike1);
    s1x=rotx;
    s1y=roty;
    s1z=rotz;

    ROT(0,0,S2,dip2,plunge2,strike2);
    s2x=rotx;
    s2y=roty;
    s2z=rotz;
}



//*************************************************************************//
// Funtion calculates node positions used in numerical integration    //
//*************************************************************************//
void Nodes()
{
    xint=b1/Nxint;
    yint=a1/Nyint;
    for (i=0;i<Nxint;i++)
        xnode1[i]=-b1/2+b1/(2*Nxint)+i*xint;
    for (k=0;k<Nyint;k++)
        ynode1[k]=-a1/2+a1/(2*Nyint)+k*yint;

    xint=b2/Nxint;
    yint=a2/Nyint;
    for (i=0;i<Nxint;i++)
        xnode2[i]=-b2/2+b2/(2*Nxint)+i*xint;
    for (k=0;k<Nyint;k++)
        ynode2[k]=-a2/2+a2/(2*Nyint)+k*yint;
```

```
}

//*****************************************************************************//
// Function translates input coordinates to coordinates relative to centre   //
// of loop.                                                                    //
//*****************************************************************************//

void Trans(float xt,float yt,float zt,float centx,float centy,float centz)
{
     transx=xt-centx;
     transy=yt-centy;
     transz=zt-centz;

}

//*****************************************************************************//
// Function determines the minimum and maximum values of the //
// induced emf's and the survey coordinates                  //
//*****************************************************************************//
void Maxmin()
{
  float dummy;

  xsmin=xs[0];
  xsmax=xs[Nsurveypts-1];
```

```
   emfxmax=emfx[0][0];
   emfxmin=emfx[0][0];
   for(i=1;i<Nsurveypts;i++){
      emfxmax=max(emfxmax,emfx[0][i]);
      emfxmin=min(emfxmin,emfx[0][i]);
   }
   dummy=(emfxmax-emfxmin)/10;
   emfxmax+=dummy;
   emfxmin-=dummy;

   emfzmax=emfz[0][0];
   emfzmin=emfz[0][0];
   for(i=1;i<Nsurveypts;i++){
      emfzmax=max(emfzmax,emfz[0][i]);
      emfzmin=min(emfzmin,emfz[0][i]);
   }
   dummy=(emfzmax-emfzmin)/10;
   emfzmax+=dummy;
   emfzmin-=dummy;


}




//*********************************************************//
//Funtion returns maximum value of two variables//
//*********************************************************//
float max(float value1, float value2)
{
   return ( (value1 > value2) ? value1 : value2);
}
```

```
//*******************************************************//
//Funtion returns minimum value of two variables//
//*******************************************************//
float min(float value3, float value4)
{
  return ( (value3 < value4) ? value3 : value4);
}



//**************//
// Graphics    //
//**************//
void Graph()
{

  int gr_left,gr_right,
      gr1_top,gr1_bottom,
      gr2_top,gr2_bottom,
      gr3_top,gr3_bottom,
      gr_size;
  float xscalefactor,yxscalefactor,yzscalefactor;
  float linebeginx,lineendx,
          linebeginy,lineendy;
  char str1[25],str2[25],buffer[40];


//INITIALIZE GRAPHICS//
  int gdriver=DETECT, gmode, errorcode;
  char msg[80];
  initgraph(&gdriver, &gmode, "");
  errorcode = graphresult();
  if (errorcode != grOk){
```

```
    printf("Graphics error: %s\n", grapherrormsg(errorcode));
    printf("Press any key to halt:");
    getch();
    exit(1);
  }



// Background colour //
  setbkcolor(WHITE);
  setcolor(BLUE);
  setlinestyle(SOLID_LINE,0,NORM_WIDTH);
  rectangle(0,0,639,479);

// Define and draw Graph windows //
  gr_right=560;
  gr_left=210;
  xscalefactor=(gr_right-gr_left)/(xsmax-xsmin);          //computing the scalefactors
  gr_size=0.5*(440-(cpmax+cpmin)*xscalefactor);

  gr1_top=10;
  gr1_bottom=gr1_top+gr_size;
  gr2_top=gr1_bottom;
  gr2_bottom=gr2_top+gr_size;
  gr3_top=gr2_bottom;
  gr3_bottom=gr3_top+(cpmax+cpmin)*xscalefactor;

  yxscalefactor=(gr1_bottom-gr1_top)/(emfxmax-emfxmin);
  yzscalefactor=(gr1_bottom-gr1_top)/(emfzmax-emfzmin);


  setfillstyle(SOLID_FILL,LIGHTGRAY);
  bar(gr_left,gr3_top,gr_right,gr3_bottom);
  setlinestyle(SOLID_LINE,0,NORM_WIDTH);
  rectangle(10,10,180,450);
```

```
  rectangle(gr_left,gr1_top,gr_right,gr1_bottom);
  rectangle(gr_left,gr2_top,gr_right,gr2_bottom);
  rectangle(gr_left,gr3_top,gr_right,gr3_bottom);


// Graph1 - x response //
  setviewport(gr_left,gr1_top,gr_right,gr1_bottom,1);
  for(j=0;j<Nchannels;j+=2){
    for(i=0;i<Nsurveypts-1;i++){                    //drawing the graph
        linebeginx=(xs[i]-xsmin)*xscalefactor;
        linebeginy=(gr1_bottom-gr1_top)-(emfx[j][i]-emfxmin)*yxscalefactor;
        lineendx=(xs[i+1]-xsmin)*xscalefactor;
        lineendy=(gr1_bottom-gr1_top)-(emfx[j][i+1]-emfxmin)*yxscalefactor;
        line(linebeginx,linebeginy,lineendx,lineendy);
    }
  }
  if(emfxmin<=0){                          //drawing zero line
   line(0,(gr1_bottom-gr1_top)+emfxmin*yxscalefactor,(gr_right-
gr_left),(gr1_bottom-gr1_top)+emfxmin*yxscalefactor);
  }


  setviewport(0,0,639,479,1);
  settextstyle(0,HORIZ_DIR,1);
  settextjustify(LEFT_TEXT,TOP_TEXT);
  gcvt(emfxmax,2,str1);
  outtextxy(gr_right+3,gr1_top+2,str1);
  settextjustify(LEFT_TEXT,BOTTOM_TEXT);
  gcvt(emfxmin,2,str2);
  outtextxy(gr_right+3,gr1_bottom-2,str2);

  settextstyle(0,VERT_DIR,1);
  settextjustify(RIGHT_TEXT,CENTER_TEXT);
  outtextxy(gr_left-10,(gr1_bottom-gr1_top)/2,"Horizontal Emf (V)");
```

```
// Graph2 - z response //
  setviewport(gr_left,gr2_top,gr_right,gr2_bottom,1);
  for(j=0;j<Nchannels;j+=2){
     for(i=0;i<Nsurveypts-1;i++){                    //drawing the graph
          linebeginx=(xs[i]-xsmin)*xscalefactor;
          linebeginy=(gr2_bottom-gr2_top)-(emfz[j][i]-emfzmin)*yzscalefactor;
          lineendx=(xs[i+1]-xsmin)*xscalefactor;
          lineendy=(gr2_bottom-gr2_top)-(emfz[j][i+1]-emfzmin)*yzscalefactor;
          line(linebeginx,linebeginy,lineendx,lineendy);
     }
  }
  if(emfzmin<=0){                          //drawing zero line
    line(0,(gr2_bottom-gr2_top)+emfzmin*yzscalefactor,(gr_right-
gr_left),(gr2_bottom-gr2_top)+emfzmin*yzscalefactor);
  }

  if(xsmin<=0){                            //drawing zero line
    setviewport(gr_left,gr1_top,gr_right,gr3_bottom,1);
    line((0-xsmin)*xscalefactor,gr3_bottom-gr1_top,(0-xsmin)*xscalefactor,0);
  }

  setviewport(gr_left,gr2_top,gr_right,gr2_bottom,1);
  settextstyle(0,HORIZ_DIR,1);

  setviewport(0,0,639,479,1);
  settextstyle(0,HORIZ_DIR,1);
  settextjustify(LEFT_TEXT,TOP_TEXT);
  gcvt(emfzmax,2,str1);
  outtextxy(gr_right+3,gr2_top+2,str1);
  settextjustify(LEFT_TEXT,BOTTOM_TEXT);
  gcvt(emfzmin,2,str2);
  outtextxy(gr_right+3,gr2_bottom-2,str2);

  settextstyle(0,VERT_DIR,1);
```

```
   settextjustify(RIGHT_TEXT,CENTER_TEXT);
   outtextxy(gr_left-10,gr1_bottom+(gr2_bottom-gr2_top)/2,"Vertical Emf (V)");



// Graph3 - model //
   setviewport(gr_left,gr3_top,gr_right,gr3_bottom,0);
   setlinestyle(SOLID_LINE,0,THICK_WIDTH);
   line((cp1x[0]-xsmin)*xscalefactor,(cp1z[0])*xscalefactor,(cp1x[1]-
xsmin)*xscalefactor,(cp1z[1])*xscalefactor);
   setlinestyle(DASHED_LINE,0,THICK_WIDTH);
   line((cp2x[1]-xsmin)*xscalefactor,(cp2z[1])*xscalefactor,(cp2x[0]-
xsmin)*xscalefactor,(cp2z[0])*xscalefactor);

   circle((-b0/2-xsmin)*xscalefactor,0,2);
   circle((b0/2-xsmin)*xscalefactor,0,2);
   settextstyle(0,HORIZ_DIR,1);
   settextjustify(CENTER_TEXT,TOP_TEXT);
   outtextxy(-xsmin*xscalefactor,5,"Source loop");

   setviewport(0,0,639,479,1);
   settextstyle(0,HORIZ_DIR,1);
   settextjustify(LEFT_TEXT,TOP_TEXT);
   outtextxy(gr_right+3,gr3_top+2,"0.0");
   settextjustify(LEFT_TEXT,BOTTOM_TEXT);
   gcvt(cpmax+cpmin,4,str1);
   outtextxy(gr_right+3,gr3_bottom-2,str1);
   settextstyle(0,HORIZ_DIR,1);
   settextjustify(CENTER_TEXT,TOP_TEXT);
   gcvt(xsmax,4,str1);
   outtextxy(gr_right,gr3_bottom+3,str1);
   gcvt(xsmin,4,str2);
   outtextxy(gr_left,gr3_bottom+3,str2);
   outtextxy(gr_left+(gr_right-gr_left)/2,gr3_bottom+10,"Survey line (m) ");
   settextstyle(0,VERT_DIR,1);
```

```
  settextjustify(RIGHT_TEXT,CENTER_TEXT);
  outtextxy(gr_left-10,gr3_top+(gr3_bottom-gr3_top)/2,"Depth(m)");

  float separation;
  separation=cp2x[0]-cp1x[0];
  separation=fabs(separation);
  settextjustify(LEFT_TEXT,TOP_TEXT);
  settextstyle(0,HORIZ_DIR,1);
  sprintf(buffer,"Separation= %d m",int(separation));
  outtextxy(gr_right-140,gr3_bottom-10,buffer);



// TEXT WINDOW //
  settextstyle(0,HORIZ_DIR,1);
  settextjustify(LEFT_TEXT,TOP_TEXT);
  outtextxy(15,45,"LOOP1 (Solid line)");
  sprintf(buffer,"Dip= %d degrees",int(Dip1));
  outtextxy(15,75,buffer);
  sprintf(buffer,"Strike= %d degrees",int(Strike1));
  outtextxy(15,95,buffer);
  sprintf(buffer,"Plunge= %d degrees",int(Plunge1));
  outtextxy(15,115,buffer);
  sprintf(buffer,"Depth = %d m",int(cp1min));
  outtextxy(15,135,buffer);
  sprintf(buffer,"Depth extent= %d m",int(b1));
  outtextxy(15,155,buffer);
  sprintf(buffer,"Strike length= %d m",int(a1));
  outtextxy(15,175,buffer);
  gcvt(cond1,2,str1);
  sprintf(buffer,"Conductance= %s S",str1);
  outtextxy(15,195,buffer);

  outtextxy(15,250,"LOOP2 (Dashed line)");
  sprintf(buffer,"Dip= %d degrees",int(Dip2));
```

```
   outtextxy(15,280,buffer);
   sprintf(buffer,"Strike= %d degrees",int(Strike2));
   outtextxy(15,300,buffer);
   sprintf(buffer,"Plunge= %d degrees",int(Plunge2));
   outtextxy(15,320,buffer);
   sprintf(buffer,"Depth = %d m",int(cp2min));
   outtextxy(15,340,buffer);
   sprintf(buffer,"Depth extent= %d m",int(b2));
   outtextxy(15,360,buffer);
   sprintf(buffer,"Strike length= %d m",int(a2));
   outtextxy(15,380,buffer);
   gcvt(cond2,2,str1);
   sprintf(buffer,"Conductance= %s S",str1);
   outtextxy(15,400,buffer);


   getch();

}




//*************************************************************//
// Function finds the minimum and maximum values     //
// of the model loops corner points (used in graphics)   //
//*************************************************************//
void Cornerpts()
{


   ROT(-b1/2,-a1/2,0,dip1,strike1,plunge1);
   cp1z[0]=l1z+rotz;
   cp1x[0]=l1x+rotx;
```

```
ROT(b1/2,-a1/2,0,dip1,strike1,plunge1);
cp1z[1]=l1z+rotz;
cp1x[1]=l1x+rotx;
ROT(b1/2,a1/2,0,dip1,strike1,plunge1);
cp1z[2]=l1z+rotz;
cp1x[2]=l1x+rotx;
ROT(-b1/2,a1/2,0,dip1,strike1,plunge1);
cp1z[3]=l1z+rotz;
cp1x[3]=l1x+rotx;

ROT(-b2/2,-a2/2,0,dip2,strike2,plunge2);
cp2z[0]=l2z+rotz;
cp2x[0]=l2x+rotx;
ROT(b2/2,-a2/2,0,dip2,strike2,plunge2);
cp2z[1]=l2z+rotz;
cp2x[1]=l2x+rotx;
ROT(b2/2,a2/2,0,dip2,strike2,plunge2);
cp2z[2]=l2z+rotz;
cp2x[2]=l2x+rotx;
ROT(-b2/2,a2/2,0,dip2,strike2,plunge2);
cp2z[3]=l2z+rotz;
cp2x[3]=l2x+rotx;

cp1max=cp1z[1];
cp1min=cp1z[1];
for(i=1;i<4;i++){
      cp1max=max(cp1max,cp1z[i]);
      cp1min=min(cp1min,cp1z[i]);
}

cp2max=cp2z[1];
cp2min=cp2z[1];
for(i=1;i<4;i++){
      cp2max=max(cp2max,cp2z[i]);
      cp2min=min(cp2min,cp2z[i]);
```

```
    }

    cpmax=max(cp1max,cp2max);
    cpmin=min(cp1min,cp2min);
}
```

REFERENCES

Adhidjaja, J.I., Hohmann, G.W., and Oristaglio, M.L., 1985, Two-dimensional transient electromagnetic responses: Geophysics, **50**, 2849-2861.

Annan, A.P., 1974, The equivalent source method in geophysics: PhD thesis, Memorial Univ of Newfoundland.

Best, M.E., and Shamas, B.R., 1976, Some modeling results for Turam type electromagnetic systems: Journal Can.Soc.ExpGeoph, **12**, 5-22.

Best, M.E., Duncan, P., Jacobs, F.J., and Scheen, W.L., 1985, Numerical modeling of the electromagnetic response of three-dimensional conductors in a layered earth: Geophysics, **50**, 665-676.

Coggon, J.H., 1971, Electromagnetic and electrical modeling by the finite element method: Geophysics, **36**, 132-1155.

Gallagher, P.R., Ward, S.H., and Hohmann, G.W., 1985, Amodel study of a thin plate in free space for the EM37 transient electromagnetic system: Geophysics, **50**, 1002-1019.

Goldman, M.M., 1983, The integral-finite-difference method for calculating transient electromagnetic fields in a horizontally stratified medium: Geophysical Prospecting, **31**, 664-686.

Goldman, M.M., and Stoyer, C.H., 1983, Finite-difference calculations of the transient field of an axially symmetric earth for vertical magnetic dipole exitation: Geophysics, **48**, 953-963.

Goldman, Y., Hubans, C., Nicoletis, S., and Spitz, S., 1986, A finite-element solution for the transient electromagnetic response of an arbitrary two-dimensional resistivity distribution: Geophysics, **51**, 1450-1461.

Hanneson, J.E., and West, G.F., 1984, The horizontal loop electromagnetic response of a thin plate in a conductive earth: Part 1-Computational method: Geophysics, **49**, 411-420.

Hanneson, J.E., 1992, The transient EM step response of a dipping plate in a conductive half-space: Geophysics, **57**, 1116-1126.

Hohmann, G.W., 1971, Electromagnetic scattering by conductors in the earth near a line source of current: Geophysics, **38**, 101-131.

Hohmann, G.W., 1975, Three dimensional I.P. and electromagnetic modeling: Geophysics, **40**, 309-324.

Khomenyuk, Yu. B., 1963, A generalized transient characteristicand its application in direct and inverse problems of the transientprocess method for certain bodies bedded in nonconducting media: Izv. Akad. Nauk SSSR, Ser. Geophys., **8**, 1234-1237.

Lamontagne, Y., and West, G.F., 1971, EM response of a rectangular thin plate: Geophysics, **36**, 1204-1222.

Lee, K.H., Pridmore, D.F., and Morrison, H.F., 1981, A hybrid three-dimensional electromagnetic modeling scheme: Geophysics, **46**, 796-805.

Leppin, Michael, 1992, Electromagnetic modeling of 3-D sources over 2-D inhomogeneities in the time domain: Geophysics, **57**, 994-1003.

Liu, Guimin, and Asten, M.W., 1993, Fast approximate solutions of transient EM response to a target Buried beneath a conductive overburden: Geophysics, **58**, 810-817.

McNeill, J.D., 1980, The application of transient electromagnetic techniques: Tech. Note 7, Geonics Ltd., Ontario, Canada.

1982, Interpretation of large-loop transmitter transient electromagnetic surveys: 52nd Ann. Internat. Mtg., Soc. Expl. Geophys., Expanded Abstracts, 373-374.

Nabighian, M.N., and Macnae, J.C., 1991, Time domain electromagnetic prospecting methods, in Nabighian, M.N., Ed. Electromagnetic methods in applied geophysics, Soc. Expl. Geophys., vol 2, 427-579.

Nabighian, M.N., and Oristaglio, M.L., 1984, Short note: On the approximation of finite loop sources by two-dimensional line sources: Geophysics, **49**, 1027-1029.

Oristaglio, M.L., and Hohmann, G.W., 1984, Diffusion of electromagnetic fields into a two-dimensional earth: A finite-difference approach: Geophysics, **49**, 870-894.

Pridmore, D.F., 1978, Three dimensional modeling of electric and electromagnetic data using the finite-element method: Ph.D thesis, University of Utah.

Pridmore, D.F., Hohmann, G.W., Ward S,H., and Sill, W.R., 1981, An investigation of finite element modeling for electrical and electromagnetic data in three dimensions: Geophysics, **46**, 1004-1024.

Rai, S.S., 1985, Transient electromagnetic response of a thin conducting plate embedded in conducting host rock: Geophysics, **50**, 1342-1349.

Raiche, A.P., 1974, An integral equation approach to three dimensional modeling: Geophysical Journal, Royal Astronomical Soc., **36**, 363-376.

SanFilipo, W.A., and Hohmann, G.W., 1985, Integral equation solution for the transient electromannetic response of a three-dimensional body in a conductive half-space: Geophysics, **50**, 798-809.

SanFilipo, W.A., Eaton, P.A., and Hohmann, G.W., 1985, The effect of a conductive half-space on the transient electromagnetic response of a three-dimensional body: Geophysics, **50**, 1144-1162.

Smith, R.S., and West, G.F., 1987, Electromagnetic induction in an inhomogeneous conductive thin sheet: Geophysics, **52**, 1677-1688.

Swift, C.M. Jnr., 1971, Theoretical magnetotelluric and Turam response from two dimensional inhohogeities, : Geophysics, **36**, 38-52

Telford, W.M., Geldart, L.P., Sheriff, R.E., 1990, Applied geophysics: Cambridge Univ. Press.

Valleé, Marc-Alex, 1981, Scale models on Transient response of multiple conductors: Res. in applied geophysics, **20**, Univ. Toronto Geophysics Lab.

Walker, P.W., and West, G.F., 1991, A robust integral equation solution for electromagnetic scattering by a thin plate in conductive media: Geophysics, **56**, 1140-1152.

Wannamaker, P.E., Hohmann, G.W., and SanFilipo, W.A., 1984, Electromagnetic modeling of three-dimensional bodies in layered earths using integral equations: Geophysics, **49**, 60-74.

Ward, S.H., and Hohmann, G.W., 1991, Electromagnetic theory for geophysical applications, in Nabighian, M.N., Ed. Electromagnetic methods in applied geophysics, Soc. Expl. Geophys., vol 2, 131-311.

Weidelt,P., 1983, The harmonic and transient response of a thin dipping dike: Geophysics, **48**, 934-952.

Wesley, J.P., 1958, Response of dyke to oscillating dipole: Geophysics, **23**, 128-133.

Wesley, J.P., 1958, Response of thin dyke to oscillating dipole: Geophysics, **23**, 134-143.